THE UNIVERSITY OF TULSA

THE GRADUATE SCHOOL

RESERVOIR DESCRIPTION BY INTEGRATION OF WELL TEST DATA AND SPATIAL STATISTICS

by

Rajiv K. Sagar

A dissertation submitted in partial fulfillment of

the requirements for the degree of Doctor of Philosophy

in the Discipline of Petroleum Engineering

The Graduate School

The University of Tulsa

1993

THE UNIVERSITY OF TULSA

THE GRADUATE SCHOOL

RESERVOIR DESCRIPTION BY INTEGRATION OF WELL TEST DATA AND SPATIAL STATISTICS

by

Rajiv K. Sagar

A DISSERTATION

APPROVED FOR THE DISCIPLINE OF

PETROLEUM ENGINEERING

By Dissertation Committee

Balmohan G Kelkar, Co-Chairperson

Rikki Thompson, Co-Chairperson

Sujeet Shenoi

Ram S. Agarwal

ABSTRACT

Sagar, R.K. (Doctor of Philosophy in Petroleum Engineering)

Reservoir Description by Integration of Well Test Data and Spatial Statistics

(166 pp. -Chapter VI)

Co-Directed by Dr. Mohan G. Kelkar and Dr. Leslie G. Thompson

(123 words)

We present an effective method to incorporate well test data in developing alternate equiprobable reservoir descriptions. In particular, we use recent analytical solutions[1,2] for well testing in heterogeneous reservoirs to describe the distribution of small scale permeability heterogeneities. The method of simulated annealing[3] is used to honor the well test and spatial statistics (variogram) constraints.

In our investigation of the problem, we are able to match the pressure and pressure derivatives of reproduced permeability fields with the pressure response of *truth* case permeability fields. We also investigate the effect of porosity heterogeneities on the pressure response in a reservoir during a drawdown test. In addition, the effect and incorporation of anisotropy on the pressure response during a drawdown test is investigated.

ACKNOWLEDGMENTS

I wish to thank Dr. Mohan Kelkar and Dr. Leslie Thompson for their invaluable assistance and encouragement as co-directors of this dissertation. I also express my gratitude to Dr. Ram Agarwal of Amoco Production Co. and Dr. Sujeet Shenoi of the University of Tulsa, for their comments and suggestions and for serving on my dissertation committee.

I acknowledge Dr. Albert Reynolds, Dr. Gilvan Feitosa, and Dr. Lifu Chu for the insightful and educational discussions we have had on the this subject.

The author is grateful to the University of Tulsa Petroleum Reservoir Exploitation Projects (TUPREP), the Department of Energy, Phillips Petroleum Company, and the University of Tulsa for funding my studies and this research project at the University of Tulsa.

This work is dedicated to my parents Vidya and Leela Sagar whose support, encouragement and sacrifices will always be treasured.

TABLE OF CONTENTS

LIST OF TABLES

LIST OF FIGURES

CHAPTER I

INTRODUCTION

Reservoir description is an integral part of reservoir management and future performance prediction. With a growing emphasis in the oil industry to enhance hydrocarbon reserves by developing mature existing fields, the need for more accurate reservoir descriptions is crucial and necessary. More accurate description of reservoirs will help in the prediction of reservoir performance at both, the primary and the secondary recovery phases. Unswept zones of oil in place can be determined and considered for infill drilling.

Present day focus and emphasis in reservoir engineering research and practical application lies in the integration of diverse sources of data for the purpose of accurate reservoir description. Geostatistical tools are widely used in industry to describe reservoir heterogeneities. However, available techniques only allow us to use data from limited sources. Very often only core, well-logs and geological information are incorporated into the model of reservoir heterogeneity. Valuable data, such as geophysical, production, and well-test data, are generally not included.

The objective of this work is to incorporate data from well-test, cores and logs to develop a more comprehensive reservoir description. Core and log data provide information about the univariate (histogram) and spatial (variogram) statistics for a reservoir property. Well test data are a measure of the dynamic performance of a reservoir and the reservoir property that describes this performance is the reservoir permeability. In addition, well-test interpretation techniques provide useful information on a scale larger

than core or log data. On this scale we can determine faults, drainage boundaries and an average reservoir permeability. On a smaller scale we can determine wellbore damage and whether the system is single or double porosity. Conventional geostatistical methods are unable to incorporate well test data. The support volume represented by a well test permeability needs to be determined as well as a procedure that relates the well test derived permeability to the distribution of small scale permeabilities within the reservoir.

The advantages of including well test data as part of the reservoir description are: (i) the well test data represent a measure of in-situ performance which is very difficult to obtain through core permeability measurements, and (ii) the scale over which the well test permeability is measured is much more representative of typical simulator grid blocks than the core measurements.

In our work we consider the transient (infinite-acting) period of a reservoir, during a drawdown test, i.e., production from a single well at a constant rate, in a heterogeneous reservoir, in which the permeability is distributed areally (x-y). Analysis of the simulated pressure vs. time data for an areally heterogeneous reservoir, is used along with the spatial statistics to describe the distribution of permeability heterogeneities.

Our analysis of the problem is presented by first addressing the forward problem. Recent developments in analytical solutions[1,2] for well testing in heterogeneous porous media are used. By using Oliver's[1] solution we are able to relate the instantaneous well test permeability derived from the pressure derivative data to an averaging technique for areally distributed grid block permeabilities within an inner and outer radii of investigation. Feitosa[2] presents an Inverse Solution Algorithm (ISA) that defines an equivalent radial permeability distribution from the pressure derivative data. We relate this permeability to an average of the grid block permeabilities within annular regions of the reservoir.

The averaging techniques for both methods are incorporated into the simulated annealing algorithm to develop alternate equiprobable reservoir descriptions that honor the imposed spatial statistics and the well test information.

By performing a numerical fluid flow drawdown simulation in the simulated permeability fields we are able to obtain a good and consistent reproduction of the pressure responses that compare favorably with the base case response. In contrast, the pressure responses of generated permeability fields that do not honor the well test constraint do not compare well with the base case responses.

We consider the effect of porosity heterogeneities on the pressure response and determine that for practical purposes the incorporation of porosity heterogeneities can be ignored when well test data is being honored.

In addition, the effect and incorporation of the pressure response due to anisotropy in a reservoir is studied. We were able to more effectively reproduce the pressure response by incorporating the well test and geostatistical information due to anisotropy in our reservoir description.

CHAPTER II

LITERATURE REVIEW

Prediction of properties in the earth sciences is inherently complex. The natural processes that have resulted in the formation of fluids in rock formations have occurred over millions of years. Due to the nature of the lithology, depositional and post-depositional environment rock formations are heterogeneous. The heterogeneities can be defined at a large scale, such as formation boundaries, or at a smaller scale, such as variations in porosity or permeability. When describing a reservoir it is important to account for the effect of scale or support volume of the source of information. Data are obtained from cores, logs, geological and geophysical information, well test analysis and production history interpretations. In using sampled information the volume over which a sample is measured has to be accounted for. For example, a permeability obtained from a core sample typically represents a volume in the order of 10^{-3} ft^3, whereas, an effective well test permeability may represent a volume in the order of 10^9 ft^3.

The conventional approach to reservoir description using geostatistics can readily accommodate the use of core and log data: specifically, permeability and porosity data. The statistics of the sample data can be defined and the support volume is a function of the size of the retrieved core or the depth of investigation of the logging instrument. Permeability values can be upscaled to represent grid blocks for the purpose of reservoir simulation studies, using the effective tensor method,[4] geometric mean,[5] and renormalization mean.[6] Porosity is upscaled using a simple arithmetic average.

First introduced in the mining industry,[7] geostatistical techniques, in recent years, have evolved and developed into practical tools for the purpose of the description of reservoir heterogeneities. Current state of the art in geostatistics not only enables us to capture the spatial variability of permeability and porosity, but also allows us to capture geologic features, such as sand bodies, shales, facies, and fractures.[8] Facies models and reservoir permeabilities and/or porosities can be simultaneously generated.[9,10] We will restrict our discussion to geostatistical techniques that describe heterogeneities in permeability and porosity, i.e., heterogeneities at smaller scale.

The geology of a reservoir determines the spatial continuity or correlation of reservoir properties. The spatial correlation and variability of a reservoir property is represented by the variogram (Figure 2.1). The variogram is determined experimentally from available data and is calculated by the following equation:[11]

$$\gamma(\vec{h}) = \frac{1}{2} E\left[\left[V(\vec{s}_i + \vec{h}) + V(\vec{s}_i)\right]^2\right], \tag{2.1}$$

where, $\vec{h}$ is the lag distance vector, $\vec{s}_i$ is the grid block location vector of the variable being modeled, V. The variogram is basically a measure of spatial continuity of a variable or property, i.e. the closer two values are spatially, the more closely their properites are related.

With the help of the variogram, kriging and conditional simulation methods are used to estimate the values of a property at unsampled locations. Kriging methods[11] provide a smooth image of the reservoir properties, whereas, stochastic conditional simulations[3,12-22] generate alternate equiprobable images which exhibit the variabilities representative of sampled data. For reservoir engineering applications, kriging methods have become less common and stochastic conditional simulation methods have become the industry norm.

Stochastic conditional simulation methods are used to generate possible descriptions of reservoir properties. The methods are stochastic since reservoir properties are

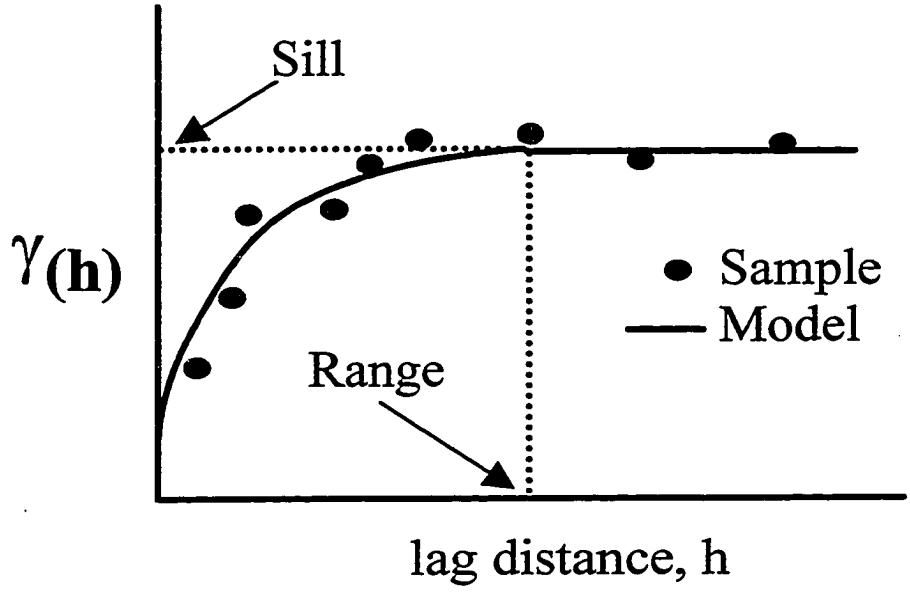

Figure 2.1 - Schematic of sample and model variograms.

represented by random variables; they are conditional since available data are honored at sampled locations; and the methods simulate several equiprobable distributions of a property in the reservoir. There are several conditional simulation techniques available in the literature. The methods range from Sequential Indicator Simulation (SIS),[12,13] Sequential Gaussian Simulation (SGS),[13] Fractal techniques,[14,15] Turning Bands Method (TBM),[16]and combinatorial optimization.[3,17-22]

In recent years, combinatorial optimization techniques for the purpose of reservoir description have become extremely popular as evidenced by the large number of studies performed and papers presented on this subject. Although these techniques are computationally demanding, the methods show promise in their robustness and flexibility to allow the incorporation of multiple constraints that can be imposed on a reservoir description when data is obtained from many sources. The methods are listed below with appropriate references for petroleum engineering applications:

- Genetic Algorithms[17,18]
- Simulated Annealing[3,19-21]
- Maximum A Posteriori (MAP)[22]
- Stochastic Hill Climbing[17]
- Neural Networks (applications are restricted to pattern recognition in well testing and log interpretations).[23]

Huang[17] and Sen et al.[18]studied and compared some of the combinatorial optimization methods for the purpose of reservoir description. This study will focus on the method of simulated annealing.

2.1 Simulated Annealing

Simulated annealing is an algorithmic approach to solving optimization problems and has its origins in the area of statistical mechanics.[24] As the name implies, simulated annealing simulates the physical process of annealing, i.e., a metal is cooled from a state of high temperature or energy to a lower temperature. The method for reservoir description was first proposed by Farmer.[19] The method was extended by others[3,19-21] to develop reservoir descriptions. A complete description of the simulated annealing algorithm is presented in Chapter IV.

2.2 Inverse Problems and Applications in Geostatistics

Inverse problems are described as a class of problems that define system parameters from physical observations. In reservoir engineering such types of problems include: estimation of interwell permeabilities and/or porosities from sample data (typical reservoir characterization problems) and interpretations of geophysical and production data that yield estimates of pertinent information, such as formation boundaries, large scale permeability, reservoir porosity,...etc.

Some authors[20,25,26] have solved the inverse problem of describing reservoir properties by honoring dynamic production data by coupling optimization techniques with conventional or simplified fluid flow simulators. Fasanino et al.[25] described a procedure for determining the permeability distribution by an inverse modeling technique. The initial reservoir description is developed using kriging.[11] Kriging generates one smoothed realization of a variable. An objective function based on a measured pressure distribution

is defined (this objective function is not the same as in annealing). The transmissibility, $\bar{k}_{wt}h$, values are iteratively modified until the method of steepest gradient descends to the smallest value of the objective function. An optimum value of $\bar{k}_{wt}h$ is specified at a few grid points until a good match between calculated and observed pressures is obtained. In this method the univariate and spatial statistics are not necessarily honored once a match has been obtained.

Long et al.[26] used an Iterated Function System(IFS) coupled with a finite element flow simulator to create fractal like distributions into a conductivity distribution to describe fracture networks in heterogeneous porous media. The IFS technique is an optimization technique similar to the method of simulated annealing. The inverse analysis optimizes IFS parameters such that flow performance from the simulation matches the observed performance.

Ouenes[20] presented an automatic history matching algorithm that simultaneously estimates relative permeability and capillary pressures for core floods using the optimization method of simulated annealing. The fully-implicit finite difference formulation of the one-dimensional diffusivity equation for multiphase flow is incorporated into the simulated annealing algorithm. A match of relative permeability and capillary pressure is obtained once the simulated results match observed cumulative production and pressure drop across the core, and breakthrough time. This application however is restricted to core floods and its extension to a reservoir study would be computationally expensive.

The three studies mentioned above show the promise of combinatorial algorithms as optimization techniques to generate reservoir properties that honor geostatistical as well as production constraints. However, these methods that couple optimization techniques with conventional numerical fluid flow simulators would require much improvement in current computational speed in order for them to become practical for full-field reservoir studies.

More recently, Hird[27] developed a conditional simulation method for reservoir description using spatial and well performance constraints. This method based on simulated annealing, does not require the use of a fluid flow simulator to solve the inverse problem. Functions defining the connectivity of a reservoir are based on the spatial arrangement of permeability. These static connectivity functions are correlated to production performance parameters, i.e., water oil ratios and water breakthrough times. The connectivity functions and the spatial statistics are then used as constraints to develop alternate reservoir descriptions. Thus dynamic production information about the reservoir is translated to quantifiable static information, which is used to solve the inverse problem of describing reservoir heterogeneities, more efficiently.

These inverse modeling techniques incorporate dynamic production data for describing reservoir properties and parameters. The pressure response during a well test is also a measure of dynamic properties of a reservoir. A dynamic property of the reservoir that most influences its performance is the permeability, and the distribution of permeability is a measure of the heterogeneity of the reservoir. In order to effectively incorporate well test information, the pressure response during a well test must be converted into equivalent static information.

2.3 Well Test Permeability

The effective radial permeability calculated by well test analysis is based on a classical analytical solution to the diffusivity equation. The solution for the infinite-acting or transient flow period can be written as:[28]

$$p_{wf} = p_i - \frac{162.6qB\mu}{\bar{k}_{wt}h}\left[\log t + \log\left(\frac{\bar{k}_{wt}}{\phi\mu c_t r_w^2}\right) - 3.2275 + .86859s\right], \qquad (2.2)$$

where the symbols used are standard and defined in the nomenclature. The slope (m) of the semilog straight line plot of pressure vs. time determines the well test permeability,

$$\bar{k}_{wt} = -162.6\frac{qB\mu}{mh}. \tag{2.3}$$

This solution is based on the assumption that the reservoir is homogeneous; however, no reservoir is homogeneous and the degree of heterogeneity is a function of the lithology, and depositional and post depositional environment of the reservoir. For practical purposes, it is assumed that the permeability determined by well test analysis is an effective permeability representing some *average* within a radius of investigation or drainage radius, which is influenced by the producing well. The classical definition of radius of influence is given by Van Poolen.[29] In physical terms it defines the radius over which all the reservoir properties have influenced the well flowing pressure.[30] It is given by the following equation:

$$r = A\sqrt{\frac{\bar{k}_{wt}t}{\phi\mu c_t}}. \tag{2.4}$$

Various authors have derived different values for the coefficient A. Lee[30] defines A to be 0.03248. As the time of the test increases more of the reservoir is influenced by the well and the radius of drainage increases. However, this definition of radius of drainage is questionable in the presence of heterogeneities.[31]

Well test derived permeabilities have been used by some authors for describing reservoirs using geostatistical techniques. De Costa e Silva[32] assumed that the well test permeability represents the permeability at the center of a grid block. Ben Rached[33] determined averages, between two arbitrary radii, of the distribution of permeability and thickness ($k_{wt}h$). He honored well test permeability by normalizing the log-derived average permeability to exactly match the permeability of the well test at the well. He did this to account for the support volume of a well test permeability.

2.4 The Radius of Investigation and the Averaging Process of a Well Test Permeability

In order to effectively incorporate well test data for the purpose of description of small scale permeability heterogeneities, one must first address the forward problem - what kind of average does the well test derived permeability represent and over what region of the reservoir is this average valid?

The reservoir permeability may be statistically distributed in a variety of ways[34] and the distribution may not necessarily be log normal. An understanding of the averaging process of layered permeabilities can be obtained from an analysis of flow through layered permeability fields.[34] For the case when bed layers are parallel to the direction of flow an arithmetic average of the permeabilities in the bed is a more appropriate average. For the case of layering in series with the beds perpendicular to the flow direction, a harmonic average is more representative. These conclusions are based on the assumption that the flow is steady state.

In the numerical simulation of a transient well test, the flow is not steady state and the arrangement of grid blocks does not necessarily produce flows in series or parallel relative to the arrangement of beds. It has been shown that the most probable behavior for an uncorrelated (i.e., spatial continuity between variables is not present) heterogeneous system approaches that of a homogeneous system with a permeability equal to the geometric mean of the individual permeabilities.[5]

Gómez-Hernández and Gorelick[35] observed that for small correlation lengths the effective permeability falls below the geometric average, and as the correlation length is increased the effective permeability approaches the harmonic average of the permeability distribution.

Recently, some authors[1,2,36,37,38] have investigated the concept of radius of investigation and the averaging process of small scale permeabilities within this radius as related to the well test permeability. The first is a stochastic approach to the problem, whereas the second is the analytical approach.

The stochastic approach is proposed by Alabert.[36] For stochastic conditioning, a permeability model must explicitly relate the test permeability to the distribution of smaller scale permeabilities. Alabert proposed guidelines to determine an optimum averaging of the distribution. A permeability field honoring some spatial and univariate statistics was developed and a drawdown test was numerically simulated in the permeability field. A single well test permeability was matched to a power average of permeabilities as circular volumes around the well were increased. The power average of the permeability is

$$\left[\bar{k}(\omega,A)\right]^{\omega} = \frac{1}{N(A)} \sum_{\bar{s}\in V(A)} k_{\bar{s}}^{\omega}, \tag{2.5}$$

where, A is similar to A defined in Equation 2.4. To eliminate boundary and wellbore effects he defines a minimum radius (r_{min}) at $t_D/r_D^2 = 120$ and a maximum radius (r_{max}) at $t_D/r_D^2 = 2500$. Alabert optimizes A to be a variable between 0.005 and 0.035. Therefore, as A varies r_{min} and r_{max} also vary defining an averaging volume $V(A)$. $\omega \in [-1,1]$, $N(A)$ is the number of grid blocks in $V(A)$ and $k_{\bar{s}}$ is the grid block permeability at location vector, $\bar{s}$. Optimum values of A and ω were determined by minimizing the mean normalized absolute difference, yielding an unbiased fit between the well test permeability and the power averaged permeability. The well test permeability was determined from the best fit slope of the semilog straight line of the pressure derivative data. For each permeability distribution an optimum A and ω were determined. Alabert also noted that as the heterogeneity of the reservoir increases ω also increases.

Deutsch and Journel[21] extended Alabert's work by incorporating his method into the simulated annealing algorithm. An optimum A and ω were determined such that the

permeability of the realization, $\bar{k}(\omega, A)$ matched the single well test permeability. The annealing algorithm was used to minimize the objective function, which includes the variogram and the power average of permeability honoring A and ω.

The analytical solutions for a heterogeneous reservoir begin by addressing the forward problem, e.g., for a well producing a single-phase fluid in an infinite acting reservoir, a mathematical solution of the diffusivity equation for heterogeneous reservoirs is presented. This is followed by tackling the inverse problem -- with the forward solution an areal or equivalent radial permeability distribution is determined.

Rosa and Horne[37] considered the pressure response at an observation well to cyclic flow rate variations at an active well. They formulated a mathematical model for the pressure behavior due to sinusoidal flow rates in reservoirs with continuously and smoothly varying radial permeability distributions. The Permeability in each zone of the equivalent reservoir was estimated by employing a non-linear regression procedure.

In this work we consider the mathematical solutions presented by Oliver[1,38] and Feitosa.[2] The analytical solutions are based on the following assumptions:

- constant rate production,
- uniformly thick reservoir with closed upper and lower boundaries,
- areally infinite reservoir,
- negligible well bore storage and skin effect,
- constant porosity, thickness and rock compressibility,
- single phase fluid with constant viscosity and compressibility,
- uniform initial pressure through the reservoir,
- negligible gravity and capillary pressure effects,
- fully penetrating well, and
- rock and fluid properties independent of pressure.

The governing equations describing the forward problem of the pressure response in an areally heterogeneous reservoir producing a slightly compressible fluid through a single well are given by the following[2] Initial Boundary Value Problem:

$$\frac{1}{r_D}\frac{\partial}{\partial r_D}\left[r_D k_D(r_D,\theta)\frac{\partial p_D}{\partial r_D}\right]+\frac{1}{r_D^2}\frac{\partial}{\partial \theta}\left[k_D(r_D,\theta)\frac{\partial p_D}{\partial \theta}\right]=\frac{\partial p_D}{\partial t_D}, \tag{2.6}$$

$$\left[p_D(r_D,\theta,t_D=0)\right]=0, \tag{2.7}$$

$$\frac{1}{2\pi}\left[\int_0^{2\pi} k_D(r_D,\theta) r_D \frac{\partial p_D}{\partial r_D} d\theta\right]_{r_D=1}=-1, \tag{2.8}$$

$$\left[\frac{\partial p_D}{\partial \theta}\right]_{r_D=1}=0, \tag{2.9}$$

$$\lim_{r_D\to\infty} p_D(r_D,\theta,t_D)=0, \tag{2.10}$$

$$p_D(r_D,\theta=0,t_D)=p_D(r_D,\theta=2\pi,t_D), \tag{2.11}$$

$$\left[\frac{\partial p_D}{\partial \theta}\right]_{\theta=0}=\left[\frac{\partial p_D}{\partial \theta}\right]_{\theta=2\pi}, \tag{2.12}$$

where the dimensionless terms are defined as:

dimensionless radius, r_D:

$$r_D = \frac{r}{r_w}, \tag{2.13}$$

dimensionless time, t_D:

$$t_D = \frac{0.006328 k_{ref} t}{\phi \mu c_t r_w^2}, \tag{2.14}$$

dimensionless pressure drop, p_D:

$$p_D = \frac{k_{ref} h}{141.2 q B \mu}\left[p_i - p(r,\theta,t)\right], \tag{2.15}$$

and

$$k_D = \frac{k(r,\theta)}{k_{ref}}, \tag{2.16}$$

where the time is measured in days and k_{ref} is an arbitrary reference value of permeability.

Oliver[1,38] investigated the averaging process of permeability variations in r and θ coordinates. He solved the diffusion equation for the pressure response of a well situated in an infinite reservoir where permeability is an arbitrary function of position, he assumed small permeability variations about some mean. Some type of averaging is inherently present when an effective permeability is determined from the slope of the semilog plot; therefore, the *averaged permeability* of the small scale permeabilities within the area of investigation is determined from the slope of the semilog plot at any instant. Oliver's solution only allows for small variations about a mean value since the overall solution is determined by a first order perturbation technique to the generalized problem. Neglecting wellbore storage and skin, the dimensionless pressure derivative for a heterogeneous reservoir is given in a dimensionless form by:

$$p'_{wD}(t_d) = \frac{\partial\, p_D}{\partial \ln t_D} = \frac{1}{2} - \frac{\varepsilon}{2\pi}\int_1^{\infty} K(\xi, t_D) \int_{-\pi}^{+\pi} f(\xi,\theta) d\theta\ d\xi, \tag{2.17}$$

where, $\varepsilon f(\xi,\theta)$ is the permeability distribution function for small variations in permeability and can be written as $\left(1 - k_{ref} / k(r,\theta)\right)$. For an equivalent purely radial system Equation 2.17 is written as:[2]

$$p'_{wD} = \frac{\partial p_D}{\partial \ln t_D} = \frac{1}{2} - \int_1^{\infty} K(r_D, t_D)\left(\frac{1}{2\pi}\int_{-\pi}^{+\pi}\left[1 - \frac{1}{k_D(r_D,\theta)}\right] d\theta\right) dr_D. \tag{2.18}$$

Note that for a homogeneous reservoir $k_D(r_D,\theta) = 1$, and Equation 2.18 gives the dimensionless pressure derivative for a homogeneous reservoir, i.e., $p'_{wD} = \frac{1}{2}$. It can be shown that the integral over θ is a normalized form of the harmonic average of permeabilities over θ. $K(r_D, t_D)$ is the weighting or kernel function and is given by:

$$\sqrt{t_D} K(r_D, t_D) = 0.5\sqrt{\frac{\pi r_D^2}{t_D}} \exp\left(-\frac{r_D^2}{2t_D}\right) W_{1/2,1/2}\left(\frac{r_D^2}{t_D}\right), \tag{2.19}$$

Equation 2.19 is valid for dimensionless times greater then 100. For further details on this solution see Reference 1. Of more importance, is the physical significance of the weighting function. The shape of this function (Figure 2.2) is used to determine the area of investigation. The inner and outer radii of the area of investigation are defined as the minimum and maximum radii at which the weighting function becomes so small that the permeabilities outside the region do not contribute to the slope of the semilog plot. A normalized plot of the weighting function (Figure 2.2) shows that 98 % of the contribution of the weighting function comes from the area encompassed by the dimensionless radii of $r_D = 0.12\sqrt{t_D}$ and $2.34\sqrt{t_D}$. Thus, the kernel function gives the weighted average of the well test permeability within these radii. Oliver claims that by using the appropriate weighting function, the average radial permeability can be estimated and that the area under the curve is a measure of the cumulative contribution to the permeability estimate.

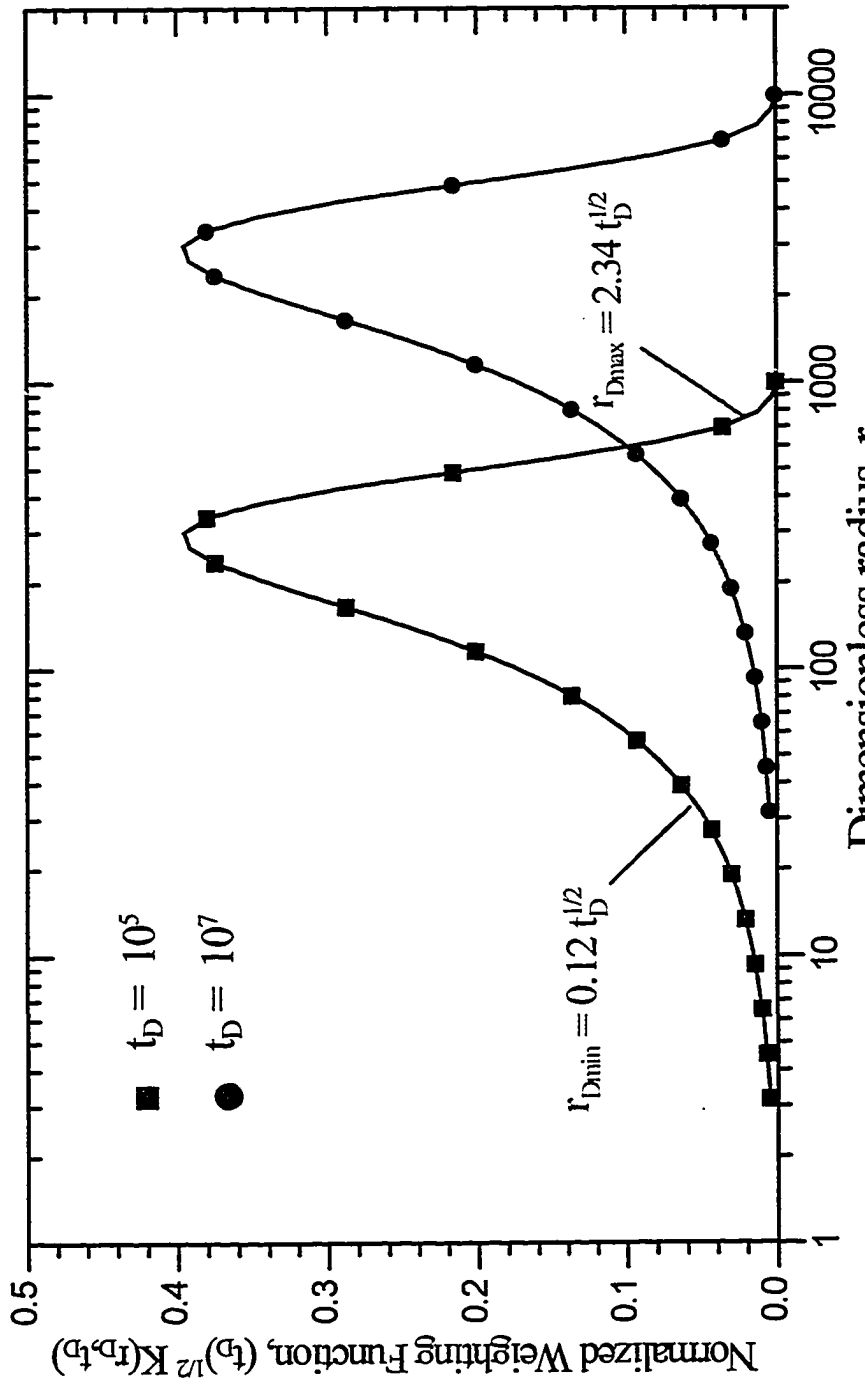

Figure 2.2 - Weighting or kernel function defining the radii of investigation , after Oliver.[1]

Feitosa[2] extended Oliver's solution and developed an Inverse Solution Algorithm (ISA) to estimate the equivalent radial permeability distribution as a function of distance from the well. The ISA algorithm has the advantage over Oliver's solution in that it can be applied to large radial variations in permeability. Instead of using a reference permeability, k_{ref}, to define the dimensionless time, t_D, it is defined in terms of an instantaneous permeability determined from instantaneous pressure derivative:

$$\hat{t}_D = \frac{0.006328\hat{k}t}{\phi\mu c_t r_w^2}, \tag{2.20}$$

where,

$$\Delta p_w' = \frac{\partial \Delta p_w}{\partial \ln t}, \tag{2.21}$$

and

$$\hat{k} = \frac{1}{2}\left[\frac{141.2qB\mu}{h\Delta p_w'}\right]. \tag{2.22}$$

ISA sequentially determines the equivalent radial permeability distribution for each zone using the following relationships:

$$\Delta\left(\frac{1}{k_{ISAn}}\right) = \frac{\frac{1}{\hat{k}_n} - \frac{1}{k_{ISAn-1}} + \sum_{i=2}^{n-1}\left[\Delta\left(\frac{1}{k_i}\right)\int_{\hat{z}_{0D}}^{\hat{z}_{i-1D}}\Omega(\hat{z}_D)d\hat{z}_D\right]}{1 - \int_{\hat{z}_{0D}}^{\hat{z}_{n-1D}}\Omega(\hat{z}_D)d\hat{z}_D}, \tag{2.23}$$

where,

$$\hat{z}_{0D} = \min\left\{\frac{1}{\sqrt{\hat{t}_D}}, 0.12\right\}, \tag{2.24}$$

$$\Omega\hat{z}_D = \sqrt{\pi}\ \ \hat{z}_D \exp\left(-\frac{\hat{z}_D^2}{2}\right) W_{\frac{1}{2},\frac{1}{2}}\left(\hat{z}_D^2\right), \tag{2.25}$$

$$\hat{z}_{0D} = \frac{1}{\sqrt{\hat{t}_D}}, \tag{2.26}$$

and

$$\hat{z}_{jD} = \frac{r_{jD}}{\sqrt{\hat{t}_D}}. \tag{2.27}$$

Once $\Delta(1/k_{ISAn})$ is calculated the permeability at zone n is determined by:

$$k_{ISAn} = \frac{1}{\frac{1}{k_{ISAn-1}} + \Delta\left(\frac{1}{k_{ISAn}}\right)}. \tag{2.28}$$

Comparisons of simulation results using the calculated radial permeability distribution and actual permeability distribution have resulted in excellent agreement between computed pressures, pressure derivatives, and permeability distributions.

Feitosa also presented analysis of the solution to areally heterogeneous reservoirs, where permeability varies in (r,θ) and (x,y). He analyzed the pressure derivatives of such distributions and determined equivalent radial permeability distributions that honor the original pressure behavior of the reservoir during a well test.

CHAPTER III

THE FORWARD PROBLEM - PERMEABILITY AVERAGE AND THE RADIUS OF INVESTIGATION

In this chapter we investigate the forward problem: from the pressure data for a single well producing in an areally heterogeneous reservoir during a drawdown test, can we determine the area of investigation and the type of permeability average represented within this area?

Two methods are investigated: Oliver's[1] solution and the Inverse Solution Algorithm (ISA) presented by Feitosa.[2]

3.1 The Base Case

The first step is to generate synthetic permeability distributions and numerically simulate pressure drawdown tests. We assume that these distributions and pressure responses are the *truth* or *base* cases. A two dimensional permeability field is generated using the Turning Bands Method (TBM).[16,39] TBM generates an unconditional correlated distribution. The distribution is unconditional since there are no available data at grid blocks that must be honored. The specified univariate and spatial statistics of the distribution are honored. For simplicity a square reservoir with square grid blocks is considered. An example of a permeability field generated using this method is shown as a greyscale map in Figure 3.1. In order to draw general conclusions, we generate numerous

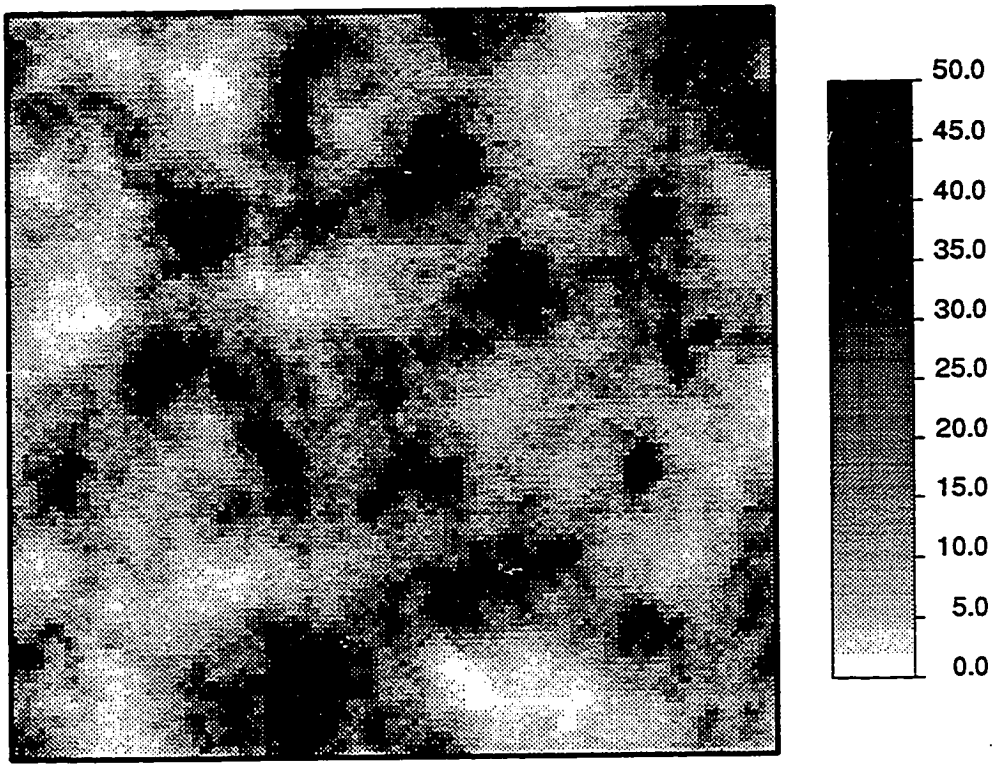

Figure 3.1 - Base case permeability distribution generated by Turning Bands (range = 600 ft, $\sigma^2_{\ln k} = 0.92$, mean = 20md).

base cases with varying degrees of heterogeneity. A summary of the univariate and spatial statistics of the generated distributions is given in Table 3.1. Using this permeability field, a numerical fluid flow simulation of a drawdown is performed on the reservoir. It is assumed that all other reservoir properties are constant and only the distribution of permeabilities is varied. The reservoir properties are given in Table 3.2.

A well producing at a constant rate is placed at the center of the grid block at the center of the reservoir. A finite difference numerical fluid flow simulation of the reservoir is performed using ECL 100,[40] a commercial reservoir simulation package. ECL 100 corrects grid block pressures to well flowing pressures using Peaceman's approximation.[41] We perform a validation run of the ECL 100 simulator. Using the reservoir parameters given in Table 3.2 and assuming a homogeneous reservoir, with k = 20 md, the numerical solution is compared to the analytical solution[28] for a square reservoir. The results, as illustrated in Figure 3.2, are satisfactory.

The pressure and pressure derivative responses for the permeability field shown in Figure 3.1 are shown in Figure 3.3. To draw general conclusions, numerous base cases are investigated. Our objective, here, is to generate a reservoir description such that the univariate and spatial statistics, and the simulated pressures and pressure derivatives are reproduced to match the base case study.

It should be noted the fluid flow simulator, ECL 100, is a finite-difference simulator and performs a harmonic average of the permeabilities at the grid block boundaries.[40] The harmonic average in the x-direction is:

$$k_{x_{i+1/2}} = \frac{x_{i+1} - x_i}{\frac{x_{i+1} - x_{i+1/2}}{k_{x_{i+1}}} + \frac{x_{i+1/2} - x_i}{k_{x_i}}}, \qquad (3.1)$$

The harmonic average in the y-direction is:

Table 3.1 - Summary of comparison for different permeability averaging techniques using Oliver's solution. The permeability derived from the best fit semi-log straight line is used to calculate t_D.

Turning Bands input parameters, μ_k = 20 md			Measures of heterogeneity		Relative error			Absolute relative error		
seed	σ^2_{lnk}	Range ft	HI	V	err($\bar{k}_{he}$)	err($\bar{k}_{ge}$)	err($\bar{k}_{ae}$)	aerr($\bar{k}_{he}$)	aerr($\bar{k}_{ge}$)	aerr($\bar{k}_{ae}$)
-15	0.4	2000	0.0795	0.33	-0.09036	-0.31868	-0.54748	0.513138	0.392082	0.547485
-4	0.25	3200	0.0497	0.22	-0.43524	-0.45448	-0.47404	0.435235	0.454482	0.474038
-3	0.5	2000	0.1242	0.39	0.222823	-0.74244	-1.80654	0.723932	0.742444	1.806539
-10	0.5	500	0.0311	0.39	1.18261	0.133535	-0.99903	1.272835	0.788592	1.225603
-22	0.92	595.41	0.1242	0.6	2.475823	0.057403	-2.89076	3.141266	1.3344	1.418949
-20	0.92	2143.84	0.4472	0.6	-0.3347	-0.4562	-0.57784	0.511436	0.542633	0.601231
-18	0.92	958.78	0.2	0.6	0.326066	-0.16675	-0.66303	0.61267	0.466313	0.697861
-16	0.92	1072	0.2236	0.6	5.276271	1.74461	-2.74124	5.366854	1.999967	2.741241
-12	0.75	1250	0.1747	0.53	3.799674	1.607549	-0.95948	3.955623	1.855726	1.272401
-11	0.75	3200	0.4472	0.53	-0.09421	-0.38604	-0.72328	0.269079	0.386039	0.723275
-7	0.75	1600	0.2236	0.53	0.666887	-0.05145	-0.74134	0.870897	0.250329	0.741335
-8	0.75	2000	0.2795	0.53	4.258866	1.719957	-1.07827	4.56714	2.142425	1.079453
-9	0.75	1000	0.1398	0.53	3.157713	0.543653	-2.01837	3.65774	2.508632	2.0854
-26	1.2	1241.69	0.4472	0.7	10.85558	3.762324	-6.27113	11.14859	4.272174	6.271128
-25	1.2	555.32	0.2	0.7	1.794496	-0.48399	-3.86832	2.291219	0.654822	3.868322
-24	1.2	220.74	0.0795	0.7	2.587599	-0.44731	-6.67754	2.690726	0.727924	6.677539
-23	1.61	193	0.1242	0.8	3.260873	-0.42692	-10.373	3.286525	0.554495	10.37296
-21	1.61	694.93	0.4472	0.8	1.478112	-0.3463	-4.50955	1.705823	0.368285	4.509553
-19	1.61	310.8	0.2	0.8	3.392921	0.70958	-4.32311	3.392921	0.719254	4.323115
-17	1.61	347.5	0.2236	0.8	1.533938	-0.00949	-4.29839	1.662844	0.493295	4.29839
Cumulative errors					2.174269	0.242667	-2.93269	2.508204	1.020205	4.194824

where,

Seed = turning bands seed number

σ^2_{lnk} =standard devation on a log normal scale

μ_k= mean permeaility

HI = Heterogeneity Index = $(\sigma^2_{lnk} range/\Delta x \times N_Y)$ (Ref. 45)

V = Dykstra Parsons Coefficient = $1-1/\exp(\sigma^2_{lnk})$ (Ref. 46)

Table 3.2 - Reservoir Properties

Number of grid blocks (x,y,z)	115x115x1
Block dimensions ($\Delta x, \Delta y, \Delta z$)	35*ft* x 35*ft* x 10*ft*
Porosity	0.3
Wellbore radius	0.5 *ft*
Total compressibility	4.9×10^{-7} psi^{-1}
Oil formation volume factor	1.2 *bbl/STB*
Oil viscosity	0.4 *cp*
Oil rate	106.3 *STB/D*
Initial pressure	2000 *psia*
No flow upper and lower boundaries	
Negligible well bore storage and skin	
Negligible gravity and capillary effects	
Fully penetrating well	

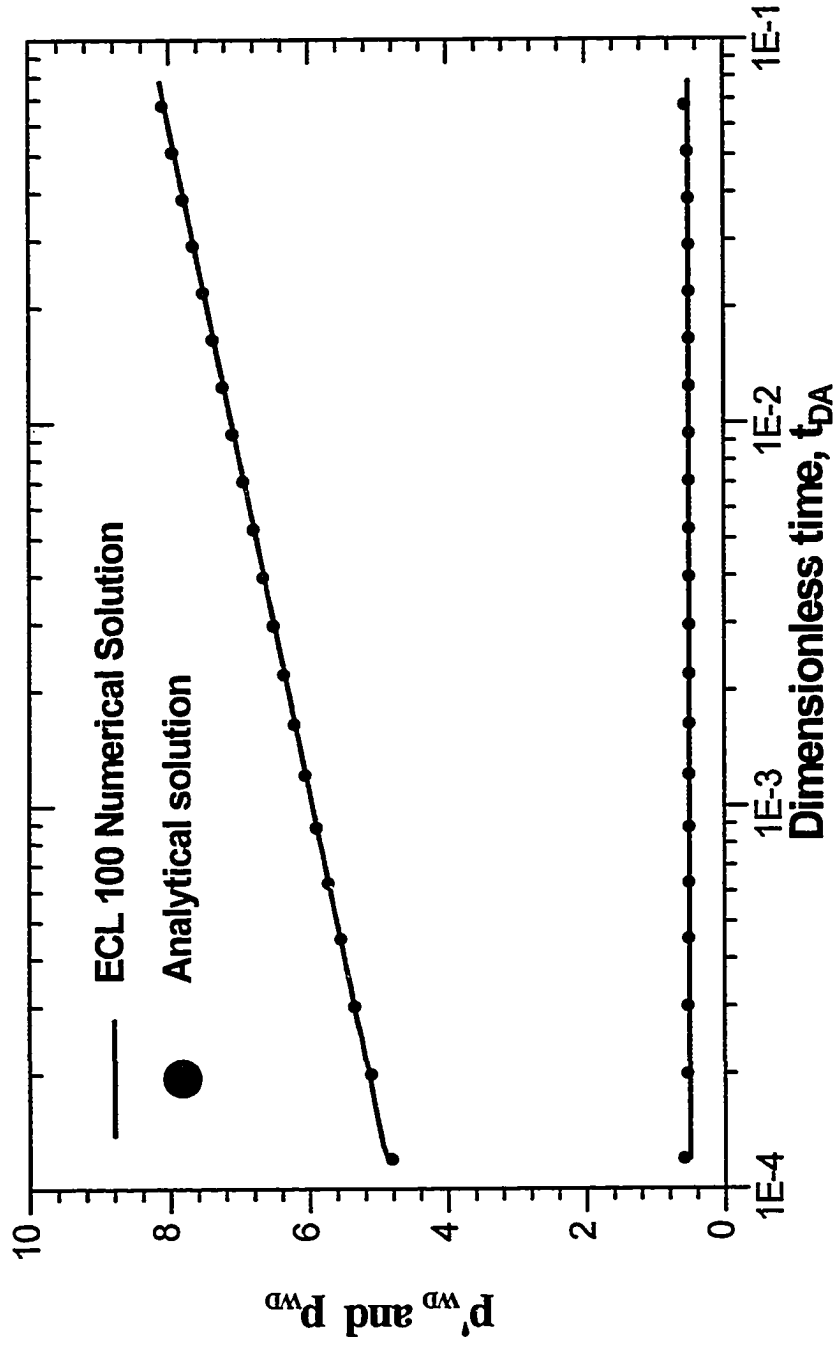

Figure 3.2 - Comparison between the analytical and numerical[29] drawdown solutions showing the dimensionless pressure and pressure derivative for a homogeneous reservoir.

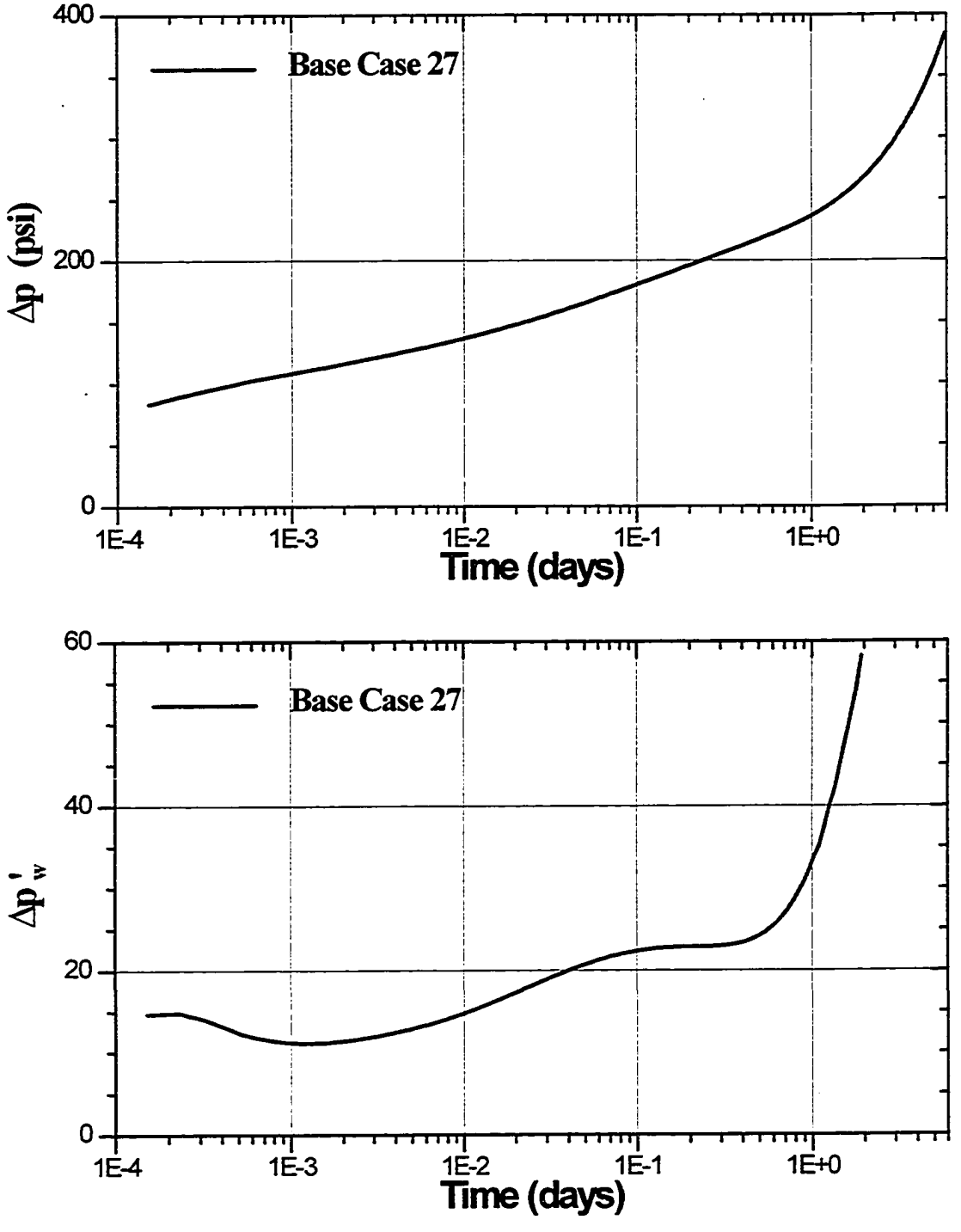

Figure 3.3 - Pressure and pressure derivative response for the permeability field shown in Figure 3.1.

$$k_{y_{j+1/2}} = \frac{y_{j+1} - y_j}{\frac{y_{j+1} - y_{j+1/2}}{k_{y_{j+1}}} + \frac{y_{j+1/2} - y_j}{k_{y_j}}}, \tag{3.2}$$

where, the nomenclature for the finite difference approximation is clearly illustrated in Figure 3.4. This calculation is correct and valid for a homogenous system with a constant permeability as evidenced by the results in Figure 3.2. However, harmonic averaging of grid blocks may not be appropriate for transient flow in a heterogeneous reservoir. Feitosa[2] showed, by example, that harmonic averaging of grid block boundaries, for single-phase transient flow in a heterogeneous reservoir, does not produce erroneous results. By comparing his finite difference radial flow simulation results to analytical solutions for radial-composite reservoirs, he showed that simulation results matched the analytical solution. The two dimensional problem in *x-y* coordinates is more complex, for which no analytical solution for permeability heterogeneity exists to show the validity of a finite difference simulation that performs harmonic averaging across the grid block boundaries. So, for this study we assume that the results given by the fluid flow simulator, that performs harmonic averaging across grid block boundaries, to be correct.

3.2 The Radius of Investigation and Averaging Process of Permeabilities

To effectively use a well test derived permeability in a stochastic conditional simulation method, the well test permeability must impose a deterministic constraint on the distribution of surrounding small scale permeabilities within the area of investigation. Therefore, an averaging model that defines the permeability distribution within the annulus of investigation has to be developed. The pressure behavior of the truth cases for varying degrees of permeability heterogeneity are used along with the analytical solutions

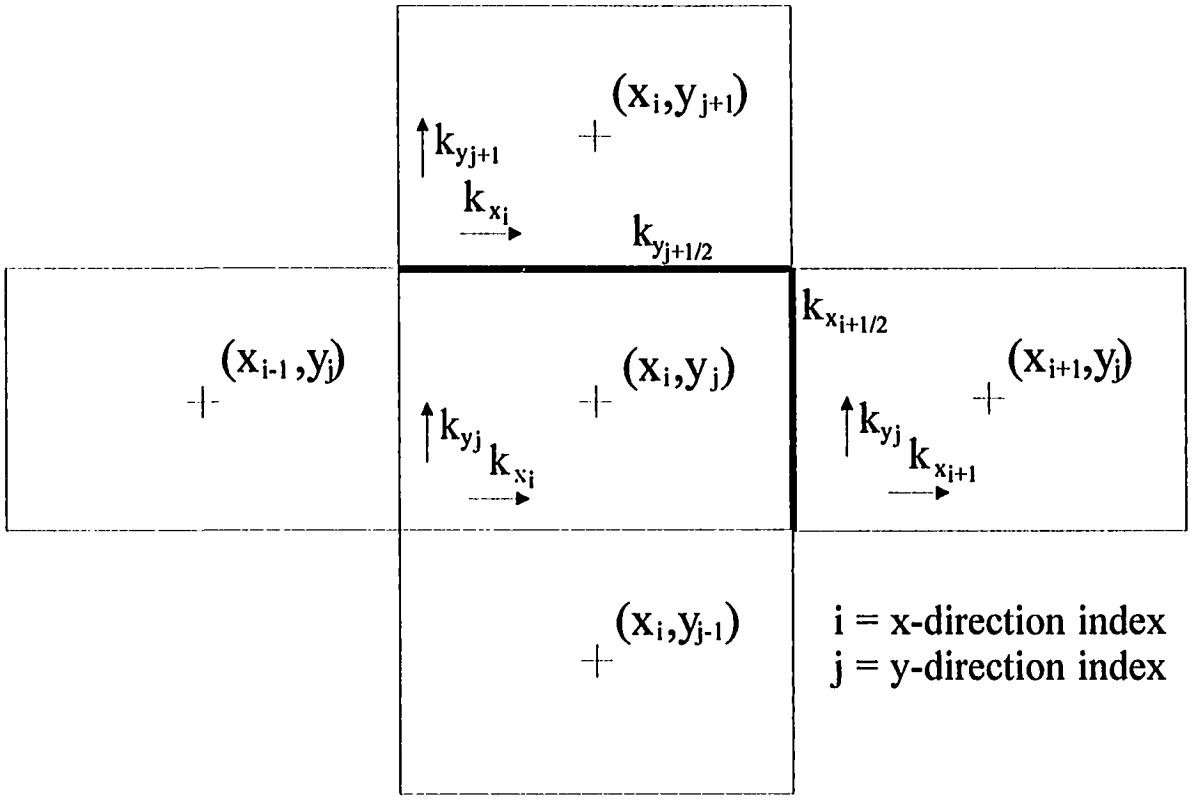

Figure 3.4 - Illustration of the nomenclature for block centered harmonic average for areal(x-y) finite difference flow simulator.

proposed by Oliver[1] and Feitosa[2] to determine the averaging process and the region of investigation.

3.2.1 Oliver's Solution

Equation 2.18[2] is the pressure derivative solution for a heterogeneous reservoir and is rewritten for convenience:

$$p'_{wD} = \frac{\partial p_D}{\partial \ln t_D} = \frac{1}{2} - \int_1^{\infty} K(r_D, t_D)\left(\frac{1}{2\pi}\int_{-\pi}^{+\pi}\left[1 - \frac{1}{k_D(r_D,\theta)}\right]d\theta\right)dr_D, \tag{3.3}$$

For our investigation, we consider only the transient flow period of the well test, for which this solution is valid, and analyze the appropriate pressure versus time data.

The annulus of investigation is the region where the kernel function is non-negligible. The kernel function (Equation 2.19) is:

$$K(r_D, t_D) = \frac{\sqrt{\pi} r_D}{2t_D}\exp\left(-\frac{r_D^2}{2t_D}\right)W_{1/2,1/2}\left(\frac{r_D^2}{t_D}\right), \tag{3.4}$$

where, $W_{1/2,1/2}$ is the Whittaker's function defined in Reference 42.

We define $k_D(r_D)$ as a dimensionless permeability, with variation in r_D:

$$k_D(r_D) = \frac{\bar{k}(r_D)}{k_{ref}}, \tag{3.5}$$

where k_{ref} is an *arbitrary average* permeability and $\bar{k}(r_D)$ is a harmonic average of permeabilities in the θ-direction. Equation 3.3 can, therefore, be written as:

$$p'_{wD} = \frac{1}{2} - \int_1^{\infty} K(r_D, t_D)\left(1 - \frac{1}{k_D(r_D)}\right) dr_D. \tag{3.6}$$

Numerical[2] and theoretical[43] analysis of the kernel function has shown that:

$$\int_1^{\infty} K(r_D, t_D) dr_D = \frac{1}{2}. \tag{3.7}$$

Substituting Equation 3.7 into 3.6, yields:

$$p'_{wD} = \int_1^{\infty} K(r_D, t_D)\left(\frac{1}{k_D(r_D)}\right) dr_D. \tag{3.8}$$

Recalling the equation (Eq. 2.22) for the instantaneous permeability, $\hat{k}$:

$$\hat{k} = \frac{1}{2}\left(\frac{141.2qB\mu}{h\Delta p'_w}\right), \tag{3.9}$$

where the instantaneous pressure derivative is:

$$\Delta p'_w = \frac{\partial \Delta p_w}{\partial \ln t} \tag{3.10}$$

and

$$\Delta p_w = p_i - p_{wf}. \tag{3.11}$$

Note p'_{wD} can also be expressed as:

$$p'_{wD} = \frac{k_{ref} h \Delta p'_w}{141.2qB\mu}. \tag{3.12}$$

Substituting Equations 3.5, 3.10 and 3.12 into Equation 3.8 gives:

$$\frac{1}{2\hat{k}} = \int_1^{\infty} K(r_D, t_D)\left(\frac{1}{\bar{k}(r_D)}\right) dr_D. \tag{3.13}$$

The above result is given in Feitosa's[2] dissertation.

For a radial reservoir, with N_r concentric annular divisions such that the "θ-averaged" radial permeability in the annulus at r_j is $\overline{k_j}$, Equation 3.13 can be represented by:

$$\frac{1}{2\hat{k}} = \sum_{j=2}^{N_r} \frac{1}{\overline{k_j}(r_{Dj})} \int_{r_{Dj-1}}^{r_{Dj}} K(r_D, t_D) dr_D, \quad \text{for } j = 1,2,.....N_r. \tag{3.14}$$

Equation 3.14 is equivalently written as:

$$\frac{1}{2\hat{k}} = \sum_{j=2}^{N_r} \frac{1}{\overline{k_j}(r_{Dj})} \frac{\int_{r_{Dj-1}}^{r_{Dj}} K(r_D, t_D) dr_D}{\int_1^{\infty} K(r_D, t_D) dr_D} \int_1^{\infty} K(r_D, t_D) dr_D. \tag{3.15}$$

Recalling Equation 3.7 and substituting it into the above equation yields:

$$\frac{1}{\hat{k}} = \sum_{j=2}^{N_r} \left[\frac{\int_{r_{Dj-1}}^{r_{Dj}} K(r_D, t_D) dr_D}{\int_1^{\infty} K(r_D, t_D) dr_D} \right] \frac{1}{\overline{k_j}(r_{Dj})}. \tag{3.16}$$

Equation 3.16 is important and fundamental to the preceding work: it explicitly relates the instantaneous permeability, $\hat{k}$, to the kernel function and a radially distributed arbitrary permeability average in the theta-direction. The equation implies that the area under the kernel function represents the weight applied to each of the permeability averages in the annular regions $(r_{j-1} \rightarrow r_j)$, and weighted harmonic average of the effective radial permeability averages is a measure of the cumulative contribution to the instantaneous well test permeability, $\hat{k}$.

3.2.1.1 Application of Oliver's Solution to an Areally (x-y) Heterogeneous Reservoir

In this section, we consider the application of Oliver's solution (in specific Equation 3.16) to an areally (x-y) heterogeneous reservoir. A method that discretizes Equation 3.16 and applies the radial solution to an equivalent areal(x-y) reservoir is presented.

For a dimensionless time, t_D, the kernel function is non-negligible between the dimensionless radii, $r_D = 0.12\sqrt{t_D}$ and $2.34\sqrt{t_D}$, where,

$$t_D = 2.637\times10^{-4}\frac{\bar{k}_{wt}t}{\phi\mu c_t r_w^2}, \tag{3.17}$$

and $\bar{k}_{wt}$ is the permeability calculated from the best fit semilog straight line equation (Eq. 2.3).

In order to discretize Oliver's solution, the reservoir is divided into annular rings defined by Coats'[44] grid:

$$r_j = \alpha^j r_o, \qquad j = 1,2,.....,N_r \tag{3.18}$$

where, $r_o = \frac{r_w \ln\alpha}{(\alpha-1)}$, $\alpha = (r_e/r_w)^{1/N_r}$ and $r_e = \min\left(\frac{\Delta x\times N_X}{2}, \frac{\Delta y\times N_Y}{2}\right)$.

For our study we assumed N_r, to be 50.

It should be noted that for a heterogeneous reservoir, there is no clear transition between the transient and pseudo-steady state flow period. Heterogeneous systems exhibit permeability streaks. The resulting fluid flow through the reservoir causes one or more of the boundaries that are closer to high permeability streaks, to be felt sooner than others. This would be especially evident in anisotropic permeability fields. The equipotential lines are not circular as they are in homogeneous reservoir. Anisotropic fields are investigated in Chapter V. For the isotropic case studies looked at in this chapter, we assume that transient flow ends when for a given flow period (time), the maximum radius of

investigation defined by Oliver's solution, $r_{D\max}$, is approximately equal to the outer radius, r_e, of the reservoir, i.e., the end of the transient period is defined by:

$$r_{D\max} = 2.34\sqrt{t_D} \le \frac{r_e}{r_w}, \tag{3.19}$$

At each time value, an annulus of investigation is defined based on the non negligible region of the kernel function.[1] Since the reservoir annular rings have been pre-defined by Coats' grid, we define the minimum and maximum radii for the annulus of investigation at each t_D by the following criteria:

$$\begin{aligned} r_{D\min} &= r_{Dj-1}, \quad r_{Dj-1} \le 0.12\sqrt{t_D} < r_{Dj} \\ r_{D\max} &= r_{Dj}, \quad r_{Dj-1} < 2.34\sqrt{t_D} \le r_{Dj}. \end{aligned} \tag{3.20}$$

Note that since the kernel function is negligible at $r_D < 0.12\sqrt{t_D}$, it must also be negligible at the Coats radius r_{Dj}. A similar argument is valid for the upper limit. A numerical integration of the kernel function using Simpson's rule[47] gives the area under the curve between $r_{D\min}$ and $r_{D\max}$. The weight of each annular region is given by:

$$w_j = \frac{\int_{r_{j-1}}^{r_j} K(r_D, t_D)}{\int_{r_{D\min}}^{r_{D\max}} K(r_D, t_D)}, \quad \text{for } j = j_{\min}, j_{\min+1}, \ldots j_{\max} \tag{3.21}$$

where, $r_{j\min}$ and $r_{j\max}$ correspond to the minimum and maximum radii defined by Equation 3.20.

A single well draining a reservoir imposes radial flow and consequently a radial solution to this problem. Permeability or reservoir properties, however, are not distributed radially but areally (x-y). Thus we must impose the radial solution on an areal permeability distribution. We need to first evaluate the correct type of averaging of grid block permeabilities within the annular rings. Note that in Oliver's solution this averaging is

harmonic. In our work we test alternate averaging methods for grid block permeabilities in the θ-direction.

An area based power averaging scheme is considered. It accounts for segments of grid blocks that only partially lie within the annulus under consideration. The equation to calculate this average permeability, $\bar{k}$, is:

$$(\bar{k}A_r)^{\omega} = \sum_{\bar{s}\in A_r} (k_{\bar{s}}A_{\bar{s}})^{\omega}, \tag{3.22}$$

where, $\bar{s}$ is the location vector of the grid block, A_r is the radial area between the r_{j-1} and r_j interval and $A_{\bar{s}}$ is the area of the grid block that falls in between these radii. The procedure used to calculate the area of such a grid block is given in Appendix A. The nomenclature is clearly illustrated in Figure 3.5. For $\omega = 1$ the arithmetic average is calculated and when $\omega = -1$ the harmonic average, i.e., the average suggested by Oliver's solution, is calculated. However, when $\omega = 0$ the geometric average cannot be calculated by Equation 3.22; instead, the following area- based geometric averaging equation is used:

$$A_r \ln \bar{k}_g = \sum_{\bar{s}\in A_r} A_{\bar{s}} \ln k_{\bar{s}}. \tag{3.23}$$

Note that if the grid block permeability, $k_{\bar{s}}$, is 0 the permeability average cannot be defined; therefore, we constrain our distribution such that permeability values are greater than 0. Equation 3.16 shows that the instantaneous permeability, $\hat{k}$, can be represented by an integral of the inverse of the radial permeability distribution within the annulus of investigation, i.e., a harmonic average of the θ-averaged radial permeability average within an annular region weighted by the function defined in Equation 3.21. In order to represent the discrete form of Equation 3.16, for an areal (x-y) heterogeneous reservoir, the instantaneous permeability, $\hat{k}$, is replaced by the equivalent permeability, $\bar{k}_e$. Therefore, the discrete form of Equation 3.16 is written as:

$$\frac{1}{\bar{k}_e} = \sum_{j=1}^{N_r} w_j \frac{1}{\bar{k}_j}. \tag{3.24}$$

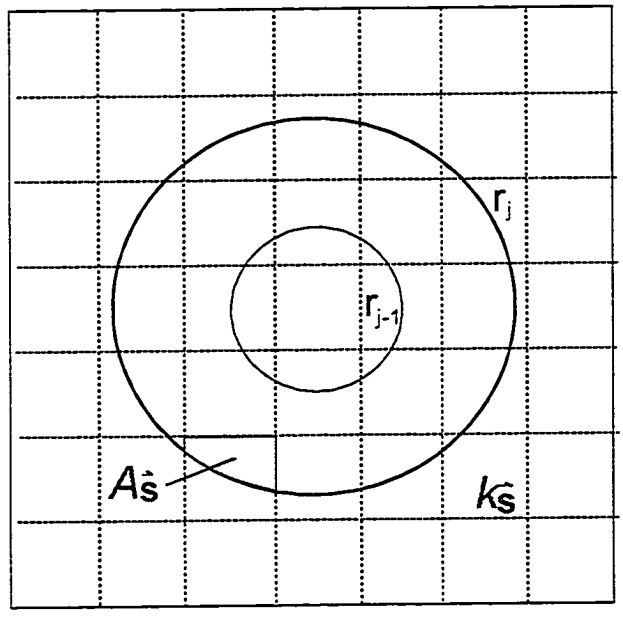

Figure 3.5 - Illustration of the nomenclature used to calculate the area based power average of grid block permeabilities in annular rings.

3.2.1.2 Numerical Experiments to Determine the Best Averaging Technique in the θ-Direction for Oliver's Solution

In Oliver's solution the averaging process in the theta direction is defined as a harmonic mean for small permeability variations about a base value. This is done so that the perturbation theory technique facilitates a solution to the generalized problem (Equations 2.6-2.12). However, in the areal permeability distributions, permeability is log normally distributed with varying degrees of heterogeneity and does *not* vary slightly about a base value. We, therefore, investigate different averaging techniques in the θ-direction using Equations 3.22 or 3.23. The instantaneous well test permeability, $\hat{k}$, (Eq. 3.10) is compared to the equivalent permeability, $\bar{k}_e$, (Eq. 3.24). Numerical experiments on the synthetic permeability distribution and pressure data have shown that a geometric average of grid block permeabilities in the theta direction, followed by a harmonic average, weighted by the kernel function, in the radial direction give a good approximation of $\hat{k}$. Figures 3.6, 3.7, and 3.8 show the comparisons between harmonic, geometric, and arithmetic averaging methods in the theta direction to the instantaneous well test permeability, respectively. The results are summarized in Table 3.1. The errors are defined as:

$$err(\bar{k}_{he}) = \frac{1}{N_t}\sum_{i=1}^{N_t} \bar{k}_{he_i} - \hat{k}_i, \tag{3.25}$$

where $\bar{k}_{he}$ is the equivalent permeability calculated by averaging harmonically in the θ-direction (Eq. 3.22) and harmonically in the radial direction (Eq. 3.24).

$$err(\bar{k}_{ge}) = \frac{1}{N_t}\sum_{i=1}^{N_t} \bar{k}_{ge_i} - \hat{k}_i, \tag{3.26}$$

where $\bar{k}_{ge}$ is the equivalent permeability calculated by averaging geometrically in the θ-direction (Eq 3.23) and harmonically in the radial direction (Eq. 3.24).

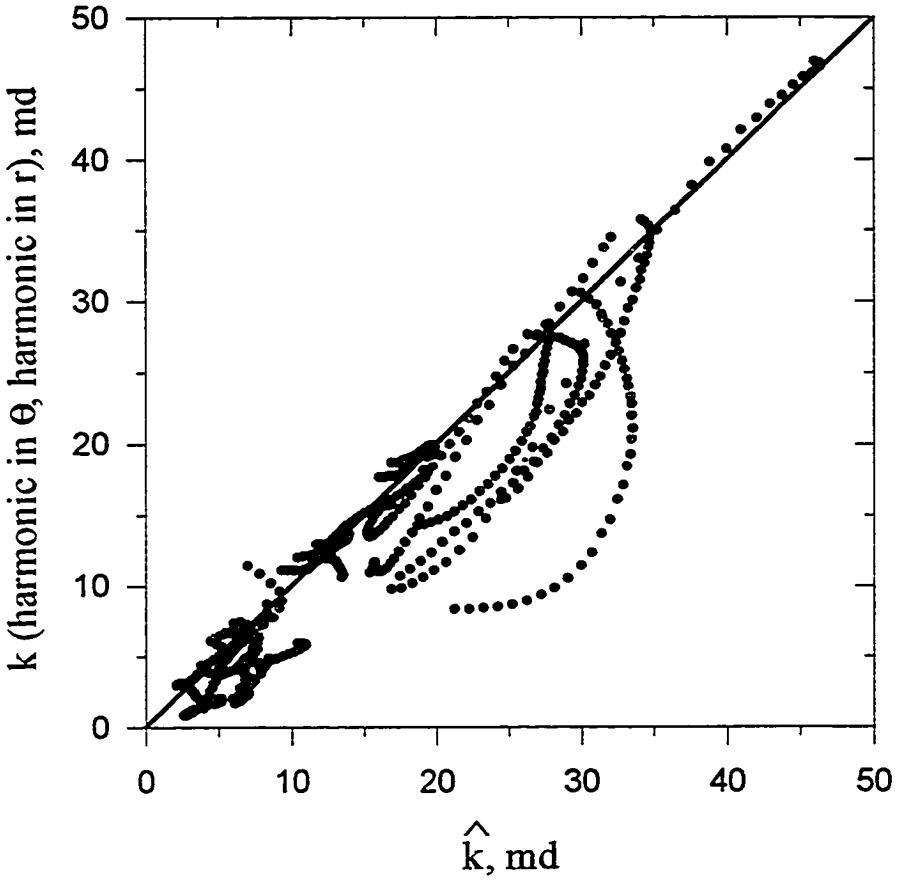

Figure 3.6- Grid block permeabilities averaged harmonically in θ and harmonically in r compared to the instantaneous well test permeability, $\hat{k}$.

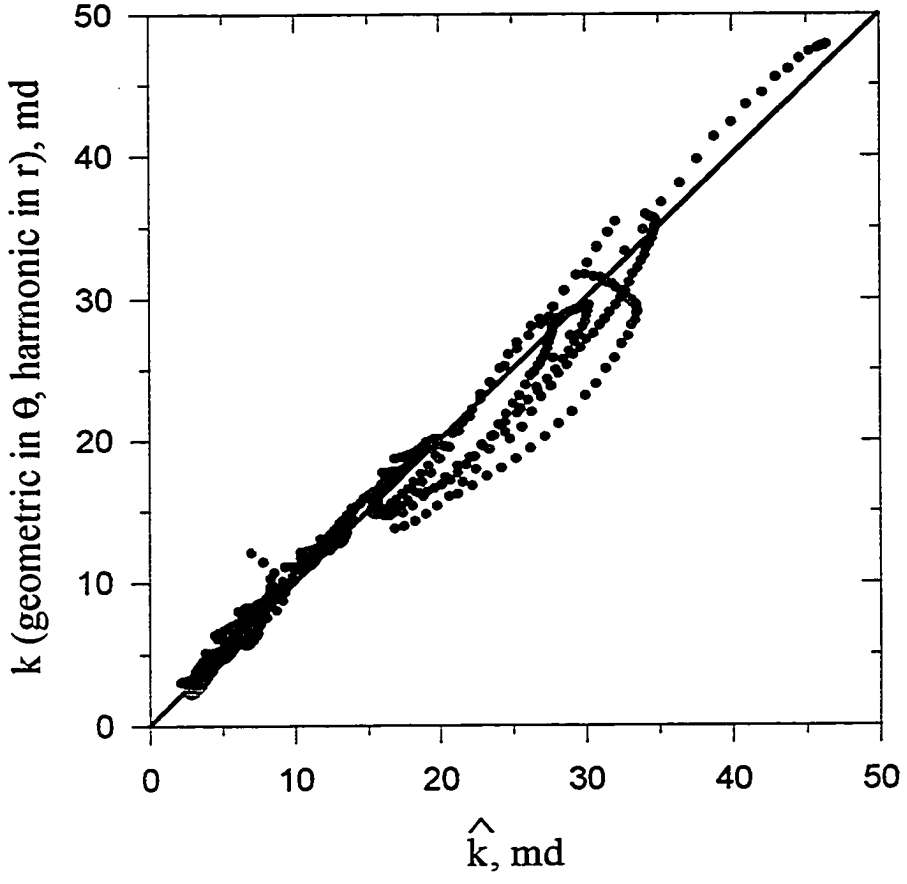

Figure 3.7 - Grid block permeabilities averaged geometrically in θ and harmonically in r compared to the instantaneous well test permeability, $\hat{k}$.

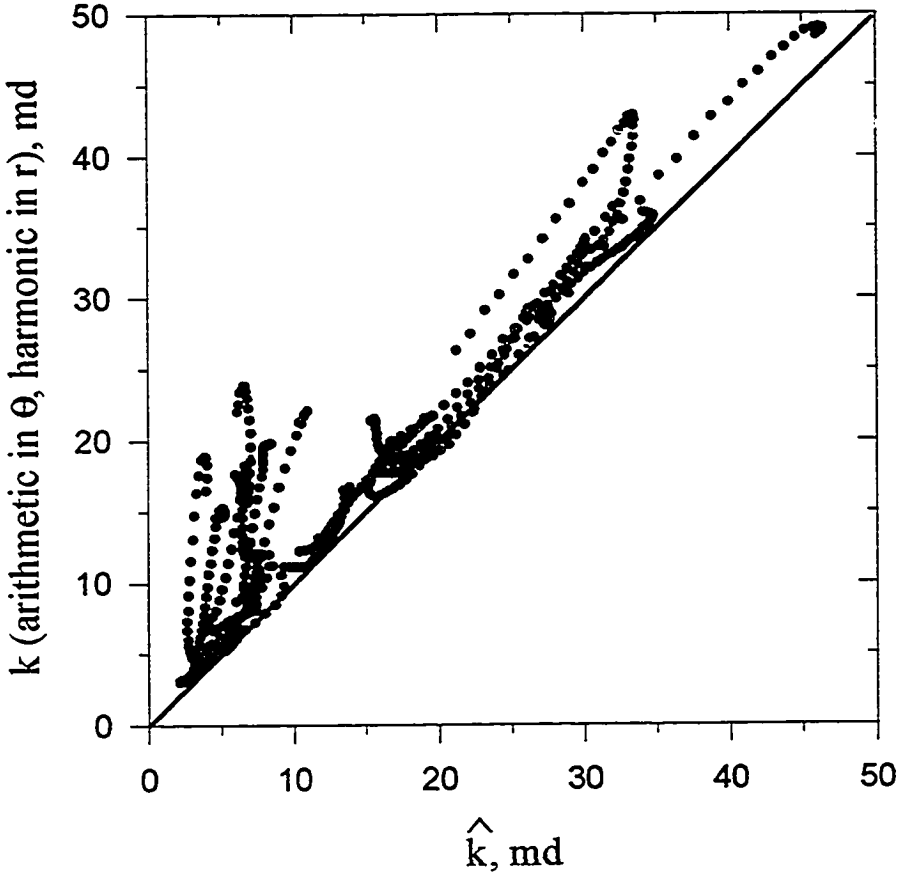

Figure 3.8 - Grid block permeabilities averaged arithmetically in θ and harmonically in r compared to the instantaneous well test permeability, $\hat{k}$..

where $\bar{k}_{he}$ is the equivalent permeability calculated by averaging harmonically in the θ-direction (Eq. 3.22) and harmonically in the radial direction (Eq. 3.24).

$$err(\bar{k}_{ge}) = \frac{1}{N_t}\sum_{i=1}^{N_t} \bar{k}_{ge_i} - \hat{k}_i, \tag{3.26}$$

where $\bar{k}_{ge}$ is the equivalent permeability calculated by averaging geometrically in the θ-direction (Eq 3.23) and harmonically in the radial direction (Eq. 3.24).

$$err(\bar{k}_{ae}) = \frac{1}{N_t}\sum_{i=1}^{N_t} \bar{k}_{ae_i} - \hat{k}_i, \tag{3.27}$$

where $\bar{k}_{ae}$ is the equivalent permeability calculated by averaging geometrically in the θ-direction (Eq 3.22) and harmonically in the radial direction (Eq. 3.24). The absolute relative errors are calculated by:

$$aerr(\bar{k}_{he}) = \frac{1}{N_t}\sum_{i=1}^{N_t} \left|\bar{k}_{he_i} - \hat{k}_i\right|, \tag{3.28}$$

$$aerr(\bar{k}_{ge}) = \frac{1}{N_t}\sum_{i=1}^{N_t} \left|\bar{k}_{ge_i} - \hat{k}_i\right|, \tag{3.29}$$

and

$$aerr(\bar{k}_{ae}) = \frac{1}{N_t}\sum_{i=1}^{N_t} \left|\bar{k}_{ae_i} - \hat{k}_i\right|. \tag{3.30}$$

Note that the harmonic average underpredicts the instantaneous well test permeability and the arithmetic average over predicts the permeability. A geometric average in the θ-direction and a harmonic average in the radial direction best approximates the instantaneous well test permeability, $\hat{k}$. Therefore, Equation 3.24, in which an area-based geometric average represents the θ-direction permeability average, is the best approximation for the discretized form of Equation 3.16.

To develop his Inverse Solution Algorithm (ISA), Feitosa[2] uses the instantaneous permeability, $\hat{k}$, to calculate an "instantaneous" dimensionless time $\hat{t}_D$ (Eq. 2.20). His

numerical experiments show that by using these "instantaneous" parameters a more accurate evaluation of the kernel function is obtained which reproduces the pressure response and permeability distribution. In this method, a pressure derivative which has large variations may result in a kernel function whose minimum radius is not guaranteed to shift forward in the domain of the reservoir for successive pressure derivative values.

Based on numerical experiments, we observed that by using $\hat{k}$, instead of the permeability derived from the best fit of the semi-log straight line to calculate the dimensionless time, t_D, made no noticeable improvements in our results. The comparison results are summarized in Table 3.3. This is probably due to the fact that the pressure derivatives of our base cases do not vary extremely.

3.2.2 The Inverse Solution Algorithm *(ISA)*^{2}

ISA determines an equivalent radial permeability distribution from well test data. Equations 2.20-2.28 describe ISA and are presented, again, for convenience. The equivalent radial permeability distribution for each zone is given by:

$$\Delta\left(\frac{1}{k_{ISAn}}\right)=\frac{\frac{1}{\hat{k}_n}-\frac{1}{k_{ISAn-1}}+\sum_{i=2}^{n-1}\left[\Delta\left(\frac{1}{k_i}\right)\int_{\hat{z}_{0D}}^{\hat{z}_{i-1D}}\Omega(\hat{z}_D)d\hat{z}_D\right]}{1-\int_{\hat{z}_{0D}}^{\hat{z}_{n-1D}}\Omega(\hat{z}_D)d\hat{z}_D}, \tag{3.31}$$

where,

$$\hat{z}_{0D}=\min\left\{\frac{1}{\sqrt{\hat{t}_D}},0.12\right\}, \tag{3.32}$$

Table 3.3 - Summary of comparison for different permeability averaging techniques using Oliver's solution. The instantaneous permeability, $\hat{k}$, is used to detrmine $\hat{t}_D$.

Turning Bands input parameters, μ_k = 20 md			Measures of heterogeneity		Relative error			Absolute relative error		
seed	σ^2_{lnk}	Range ft	HI	V	err($\bar{k}_{he}$)	err($\bar{k}_{ge}$)	err($\bar{k}_{ae}$)	aerr($\bar{k}_{he}$)	aerr($\bar{k}_{ge}$)	aerr($\bar{k}_{ae}$)
-15	0.4	2000	0.0795	0.33	-0.134	-0.356	-0.577	0.546	0.427	0.577
-4	0.25	3200	0.0497	0.22	-0.458	-0.477	-0.496	0.458	0.477	0.496
-3	0.5	2000	0.1242	0.39	0.304	-0.565	-1.521	0.629	0.565	1.520
-10	0.5	500	0.0311	0.39	1.634	0.623	-0.466	1.643	1.085	1.341
-22	0.92	595.41	0.1242	0.6	3.971	1.453	-1.619	3.971	1.498	2.063
-20	0.92	2143.84	0.4472	0.6	-0.547	-0.637	-0.727	0.547	0.637	0.727
-18	0.92	958.78	0.2	0.6	0.286	-0.176	-0.645	0.580	0.535	0.692
-16	0.92	1072	0.2236	0.6	5.955	2.081	-2.838	5.963	2.266	2.838
-12	0.75	1250	0.1747	0.53	4.041	1.710	-1.020	4.081	1.810	1.081
-11	0.75	3200	0.4472	0.53	-0.184	-0.450	-0.757	0.299	0.450	0.757
-7	0.75	1600	0.2236	0.53	0.647	-0.085	-0.782	0.895	0.267	0.782
-8	0.75	2000	0.2795	0.53	4.933	2.147	-0.948	5.111	2.414	0.948
-9	0.75	1000	0.1398	0.53	5.858	2.943	0.084	5.932	3.244	1.389
-26	1.2	1241.69	0.4472	0.7	12.200	4.254	-6.825	12.21	4.507	6.825
-25	1.2	555.32	0.2	0.7	1.487	-0.515	-3.464	2.014	0.688	3.464
-24	1.2	220.74	0.0795	0.7	2.461	-0.430	-6.371	2.635	0.724	6.371
-23	1.61	193	0.1242	0.8	3.147	-0.408	-10.09	3.263	0.524	10.088
-21	1.61	694.93	0.4472	0.8	NO SOLUTION					
-19	1.61	310.8	0.2	0.8	0.349	0.729	-4.752	3.563	0.737	4.752
-17	1.61	347.5	0.2236	0.8	1.790	0.231	-3.727	1.848	0.597	3.727
Cumulative errors					2.627	0.588	-2.617	2.902	1.196	3.711

where,

Seed = turning bands seed number

σ^2_{lnk} = standard devation on a log normal scale μ_k = mean permeaility

HI = Heterogeneity Index = $(\sigma^2_{lnk} range/\Delta x \times N_X)$ (Ref. 45) V = Dykstra Parsons Coefficient = $1-1/\exp(\sigma^2_{lnk})$ (Ref. 46)

$$\Omega\hat{z}_D = \sqrt{\pi}\ \ \hat{z}_D \exp\left(-\frac{\hat{z}_D^2}{2}\right) W_{\frac{1}{2},\frac{1}{2}}\left(\hat{z}_D^2\right), \tag{3.33}$$

$$\hat{z}_{0D} = \frac{1}{\sqrt{\hat{t}_D}}, \tag{3.34}$$

$$\hat{z}_{jD} = \frac{r_{jD}}{\sqrt{\hat{t}_D}}, \tag{3.35}$$

and

$$\hat{t}_D = \frac{0.006328\hat{k}_n t_n}{\phi\mu c_t r_w^2}, \tag{3.36}$$

where $\hat{k}_n$ is the instantaneous permeability given by Equation 3.9.

Once $\Delta(1/k_{ISAn})$ is calculated, the permeability at zone n is determined by:

$$k_{ISAn} = \frac{1}{\frac{1}{k_{ISAn-1}} + \Delta\left(\frac{1}{k_{ISAn}}\right)}. \tag{3.37}$$

The radius of investigation for this solution at zone n is defined as:

$$r_n = 2.0\sqrt{\frac{0.006328\hat{k}_n t_n}{\phi\mu c_t}}, \tag{3.38}$$

Figure 3.9 shows the equivalent radial permeability distribution obtained from ISA for the pressure response shown in Figure 3.3.

3.2.2.1 Application of ISA to Areally (x-y) Heterogeneous Reservoir

The permeability distribution, generated by ISA is a piece wise linear polynomial (Figure 3.9). In our application to an areal permeability field, we must define the

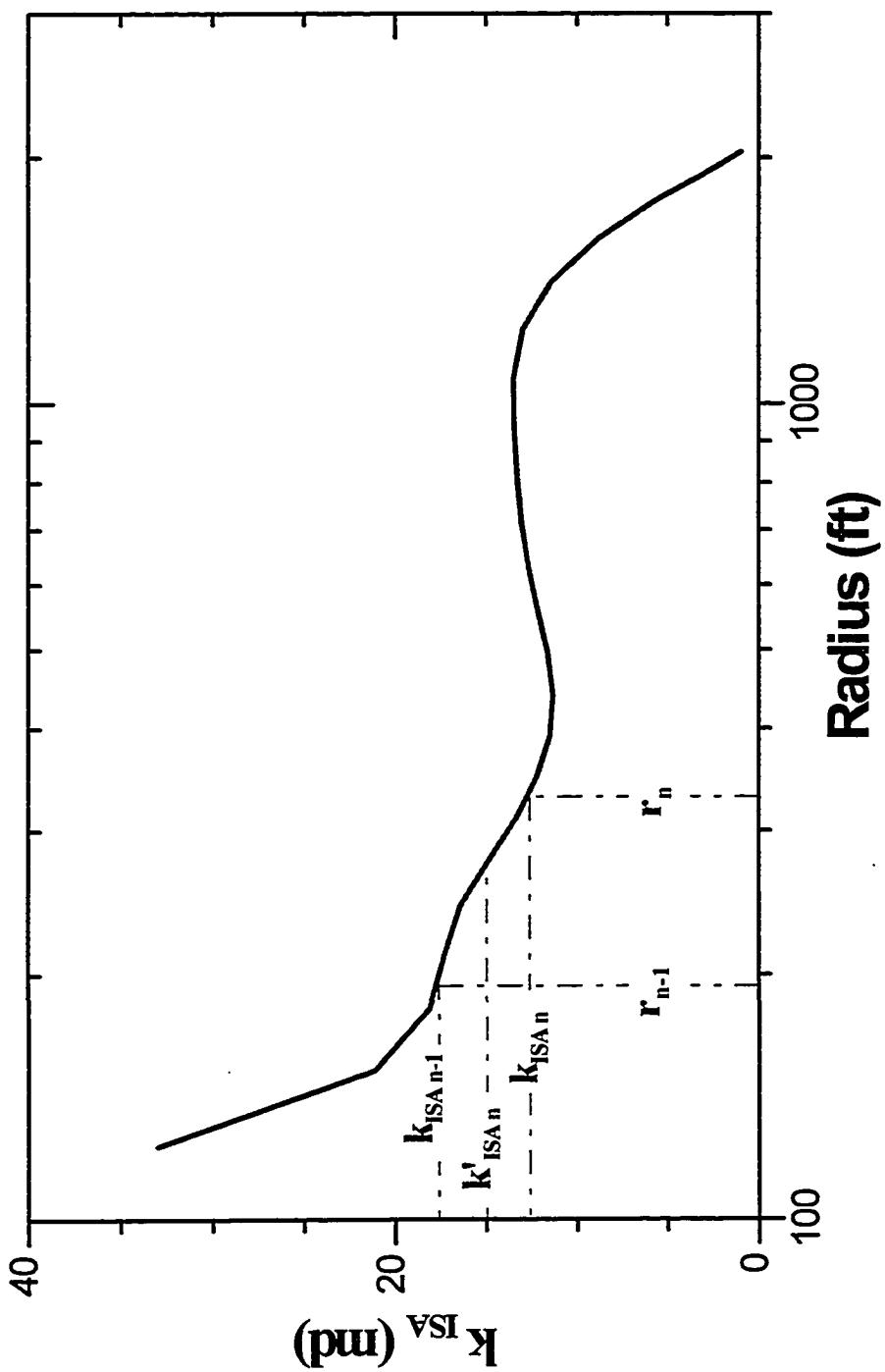

Figure 3.9- Equivalent radial permeability distribution determined by ISA for the pressure response shown in Figure 3.3.

equivalent ISA permeability within an inner and outer radius of investigation. We define k'_{ISAn} as the permeability which is linearly interpolated between k_{ISAn-1} and k_{ISAn}, for the inner and outer radius of investigation, r_{n-1} and r_n, respectively (see Figure 3.9). Therefore, for each annular region over which k'_{ISAn} is defined, the minimum radius, is defined by r_{n-1} and the maximum radius is defined by r_n.

Feitosa showed an example in which permeability is varied in r and θ. A numerical fluid flow simulation is performed using a r-θ flow simulator. He observed that if he replaces the areally (r-θ) heterogeneous reservoir with a radial reservoir where the permeability in each Coat's grid annulus was computed as the *geometric average* of the grid block permeabilities within the annulus, he obtained a pressure derivative that best matches the pressure derivative from the areally heterogeneous reservoir.

3.2.2.2 Numerical Experiments to Determine the Best Averaging Technique in the θ-Direction for ISA

We study the application of ISA derived radial permeabilities to our areal (x-y) permeability distribution. A procedure similar to the one used to determine the best type of average for Oliver's solution is used. Equations 3.22 and 3.23 are used to calculate the arithmetic, harmonic, and geometric permeability averages within the ISA defined radii of investigation. Figures 3.10 - 3.12 compare the different averaging techniques to the ISA permeability distribution. Table 3.4 summarizes the results. The errors are defined as:

$$err(\bar{k}_h) = \frac{1}{N_r}\sum_{j=1}^{N_r} \bar{k}_{h_j} - k_{ISAj}, \tag{3.39}$$

where $\bar{k}_h$ is the harmonic average of grid block permeabilities in the θ-direction (Eq. 3.22) between the inner and outer radii of investigation.

$$err(\bar{k}_g) = \frac{1}{N_r}\sum_{j=1}^{N_r} \bar{k}_{g_j} - k_{ISAj}, \tag{3.40}$$

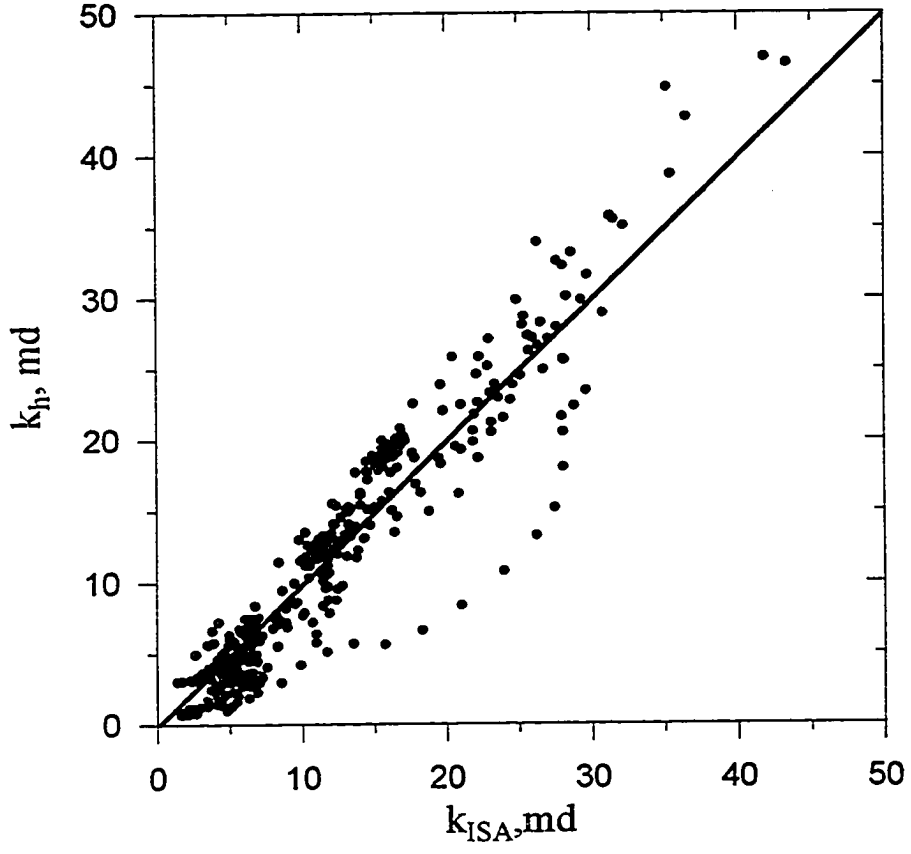

Figure 3.10- Grid block permeabilities averaged harmonically in θ compared to the ISA well test permeability distribution, k_{ISA}.

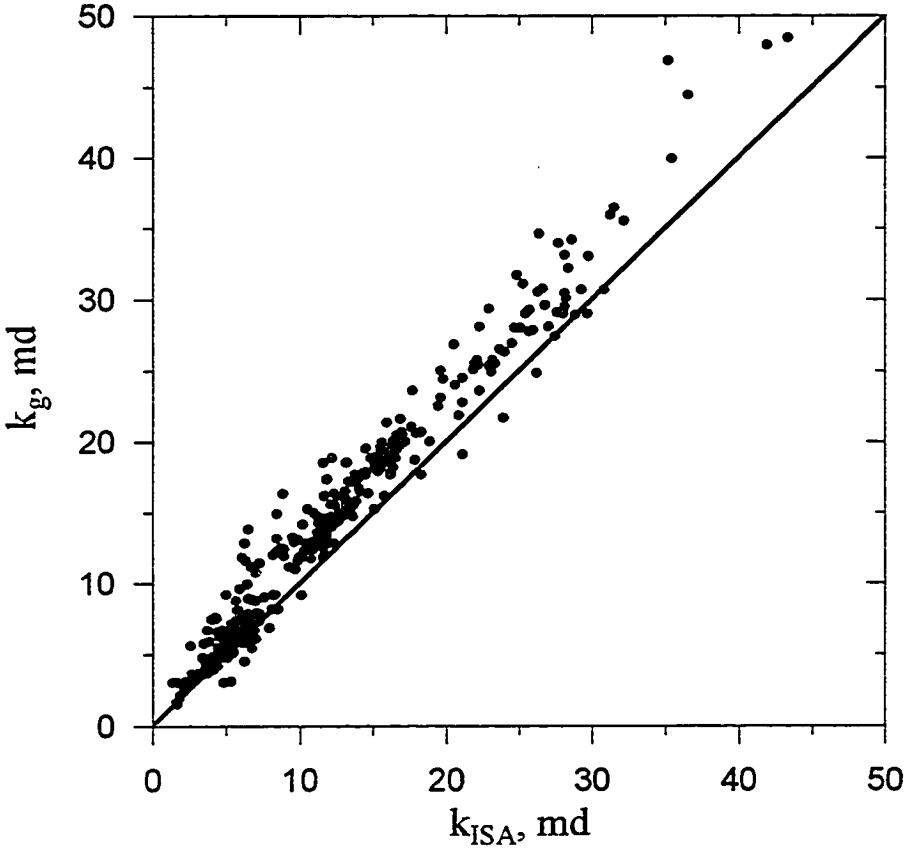

Figure 3.11- Grid block permeabilities averaged geometrically in θ compared to the ISA well test permeability distribution, k_{ISA}.

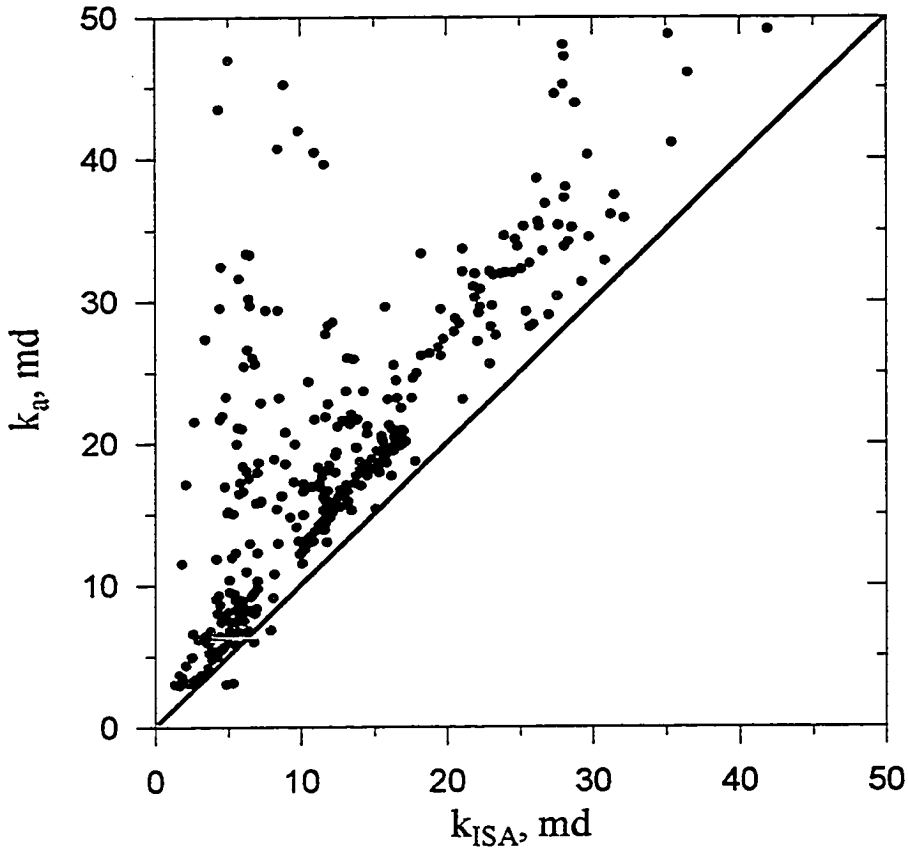

Figure 3.12- Grid block permeabilities averaged arithmetically in θ compared to the ISA well test permeability distribution, k_{ISA}.

Table 3.4 - Summary of comparison for different permeability averaging techniques compared to the ISA permeability.

Turning Bands input parameters, μ_k = 20 md			Measures of heterogeneity		Relative error			Absolute relative error		
seed	σ^2_{lnk}	Range ft	HI	V	$err(\bar{k}_h)$	$err(\bar{k}_g)$	$err(\bar{k}_a)$	$aerr(\bar{k}_h)$	$aerr(\bar{k}_g)$	$aerr(\bar{k}_a)$
-15	0.4	2000	0.0795	0.33	-2.905	-3.168	-3.433	2.905	3.168	3.433
-4	0.25	3200	0.0497	0.22	-3.175	-3.200	-3.224	3.175	3.200	3.224
-10	0.5	500	0.0311	0.39	-1.695	-2.918	-4.318	1.724	2.919	4.318
-22	0.92	595.41	0.1242	0.6	-0.267	-3.032	-6.783	1.745	3.032	6.784
-20	0.92	2143.84	0.4472	0.6	-0.639	-0.779	-0.920	1.056	1.196	1.336
-18	0.92	958.78	0.2	0.6	-0.357	-0.823	-1.287	0.609	0.941	1.402
-16	0.92	1072	0.2236	0.6	0.817	-2.928	-7.870	1.655	2.928	7.869
-12	0.75	1250	0.1747	0.53	-0.425	-2.782	-5.688	1.243	2.782	5.688
-7	0.75	1600	0.2236	0.53	-1.011	-1.995	-3.053	1.563	1.995	3.053
-8	0.75	2000	0.2795	0.53	-0.403	-3.454	-7.080	2.319	3.454	7.080
-9	0.75	1000	0.1398	0.53	-1.652	-4.217	-7.026	3.221	4.217	7.026
-26	1.2	1241.69	0.4472	0.7	6.647	-1.004	-12.655	7.417	1.813	12.655
-25	1.2	555.32	0.2	0.7	1.660	-1.637	-8.773	2.188	1.671	8.773
-24	1.2	220.74	0.0795	0.7	1.677	-2.174	-11.740	1.940	2.340	11.74
-23	1.61	193	0.1242	0.8	2.262	-1.667	-14.936	2.539	1.968	14.963
-19	1.61	310.8	0.2	0.8	2.355	-0.744	-7.715	2.420	1.028	7.715
-17	1.61	347.5	0.2236	0.8	1.177	-0.660	-10.65	1.350	0.806	10.714
Cumulative errors					0.134	-1.152	-4.846	2.221	2.271	6.831

where,
Seed = turning bands seed number

σ^2_{lnk} =standard devation on a log normal scale

$\mu_{k=}$mean permeaility

HI = Heterogeneity Index = $(\sigma^2_{lnk} range/\Delta x \times N_X)$ (Ref. 45)

V = Dykstra Parsons Coefficient = $1-1/\exp(\sigma^2_{lnk})$ (Ref. 46)

where $\bar{k}_g$ is the geometric average of grid block permeabilities in the θ-direction (Eq. 3.23) between the inner and outer radii of investigation.

$$err(\bar{k}_a) = \frac{1}{N_r}\sum_{j=1}^{N_r} \bar{k}_{a_j} - k_{ISAj}, \tag{3.41}$$

where $\bar{k}_a$ is the arithmetic average of grid block permeabilities in the θ-direction (Eq. 3.22) between the inner and outer radii of investigation. The absolute relative errors are calculated by:

$$aerr(\bar{k}_h) = \frac{1}{N_r}\sum_{j=1}^{N_r} \left|\bar{k}_{h_j} - k_{ISAj}\right|, \tag{3.42}$$

$$aerr(\bar{k}_g) = \frac{1}{N_r}\sum_{j=1}^{N_r} \left|\bar{k}_{g_j} - k_{ISAj}\right|, \tag{3.43}$$

and

$$aerr(\bar{k}_a) = \frac{1}{N_r}\sum_{j=1}^{N_r} \left|\bar{k}_{a_j} - k_{ISAj}\right|. \tag{3.44}$$

Note, that both harmonic and geometric averaging in the θ-direction of the areal permeability field give good approximations to the ISA radial permeability distribution. The best averaging technique for ISA is studied further in Chapter V, where the inverse problem is solved; i.e. an areal permeability distribution honoring geostatistical and ISA equivalent permeabilities is generated. The pressure response of permeability fields honoring ISA by performing both harmonic and geometric averaging in the θ–direction are compared to the base case pressure response.

CHAPTER IV

SIMULATED ANNEALING ALGORITHM

In this chapter we outline the simulated annealing algorithm to solve the inverse problem: assuming the permeability field is unknown, can we estimate the true permeability field based on the available data? We assume that the univariate and spatial statistics of the distribution and the transient pressure response of the permeability field are known a-priori. Thus the resulting reservoir description should honor the spatial and univariate statistics and the well test data. The stochastic conditional simulation method of simulated annealing is used to develop a reservoir description that honors these constraints. The observations made in Chapter III, concerning the application of Oliver's[1] method and Feitosa's[2] Inverse Solution Algorithm (ISA) to an areally (x-y) heterogeneous reservoir, are used to honor the well test constraint. These observations are:

(i) For Oliver's solution, the instantaneous well test permeability, $\hat{k}$, can be approximated by an equivalent permeability, $\bar{k}_e$. $\bar{k}_e$ is an area-based geometric average of grid block permeabilities in the θ-direction within the annular regions defined by Coats' grid, which is followed by a harmonic average in the radial direction, between the minimum and maximum radii of investigation defined by $r_{D\min} = 0.12\sqrt{t_D}$ and $r_{D\max} = 2.34\sqrt{t_D}$. Oliver's kernel function is used to determine appropriate weights.

(ii) The equivalent radial permeability distribution determined by ISA can be approximated by an area-based harmonic or geometric average of grid block permeabilities in the θ-direction, within the annular regions defined by ISA.

The original simulated annealing algorithm code written in ANSI FORTRAN 77 by Pérez,[3] is modified to include the constraints imposed by the well test information. The reservoir description process must honor the following constraints: (i) the cumulative distribution function (cdf), (ii) the conditioning data at sampled locations, (iii) the variogram models, and (iv) the well test information. A description of the algorithm is presented and wherever possible the nomenclature defined by Pérez is used. For the sake of clarity and completeness some of the work presented by Pérez is summarized and presented again. We first describe the calculation of important components of the simulated annealing algorithm. Then the actual simulation process is described.

4.1 Generation of the Simulation Grid

A two-dimensional rectangular grid with N_x grid blocks in the x-direction and N_y grid blocks in the y-direction is defined. The size of each grid block is $\Delta x \times \Delta y$. The coordinates of the center of the grid block (x_i, y_i) are

$$x_i = O_x + i\Delta x, \quad \text{for } i = 1,2,.....N_x \tag{4.1}$$

and

$$y_j = O_y + j\Delta y, \quad \text{for } j = 1,2,.....N_y, \tag{4.2}$$

where, $(O_x O_y)$ are the coordinates of the origin typically defined to be at the lower left corner of the two-dimensional grid.

In the simulated annealing algorithm, the grid block location vector, $\bar{s} = (x_i, y_j)$, is referenced by a single index, l, which defines the grid-block location index (i,j) in the algorithm:

$$j = 1 + \mathrm{INT}\left[\frac{l-1}{N_x}\right]$$
and
$$i = l - (j-1)N_x, \tag{4.3}$$

where, l = 1,2...N_s and N_s is the total number of simulation points, i.e., $N_x \times N_y$. INT truncates the number in brackets to an integer value.

The simulation variable in our study is the grid block permeability and is defined at the location vector, $\bar{s}$, as $k_{\bar{s}}$. The value of each grid block permeability is assigned by sampling the cumulative distribution function (cdf). The discrete cdf can be represented as C_j classes, for j=1,..,N_f class intervals. By sequentially visiting each grid block in the domain, the permeability at each grid block is assigned:

$$k_{\bar{s}} = C_{iR} - (C_{iR} - C_{iR-1})\left[\frac{iR}{N_f} - R\right]N_f, \tag{4.4}$$

where

$$iR = \mathrm{INT}(R \times N_f) + 1 \tag{4.5}$$

and R is a random number sampled from a uniform distribution between [0,1]. The above equations form the constraint for the cdf.

The conditioning data constraint is specified by assigning the permeability at specified locations, i.e.,

$$k_{\bar{s},c} = k(c)_{\bar{s}}, \tag{4.6}$$

where $k(c)_{\bar{s}}$ is the sampled permeability at the conditioning point location. The values of the conditioning points remain fixed throughout the simulation.

This procedure yields an initial uncorrelated permeability distribution that honors the cdf and the conditioning data.

4.2 Sample Variogram

The sample variogram of the permeability distribution is calculated by:

$$\gamma_s(\bar{h}_{l,i}) = \frac{1}{2N_p(\bar{h}_{l,i})} \sum_{j=1}^{N_p(\bar{h}_{l,i})} \left[k(\bar{s}_j + \bar{h}_{l,i}) - k(\bar{s}_j)\right]^2, \tag{4.7}$$

where $\bar{h}_{l,i}$ is the lag distance vector (or separation distance between points), $N_p(\bar{h}_{l,i})$ is the number of pairs within the simulation grid corresponding to the lag $\bar{h}_{l,i}$, $\bar{s}_j$ is the location vector of the grid block. The index i refers to the direction and the index l refers to the lag distance considered for a given direction. Spatial relations can be defined in the three principle directions and anisotropy considered such that three dimensional anisotropic realizations are generated.

A variogram model, γ_o, is defined by fitting one of the conventional models[11] to the available data. In our case, we assume that model variogram is known a-priori and is the model variogram of the base case permeability distribution.

4.3 Initial Well Test Information

The major modifications to the simulated annealing code developed by Pérez are in the inclusion of the well test information. The modified code must allow for the most efficient updating of the energy function (described in Section 4.10). In order to achieve this, variables important for the inclusion of well test information are determined in the initial part of the algorithm. The reasons for defining these variables become evident when the well test energy function component is calculated and the update performed.

1. The area of each grid block within Coats' pre-defined radial grid

This is done by calculating the area of the grid block, $A_{\bar{s},j}$, that falls within the pre-defined Coats' grid. The index j defines the Coats' grid annulus, where $j = 1,...,N_r$. N_r is the number of radial grid divisions. The area of each grid block is calculated as outlined in Appendix A. This method accounts for segments of grid blocks that only partially lie within the annulus under consideration. If the grid block lies outside the pre-defined annulus the algorithm assigns a value of 0 to the grid block area (see Figure 4.1), based on the following criteria:

$$r_{c\max} < r_{j-1} \quad and \quad r_{c\min} > r_j \Rightarrow A_{\bar{s},j} = 0, \quad for \quad j = 1,2,....N_r, \tag{4.8}$$

where, $r_{c\min}$ and $r_{c\max}$ are the minimum and maximum radii to the corners of the grid block, $A_{\bar{s},j}$, respectively. This is clearly illustrated in Figure 4.1 with the appropriate nomenclature. For the purpose of updating the well test component of the energy function (Section 4.10), these values are stored in a two dimensional array. For example a reservoir with dimensions $N_x \times N_y$ and N_r radial Coats' grids, requires the areas to be stored in an array of dimensions $\left(N_x \times N_y, N_r\right)$.

2. The area based geometric average of permeabilities, $\bar{k}_{gj}$, (Eq. 3.23) within the pre-defined Coats' radial grid is calculated by:

$$\bar{k}_{gj} = \exp\left[\frac{\sum_{\bar{s}\in A_{rj}} A_{\bar{s},j} \ln k_{\bar{s}}}{A_{rj}}\right] \quad for \quad j = 1,2....N_r, \tag{4.9}$$

where A_{rj} is the area of the annular region between r_{j-1} and r_j. The averaged permeabilities $\bar{k}_{gj}$, and the annular areas, A_{rj}, are stored in arrays of dimension N_r. Note that if $\bar{s} \notin A_{rj}$, the contribution of $k_{\bar{s}}$ to $\bar{k}_{gj}$ is 0.

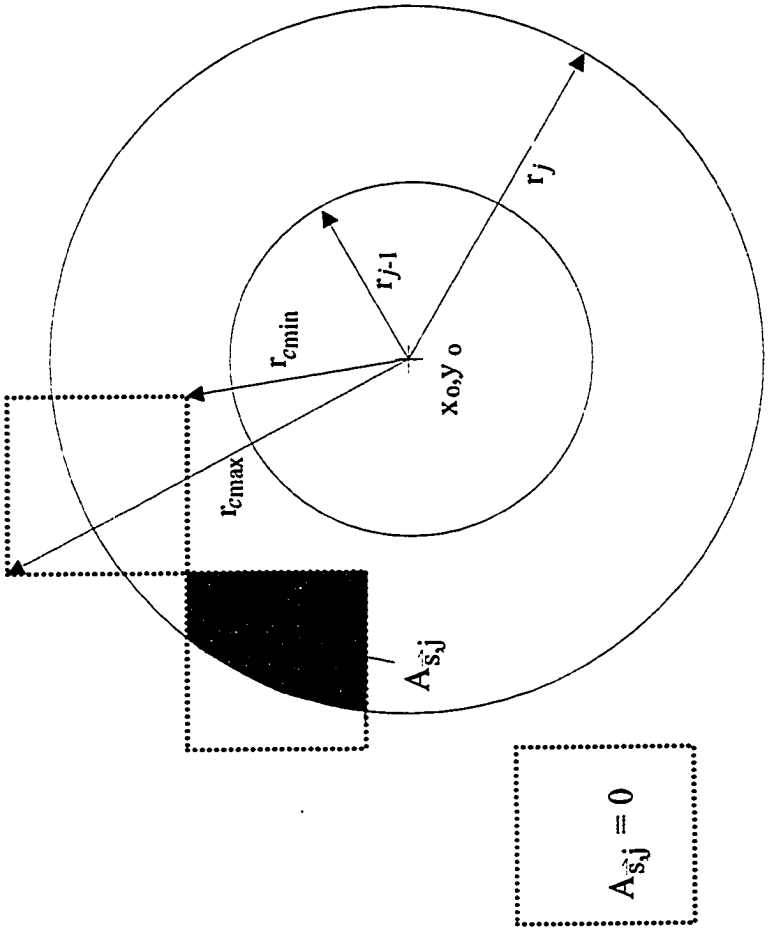

Figure 4.1 - Illustration of nomenclature describing grid block location and area within inner and outer radii.

If ISA is being used then, either $\bar{k}_{gj}$ or $\bar{k}_{hj}$ approximates the equivalent radial permeability, $\bar{k}_{ISA}$. $\bar{k}_{hj}$ is calculated from Equation 3.22 to be:

$$\bar{k}_{hj} = \frac{1}{A_{rj} \sum_{\bar{s} \in A_{rj}} \frac{1}{A_{\bar{s},j} k_{\bar{s}}}} \quad for \quad j = 1,2....N_r. \tag{4.10}$$

Note that for ISA, as described in Section 3.2.2.1, we do not have a radial Coats' grid division; the radial grid is defined by the algorithm itself. However, we still consider N_r radial divisions (defined by ISA) and the above relations (Eqs. 4.8-4.10) still apply.

3. The equivalent permeability, $\bar{k}_e$, for Oliver's method is calculated by:

$$\frac{1}{\bar{k}_e} = \sum_{j=1}^{N_r} w_j \frac{1}{\bar{k}_{gj}}, \tag{4.11}$$

where w_j is the weight, in the annulus between the radii r_{j-1} and r_j, that contributes to the equivalent permeability. The weights are calculated by Equation 3.21, which is presented again for convenience:

$$w_j = \frac{\int_{r_{j-1}}^{r_j} K(r_D, t_D)}{\int_{r_{D\min}}^{r_{D\max}} K(r_D, t_D)}, \quad \text{for} j = j_{\min}, j_{\min+1}, ..., j_{\max}, \tag{4.12}$$

where, $r_{j\min}$ and $r_{j\max}$ correspond to the minimum and maximum radii defined by Equation 3.20. The values for the above variables are stored in arrays of dimension N_t for $\bar{k}_e$ and N_t, N_r for w.

The computer storage requirements of the above additions to the annealing algorithm are large. However, this ensures that the computational cost in recalculating the energy function due to a swap is minimized (see Section 4.10).

4.4 Objective Function

The basic goal of the simulated annealing algorithm is to describe a configuration of variables such that a global minimum of the objective function is obtained.

The objective function defines the difference between a function of sample data and a desired model that the sample data must fit. This can be the difference between the sample and model variograms or the difference between the permeability derived from pressure transient data and some averaging process of permeabilities. When multiple constraints are imposed on the reservoir description the objective function is divided into principle components that describe each imposed constraint. In our study, the objective functions or energies for the following constraints are defined: (i) the energy of the variogram component and (ii) the energy of the constraint imposed by well test information using either Oliver's method or ISA.

4.4.1 Energy Function - Variogram Constraint

The variogram energy function, E_1^k, is calculated as the square root of the sum in N_d directions and for N_h lags of the normalized difference between the model variogram and sample variogram at the k^{th} iteration step of the algorithm:

$$E_1^k = \sqrt{\sum_{i=1}^{N_d}\sum_{l=1}^{N_{hi}}\left[\frac{\gamma_s^k(\bar{h}_{l,i}) - \gamma_o(\bar{h}_{l,i})}{\gamma_o(\bar{h}_{l,i})}\right]^2}, \qquad (4.13)$$

$\gamma_s^k(\bar{h}_{l,i})$ is the variogram of the permeability distribution at the iteration level k calculated by Equation 4.7. $\gamma_o(\bar{h}_{l,i})$ is the model variogram that the sample variogram must ultimately match.

A normalizing constant of the variogram energy function, E_{01} is also defined. It is the normalizing constant of the variogram constraint and is determined in the initial part of the algorithm. It is determined by calculating the energy of the variogram at initial conditions:

$$E_{01} = \sqrt{\sum_{i=1}^{N_d}\sum_{l=1}^{N_{hi}}\left[\frac{\gamma_s^o(\bar{h}_{l,i}) - \gamma_o(\bar{h}_{l,i})}{\gamma_o(\bar{h}_{l,i})}\right]^2}. \qquad (4.14)$$

$\gamma_s^o(\bar{h}_{l,i})$ is the variogram of the permeability for the initial uncorrelated distribution.

The well test information constraint can be represented by either Oliver's method or ISA, the energy function for incorporating both methods is presented.

4.4.2 Energy Function - Well Test Constraint (Oliver's Method)

In Chapter III we concluded that for Oliver's solution the equivalent permeability, $\bar{k}_e$, (Eq. 4.11) is approximately equal to the instantaneous well test permeability, $\hat{k}$ (Eq. 3.9). Based on this observation, if we simulate the annealing procedure until $\bar{k}_e \approx \hat{k}$ for each t_D, we should be able to reproduce the pressure response of the reservoir. For our N_t sets of pressure derivative data, we compute N_t associated regions of investigation. Each region is defined in the limits of $r_{D\min} = 0.12\sqrt{t_D}$ and $r_{D\max} = 2.34\sqrt{t_D}$. Note that since $r_{D\min}$ for the current pressure derivative data point may be less than $r_{D\max}$ for the previous pressure derivative data point, i.e., $r_{D\min i} < r_{D\max i-1}$ for i=1,2.....N_p there may be some overlap between the different radii of investigation.

The energy function of the well test constraint imposed by Oliver's method is calculated by:

$$E_2^k = \sqrt{\sum_{i=1}^{N_t}\left[\frac{\bar{k}_e^k - \hat{k}_i}{\hat{k}_i}\right]^2}, \tag{4.15}$$

where $\bar{k}_e^k$ is the equivalent permeability determined by Equation 4.11 at the k^{th} iteration level of the simulation. $\hat{k}$ is the instantaneous permeability derived from the instantaneous pressure derivative.

The initial energy function for Oliver's method incorporating the well test component, E_{02}, is defined as:

$$E_{02} = \sqrt{\sum_{i=1}^{N_t}\left[\frac{\bar{k}_{e,i}^o - \hat{k}_i}{\hat{k}_i}\right]^2}, \tag{4.16}$$

where $\bar{k}_e^o$ is the equivalent permeability for the initial uncorrelated distribution calculated by Equation 4.11.

4.4.3 Energy Function -Well Test Constraint (ISA)

In Chapter III we observed that the ISA equivalent permeability, k_{ISA}, (Eqs. 3.31-3.38) is best approximated by either the area-based geometric (Eq. 4.9) or harmonic average (Eq. 4.10) of grid block permeabilities between the annulus of investigation. The component of the energy function incorporating the equivalent ISA radial permeability distribution is given by:

$$E_2^k = \sqrt{\sum_{j=1}^{N_r}\left[\frac{\bar{k}_j^k - k_{ISAj}}{k_{ISAj}}\right]^2}, \tag{4.17}$$

where $\bar{k}_j^k$ is either the area-based geometric (Eq. 4.9) or harmonic (Eq. 4.10) average of grid block permeabilities within the pre-defined annular regions at the k^{th} iteration level of the simulation and k_{ISA} is the equivalent ISA radial permeability distribution given by Equations 3.31-3.38.

The normalizing coefficient of the energy function incorporating ISA is given by:

$$E_{02} = \sqrt{\sum_{j=1}^{N_r} \left[\frac{\bar{k}_j^o - k_{ISAj}}{k_{ISAj}} \right]^2}, \tag{4.18}$$

where $\bar{k}_j^o$ is either the area-based geometric or harmonic average of grid block permeabilities for the initial uncorrelated distribution.

4.5 Objective Function Weights

Combinatorial optimization techniques allow us to incorporate additional constraints into the objective function. This is done by dividing the objective function into components describing each constraint that must be honored. In order to simultaneously honor the variogram and the well test constraint, the energies of the two components are weighted and added together, to yield the overall energy function:

$$E^k = \frac{\psi_1}{E_{01}} E_1^k + \frac{\psi_2}{E_{02}} E_2^k, \tag{4.19}$$

E_{01} (Eq. 4.14) and E_{02} (Eq. 4.16 or Eq. 4.18) are the normalizing constants of the variogram and well test components of the energy function, respectively. E_1^k (Eq. 4.13) and E_2^k (Eq. 4.15 or Eq. 4.17) are the energy functions of the variogram and well test components, respectively.

ψ_1 and ψ_2 are the weights assigned to each component of the energy function such that on an average each component contributes *equally* to the change in the overall

objective function.[20] The weights are computed numerically in the initial phase of the algorithm by performing sufficient, M, interchanges such that stable estimates of the weights are obtained. The equation to calculate the weight for the variogram constraint, ψ_1, is given by:

$$\psi_1 = \frac{\frac{1}{M}\sum_{k=1}^{M}\frac{|E_1^k - E_{01}|}{E_{01}}}{\frac{1}{M}\sum_{k=1}^{M}\frac{|E_1^k - E_{01}|}{E_{01}} + \frac{1}{M}\sum_{k=1}^{M}\frac{|E_2^k - E_{02}|}{E_{02}}}. \tag{4.20}$$

The weight for the well test constraint, ψ_2, is similarly determined:

$$\psi_2 = \frac{\frac{1}{M}\sum_{k=1}^{M}\frac{|E_2^k - E_{02}|}{E_{02}}}{\frac{1}{M}\sum_{k=1}^{M}\frac{|E_2^k - E_{02}|}{E_{02}} + \frac{1}{M}\sum_{k=1}^{M}\frac{|E_1^k - E_{01}|}{E_{01}}}. \tag{4.21}$$

In order to achieve a general value of the minimum number of iterations to achieve a stable estimate of the weighting functions, the iterations are normalized by dividing the iterations by the total number of simulation points, N_S, to determine the number of cycles. Figure 4.2 shows that 0.06 cycles of iterations, provide weights which converge to a stable value. Note that the weight for the well test energy function is less than that for the variogram.

The simulated annealing algorithm must simultaneously satisfy the variogram, the conditioning data constraints, and the instantaneous well test permeabilities or the ISA radial permeability distribution. The overall energy function (Equation 4.19) must converge to a value of 0 within some tolerance.

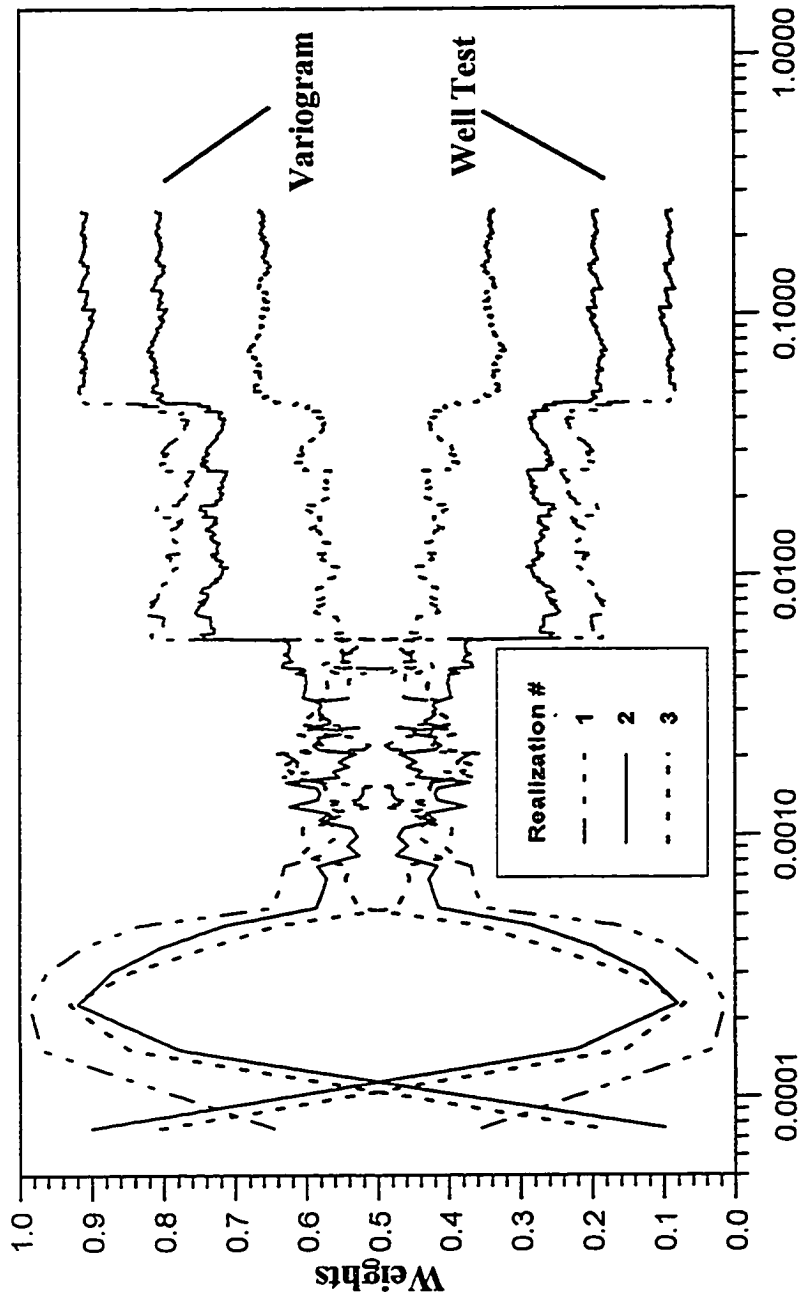

Figure 4.2 - Estimated objective function weights for a different number of iteration cycles and realizations.

4.6 The Interchange Mechanism

In order to allow for convergence of the objective function, perturbations are made to the simulation domain. The perturbation can be a two point or single point swap.

For the two point swap the exchange points in the reservoir are randomly selected as follows:

$$I_1 = 1 + \mathrm{INT}(N_s R_1), \tag{4.22}$$

and

$$I_2 = 1 + \mathrm{INT}(N_s R_2), \tag{4.23}$$

where R_1 and R_2 are random numbers generated from a uniform distribution in the range [0,1] and INT truncates the number in brackets to an integer. For the single point swap only one exchange point is randomly selected by using either of the above equations. The algorithm also ensures that the selected swap point or points do not coincide with any of the conditioning data.

For the single point swap a possible new permeability value is determined by sampling the original cdf. Equations 4.4 and 4.5 are used to calculate the new permeability value. Since the permeability at the exchange point must make a significant change on the objective function, the algorithm also ensures that the permeability of the selected grid block is significantly different from the original permeability. This is achieved by ensuring that the difference between the original permeability value and the new permeability value at the swap point is greater than the smallest magnitude of the difference between consecutive class limits. For the two point swap, this is represented as:

$$\left|k(\bar{s}_{l_1}) - k(\bar{s}_{l_2})\right| > \mathrm{MIN}(C_i - C_{i-1}), \quad \text{for } i = 1, 2, \ldots\ldots N_f. \tag{4.24}$$

A similar criterion can be defined for the single point swap.

4.7 Metropolis Condition

Variables in the system are *interchanged* or *swapped* until the objective function is minimized. Variations of the simulated annealing algorithm as applied to reservoir description exist in the literature. The differences are based on the acceptance criteria of a swap. These include the greedy algorithm, the heat bath algorithm, and the Metropolis condition.[17,18] In this work only the Metropolis acceptance criteria[48] will be considered and is described as follows. The exchange of two permeability values or the swap is accepted if the value of the energy function is reduced. The exchange may also be accepted if the energy function is increased. The Metropolis condition[48] calculates the probability of the transition between two states of the objective function:

$$P(\Delta E^k, T_r) = \begin{cases} 1, & \Delta E^k \le 0 \\ \exp\left(\dfrac{-\Delta E^k}{T^r}\right) & \Delta E^k > 0, \end{cases} \tag{4.25}$$

where the index k denotes an iteration within a step, represented by index r. The change in the objective function, ΔE_k, due to one interchange is:

$$\Delta E^k = E' - E^k. \tag{4.26}$$

T^r is the control parameter calculated by:

$$T^r = \alpha T^{r-1}, \tag{4.27}$$

α is the convergence rate factor and is a constant value in the range $0 < \alpha < 1$.

If $\Delta E^k \le 0$ the exchange is always accepted according to Equation 4.25. However, if $\Delta E^k \ge 0$, then a random number, R, from a uniform distribution in the range [0,1] is compared to $P(\Delta E^k, T^r)$ (Eq. 4.25). If $R \le P(\Delta E^k, T^r)$ the proposed interchange is accepted.

The use of the metropolis condition increases the probability of convergence of the algorithm to a global rather than a local minimum.

4.8 The Initial Control Parameter

The effect of the control parameter is evident from the Metropolis condition; if the value of the control parameter is high then more of the iterations proposed by the interchange mechanism will be accepted. The initial control parameter, T^o, is determined for the first step (r=1), numerically in the initial phase of the algorithm. The value of the initial control parameter determines the performance and efficiency of simulated annealing. If the control parameter is too high then most of the swaps are accepted leaving the simulation variable essentially uncorrelated. If its value is too low, then the simulation may converge to a local minimum. An appropriate value for T^0 is derived by Aarts and Korst.[49] It is determined in the initial phase of the algorithm and is given by:

(4.28)

$$T_o = \frac{\overline{\Delta E}^+}{\ln\left[\frac{m_2}{\chi_{initial} m_2 - (1-\chi_{initial}) m_1}\right]},$$

$\overline{\Delta E}^+_{initial}$ is the mean of m_2 positive changes in the objective function

$$\overline{\Delta E}^+_{initial} = \frac{1}{m_2}\sum_{i=1}^{m_2} \Delta E^+_{initial}, \tag{4.29}$$

$\Delta E^+_{initial}$ represents a positive change in the energy function. This is numerically determined by performing sufficient iterations in the initial phase of the algorithm. The change in the objective function at each iteration is given by:

$$\Delta E^k_{initial} = E^k_{initial} - E_o, \tag{4.30}$$

for $k = 1,.....,M_{initial}\,N_s$, where E^0 is the initial objective function. For the total number of iterations there are m_1 iterations for $\Delta E^k_{initial} \leq 0$ and m_2 iterations for $\Delta E^k_{initial} > 0$.

By performing numerical experiments, Pérez determined that $M_{initial} = 0.25$ is sufficiently large to allow for a stable estimate of the mean change in the objective function. He also defines the initial acceptance ratio, $\chi_{initial}$, to be 0.99 which is sufficiently large such that most of the proposed exchanges are accepted.

4.9 Maximum Number of Iterations per Step

The method developed by Pérez to calculate the maximum number of total iterations per step is outlined. The method calculates the maximum number of iterations per step by estimating the acceptance ratio for the subsequent step. The maximum number of steps defined by Pérez is 1000. The acceptance ratio for each step is defined by:

$$\chi^{r+1} = \frac{(\chi^r)^2}{\chi^{r-1}}, \tag{4.31}$$

for $r = 1,2,....1000$ and for $r = 1$, $\chi^1 = 1$.

The maximum number of iterations per step are calculated by:

$$M_t^{r+1} = M_a \frac{\chi^{r-1}}{(\chi^r)^2}, \tag{4.32}$$

where the recommended value for M_a is $5.0N_s$. Numerical experiments recommend the coefficient value of 5.0 is ideal and allows for sufficient iterations per step.

4.10 Energy Function Update Mechanism

In the simulated annealing algorithm most of the computational effort is spent on updating the constraints imposed by the variogram and well test information, once a perturbation or swap has been made. Thus the update code must be efficient with minimum computations to reduce the overall computational cost. The permeabilities at the swap points, $\vec{s}_{l1}$ and $\vec{s}_{l2}$, result in a change in the energy function for each component. We present the update formulations for the two point swap for the variogram and well test component of the energy function and the update formulation for the single point swap for only the variogram component. The update formulations presented here allow us to determine the new variogram and permeability average efficiently with minimal computational cost.

4.10.1 Variogram Energy Function Update

The update mechanism for the variogram component of the energy function was described by Pérez and is presented here for the sake of completeness. The new sample variogram, $\gamma_s'(\vec{h}_a)$, calculated at an arbitrary lag distance, $\vec{h}_a$ is

$$\gamma_s'(\vec{h}_a) = \gamma_s(\vec{h}_a) + \lambda(\vec{h}_a), \tag{4.33}$$

where $\gamma_s(\vec{h}_a)$is the original variogram value at $\vec{h}_a$. $\lambda(\vec{h}_a)$ is the variogram correction term which consists of removing the contribution to the variogram of the permeability at one exchange point and adding the contribution of permeability at the other exchange point for the two point swap or the permeability sampled from the cdf for the single point swap.

For the two point swap the correction term at the lag distance, $\bar{h}_a$ is

$$\lambda(\bar{h}_a) = \frac{1}{2N_p(\bar{h}_a)}\left[\lambda^+_{I1} + \lambda^-_{I1} + \lambda^+_{I2} + \lambda^-_{I2}\right], \tag{4.34}$$

where, N_p is the number of pairs for the lag, $\bar{h}_a$. For the single point swap $\lambda^+_{I2} = 0$ and $\lambda^-_{I2} = 0$.

For the exchange at $\bar{s}_{I1}$ the correction components are:

$$\lambda^+_{I1} = -d_{1,2}k(\bar{s}_{I1} + \bar{h}_a) + D_{1,2} \tag{4.35}$$

and

$$\lambda^-_{I1} = -d_{1,2}k(\bar{s}_{I1} - \bar{h}_a) + D_{1,2}.$$

For the exchange at $\bar{s}_{I2}$ the correction components are:

$$\lambda^+_{I2} = -d_{1,2}k(\bar{s}_{I2} + \bar{h}_a) + D_{1,2} \tag{4.36}$$

and

$$\lambda^-_{I2} = -d_{1,2}k(\bar{s}_{I2} - \bar{h}_a) + D_{1,2},$$

where

$$D_{1,2} = [k_{\bar{s}I1} + k_{\bar{s}I2}][k_{\bar{s}I1} - k_{\bar{s}I2}] \tag{4.37}$$

and

$$d_{1,2} = 2[k_{\bar{s}I1} - k_{\bar{s}I2}]. \tag{4.38}$$

Note that for the single point swap $k_{\bar{s}I2}$ is substituted by the permeability value sampled from the cdf.

Most of the computational cost in the simulated annealing algorithm is due to the update of the energy function. Since the number of computations for the single point swap are less than that of the two point swap, the single point swap formulation speeds up the algorithm. However, note that for the single point swap the cdf constraint of the algorithm is no longer satisfied.

The new variogram objective function due to the swap is written as:

$$E_1' = \sqrt{\sum_{i=1}^{N_d}\sum_{l=1}^{N_{h,l}}\left[\frac{\gamma_s^k(\bar{h}_{l,i}) + \lambda^k(\bar{h}_{l,i}) - \gamma_o(\bar{h}_{l,i})}{\gamma_o(\bar{h}_{l,i})}\right]^2}. \tag{4.39}$$

4.10.2 Well Test Component Update

The correction term for the well test component is a correction to the geometric permeability average in the theta direction, $\bar{k}_{gj}$, for each pressure derivative data point considered. The correction removes the contribution of permeability at one exchange point and adds the contribution of permeability to the other exchange point. Equation 4.10 is modified to account for the change of two exchanged locations $\bar{s}_{l1}$ and $\bar{s}_{l2}$ on the geometric permeability average, $\bar{k}_{gj}$:

$$\begin{aligned}\bar{k}_{gj}' = \exp[\{&A_{\eta_j}\ln\bar{k}_{gj} + A_{\bar{s}_{l2},j}\ln k_{\bar{s}_{l1}} - A_{\bar{s}_{l2},j}\ln k_{\bar{s}_{l2}} \\ &+ A_{\bar{s}_{l1},j}\ln k_{\bar{s}_{l2}} - A_{\bar{s}_{l1},j}\ln k_{\bar{s}_{l1}}\}/A_{\eta_j}],\end{aligned} \tag{4.40}$$

where $j = 1,2,3,.....N_r$

If the grid block at $\bar{s}$ falls completely outside the annular region between j-1 and j, then since $A_{\bar{s},j} = 0$, the contribution of the permeability $k_{\bar{s}}$, to the permeability average is 0 (see Figure 4.1). We then calculate the equivalent permeability, $\bar{k}_e$, for the correction term:

$$\frac{1}{\bar{k}_e'} = \sum_{j=1}^{N_r} w_j \frac{1}{\bar{k}_{gj}'}. \tag{4.41}$$

For Oliver's method the well test component of the energy function is calculated by the following equation:

$$E_2' = \sqrt{\sum_{i=1}^{N_t} \left[\frac{\bar{k}_e' - \hat{k}_i}{\hat{k}_i} \right]^2} \tag{4.42}$$

For the Inverse Solution Algorithm if the geometric average is used to approximate the equivalent radial permeability distribution, then only the update equation, Equation 4.12, is needed to determine the equivalent permeability. If the harmonic average is used to approximate the ISA permeability distribution then the following update equation is used:

$$\bar{k}_{hj}' = \frac{A_{rj}}{A_{rj}\bar{k}_{hj} + A_{\bar{s}_{j2},j}k_{\bar{s}_{j1}} - A_{\bar{s}_{j2},j}k_{\bar{s}_{j2}} + A_{\bar{s}_{n},j}k_{\bar{s}_{j2}} - A_{\bar{s}_{n},j}k_{\bar{s}_{j1}}}, \tag{4.43}$$

For ISA the well test component of the energy function is calculated by:

$$E_2' = \sqrt{\sum_{j=1}^{N_r} \left[\frac{\bar{k}_j' - \hat{k}_j}{\hat{k}_{ji}} \right]^2}, \tag{4.44}$$

where $\bar{k}'$ is either the area-based geometric or harmonic average of grid block permeabilities in annular rings defined by Equation 4.40 or 4.43, respectively.

4.11 Simulation Process

In this section we present a step by step outline of the simulated annealing algorithm. The algorithm is summarized in the flow chart shown in Figure 4.3. Numbers in the flow chart indicate a step in the algorithm below.

1. Generate the initial uncorrelated permeability distribution by the method described in Section 4.1
2. Calculate the sample variogram (Section 4.2) and the initial well test information (Section 4.3) for the initial distribution. The initial well test

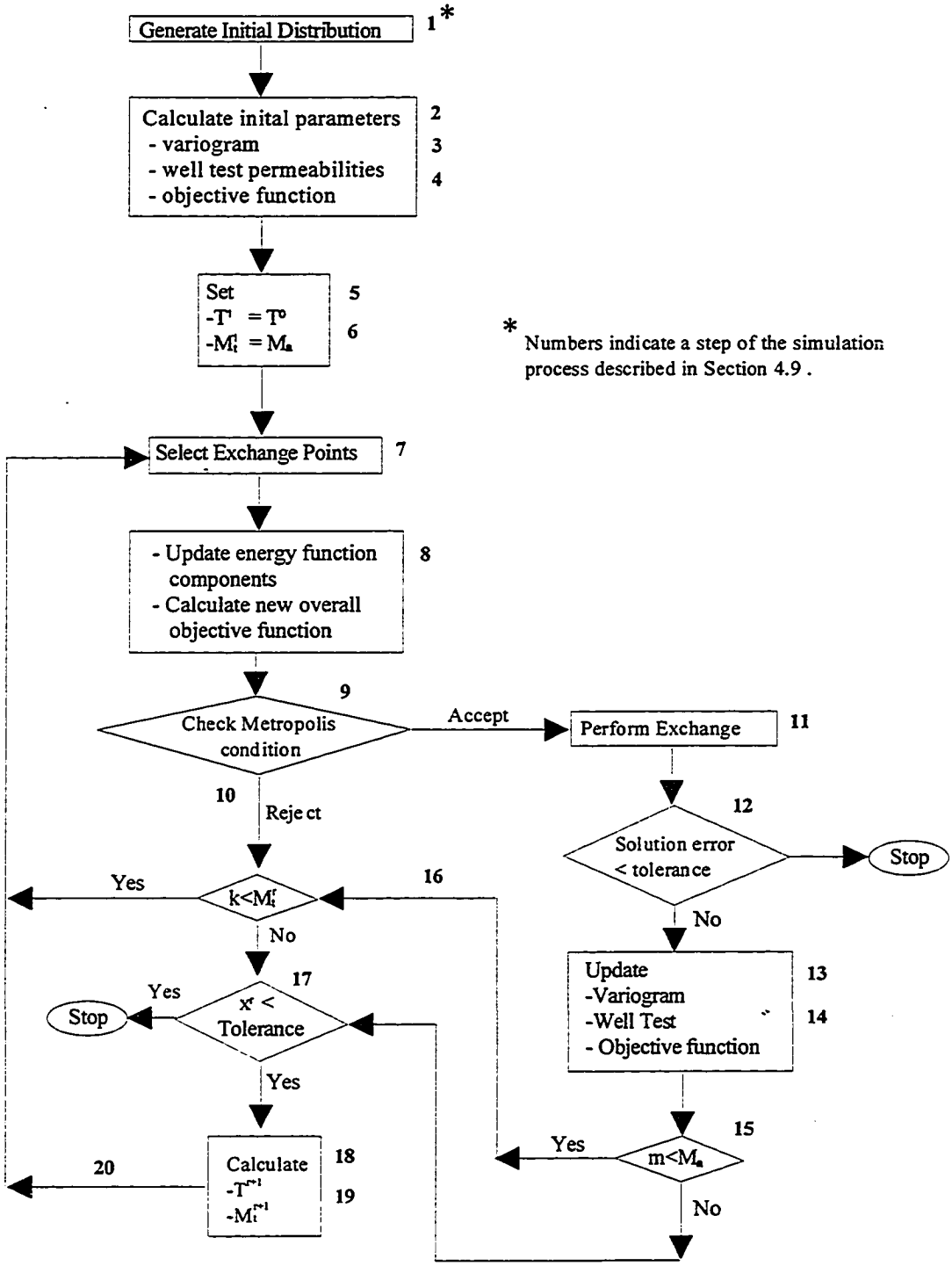

Figure 4.3 - Simulated annealing flow chart , incorporating geostatistical and well test information

information includes (i) the area of each grid block within the predefined radial grid (ii) the area-based geometric or harmonic grid block permeabilities within each annular region and/or (iii) for Oliver's method only, the equivalent permeability and corresponding weights determined by the kernel function.

3. Calculate each of the normalizing constants for each of the component objective functions (Section 4.4).
4. Calculate the component objective function weights by the procedure given in Section 4.5.
5. Calculate the value of the initial control parameter, T^o (Section 4.8) and set $T^l = T^o$.
6. For the first step, set the maximum number of iterations per step equal to M_a, i.e., $M_t^1 = M_a$ (Section 4.9).
7. Using the interchange mechanism described in Section 4.6 select two random locations in the simulation domain, $\vec{s}_{I1}$ and $\vec{s}_{I2}$.
8. Calculate the update of each component of the energy function (variogram and well test) using the procedure outlined in Section 4.10 and calculate the new overall energy function (Section 4.5).
9. By the procedure outlined in Section 4.7 check if the metropolis condition accepts the proposed interchange.
10. If the interchange is not accepted return to step 7.
11. If the interchange is accepted, then permanently exchange the permeabilities at the two selected swap points by assigning the original permeabilities at the swap points to temporary variables, i.e., $TV_1 = k_{\vec{s}_{I1}}$ and $TV_2 = k_{\vec{s}_{I2}}$. Then assign the permeability values at the new location: $k_{\vec{s}_{I1}} = TV_2$ and $k_{\vec{s}_{I2}} = TV_1$.
12. Check for convergence; if the tolerance condition of the objective function is satisfied. For Oliver's method this convergence criterion is,

$$\frac{E_1^k}{\sum_{i=1}^{N_d} N_{h,i}} + \frac{E_2^k}{N_{wt} + N_r} \leq \varepsilon_v. \tag{4.45}$$

For ISA the convergence criterion is

$$\frac{E_1^k}{\sum_{i=1}^{N_d} N_{h,i}} + \frac{E_2^k}{N_r} \leq \varepsilon_v. \tag{4.46}$$

ε_v is a convergence tolerance close to 0. If the convergence criteria are satisfied, then the simulation is stopped.

13. Update the sample variogram and corresponding variogram energy function for the next iteration level:

$$\gamma_s^{k+1}(\bar{h}_{l,i}) = \gamma_s'(\bar{h}_{l,i}) \quad \text{for } l = 1,\ldots N_{h,i} \text{ and } i = 1,\ldots N_d. \tag{4.47}$$

and

$$E_1^{k+1} = E_1'. \tag{4.48}$$

14a. For Oliver's method, update the area-based geometric average of the grid block permeabilities within annular regions, the equivalent permeability and the corresponding energy function:

$$\bar{k}_{g,j}^{k+1} = \bar{k}_{g,j}', \quad \text{for } j = 1,\ldots\ldots, N_r, \tag{4.49}$$

$$\bar{k}_{e,i}^{k+1} = \bar{k}_{e,i}', \quad \text{for } i = 1,\ldots\ldots N_t, \tag{4.50}$$

and

$$E_2^{k+1} = E_2'. \tag{4.51}$$

14b. For ISA update the area-based geometric or harmonic average of the grid block permeabilities within annular regions and the corresponding energy function:

$$\bar{k}_{g,j}^{k+1} = \bar{k}_{g,j}', \quad \text{for } j = 1,\ldots\ldots, N_r, \tag{4.52}$$

or

$$\overline{k}_{h,j}^{k+1} = \overline{k}_{h,j}^{r}, \quad \text{for } j = 1,\ldots\ldots,N_r, \tag{4.53}$$

and

$$E_2^{k+1} = E_2^{r}. \tag{4.54}$$

15. Check if the number of iterations is less than the maximum number of allowable iterations, if $m > M_a$ go to 17 or if $m \leq M_a$ go to 16.

16. Check if the number of iterations in a step r does not exceed the maximum number of total iterations per step, M_t^r. If $k \geq M_t^r$ then go to step 17. If $k < M_t^r$ then go to step 7.

17. Check the acceptance ratio tolerance for the current step. The acceptance ratio is the fraction of the total iterations in a step which were accepted by the metropolis condition (Section 4.7) and is given by

$$\chi^r = \frac{m}{k} \tag{4.55}$$

where m is the number of accepted iterations in the step r and k is the total number of iterations. The convergence criteria is

$$\chi^r \leq \varepsilon_a \tag{4.56}$$

ε_a is a convergence tolerance close to 0. If the convergence criteria is satisfied the simulation is stopped. This convergence does not imply a convergence of the objective function but ensures the algorithm does not run for extremely long times.

18. Calculate the control parameter for the next step using the procedure outlined in Section 4.7

19. Calculate the maximum number of iterations for the next step as described in Section 4.8.

20. Proceed to step 7.

CHAPTER V

RESERVOIR DESCRIPTION

In this chapter, we apply the simulated annealing algorithm to develop reservoir descriptions that simultaneously honor the spatial statistics (variogram) and the well test information, using the procedure described in Chapter IV. From the pressure transient response of a single well producing during a drawdown test in a heterogeneous reservoir, both Oliver's method and ISA are used to reproduce the permeability distribution. The reproduced reservoir images and their pressure and pressure derivatives are compared to their respective base cases. We also investigate the efficiency, in terms of computational cost, for both methods.

The effect of porosity variations on the pressure response for a single well producing in a heterogeneous porous medium is also investigated.

We consider the effect of anisotropy on the pressure response during a drawdown test. A gridding scheme for simulated annealing is developed; it allows for the incorporation of the pressure response due to anisotropy into an isotropic domain.

5.1 Incorporation of Well Test Data

Using the simulated annealing algorithm described in Chapter IV, permeability fields are reproduced such that the spatial and univariate statistics and the pressure transient data of the synthetic base case are honored. A numerical fluid flow drawdown

simulation of the regenerated permeability field is performed using ECL 100. The reservoir properties are the same as in the base cases and are summarized in Table 3.2. The pressures and pressure derivatives are compared to the base case pressure responses. The input parameters for the simulated annealing algorithm are:

- the univariate statistics (cdf),
- the spatial statistics (variogram),
- the conditioning data,
- the instantaneous permeability, $\hat{k}$, for N_t time steps for Oliver's solution, or
- the equivalent radial permeability distribution, $\bar{k}_{ISA}$, determined by ISA.

Each distribution is conditioned such that the center grid block permeability where the well is located is the permeability of the base distribution. It should be noted that Turning Bands does a poor job of reproducing the input variogram. Therefore, the variogram of the base distribution was recalculated using the Xgam program in GSLIB.[13] We present both the Oliver's solution and ISA results.

5.1.1 Oliver's Solution Results

Example 1

In the first example, we consider the permeability field shown in Figure 3.1 and corresponding pressure response shown in Figure 3.3 as the truth case. From a qualitative global radial perspective we observe that the permeability field in this example exhibits a region of higher permeability near the flowing well located at the center of the reservoir

and reduced permeability nearer the outer no-flow boundaries. This effect is also shown by the pressure derivative which has a lower value at early times and a higher value at later times. Typical well test interpretation of the pressure derivative would indicate the behavior of two-zone composite reservoir.

The input parameters for the simulated annealing algorithm are summarized in Table 5.1 Multiple realizations, honoring the same constraints, are generated by changing only the seed value to generate random numbers. Figure 5.1a is the base case permeability distribution and Figures 5.1b-5.1f are multiple realizations honoring the same constraints. A comparison between the pressures and pressure derivatives of the base case and simulated cases are shown in Figure 5.2.

The match between the pressures and the pressure derivatives of the base case and simulated cases show a good agreement. The simulation statistics also show an excellent match between the input and simulated variogram. Figure 5.3 shows the pressures and pressure derivatives of realizations generated by constraining them only to the univariate and spatial statistics, but *not* to pressure transient data. Note that for these cases the pressure response is reproduced poorly.

Example 2

We also present a second case study, where the permeability has a higher variance indicating a higher degree of heterogeneity. The base case permeability field is shown in Figure 5.4a and the reproduced permeability distributions are shown in Figure 5.4b-5.4f. Figure 5.5 shows the fluid flow simulation results of the pressure responses compared to the base case pressure response. Figure 5.6 shows pressure responses of reproduced permeability fields that do not honor the well test constraint. Once again, we observe that the pressure response is more effectively reproduced when the well test constraint is taken into consideration.

Table 5.1 - Simulated Annealing Input Data-Oliver's Solution

Number of grid blocks (x,y,z)	115x115x1
Block dimensions ($\Delta x, \Delta y, \Delta z$)	35*ft* x 35*ft* x 10*ft*
Variogram type	Spherical - isotropic
Sill	440.0
Range	590.0 *ft*

Well Test Information

n	t (days)	r_{min}	r_{max}	$\hat{k}$
1	1.16×10^{-3}	5.4	105.6	32.41
2	2.29×10^{-3}	7.6	148.3	31.22
3	4.37×10^{-3}	10.5	204.9	28.60
4	9.08×10^{-3}	15.1	295.4	24.86
5	1.93×10^{-2}	22.1	430.7	20.98
6	3.46×10^{-2}	29.6	576.3	18.54
7	5.71×10^{-2}	38.0	740.5	17.08
8	8.74×10^{-2}	47.0	916.3	16.29
9	1.25×10^{-1}	56.1	1093.5	15.92
10	2.19×10^{-1}	74.3	1449.5	15.76
11	2.90×10^{-1}	85.6	1668.4	15.71
12	4.12×10^{-1}	102.0	1988.6	15.38

Conditioning Data	$x(ft)$	$y(ft)$	$z(ft)$	$k_{\bar{s}}(md)$
	2012.5	2012.5	17.5	34.3

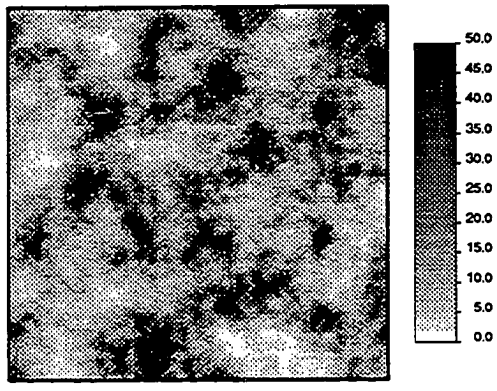

Figure 5.1a - Base case permeability distribution generated by Turning Bands (range = 600 ft $\sigma^2_{\ln k} = 0.92$).

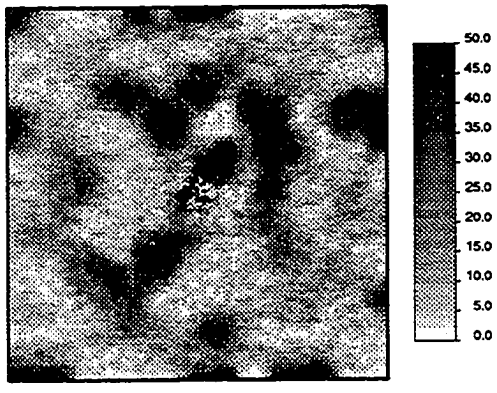

5.1b (Seed = 107935)

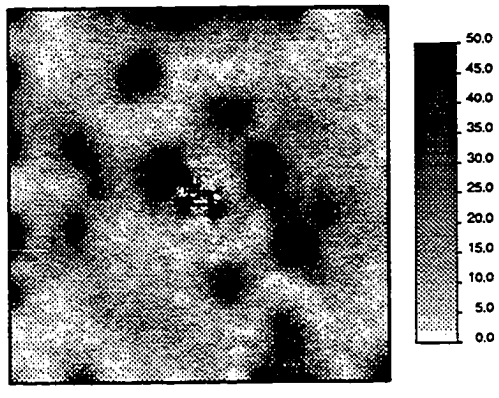

5.1c (Seed = 1079602)

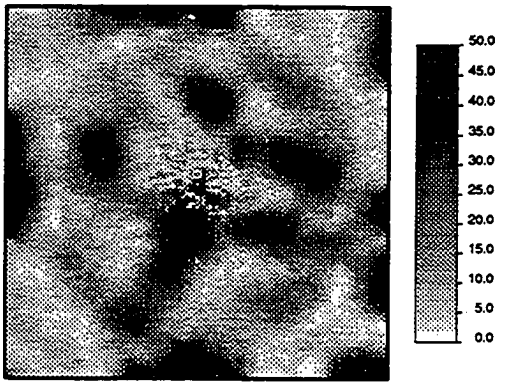

5.1d (Seed = 1079623)

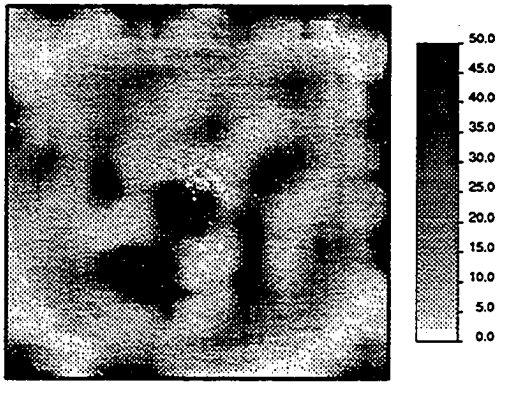

5.1e (Seed = 1079635)

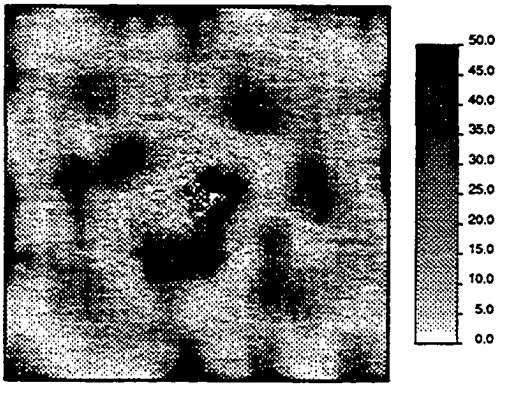

5.1f (Seed = 1079602)

Figure 5.1b - 5.1f - Simulated permeability distributions honoring variogram and Oliver well test constraints

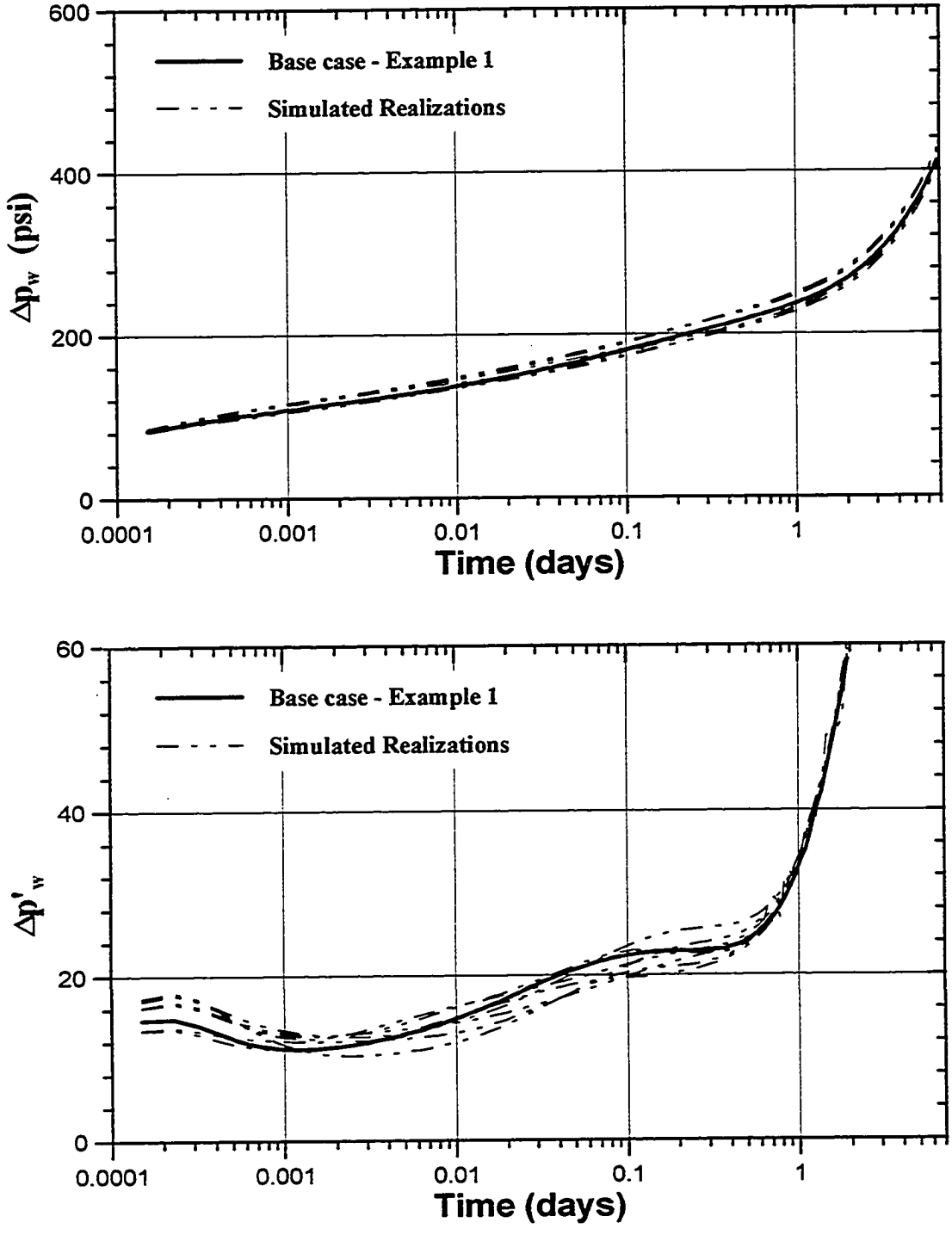

Figure 5.2 - Pressures and pressure derivatives of simulated permeability realizations honoring variogram and well test constraints compared to the base case response for example 1.

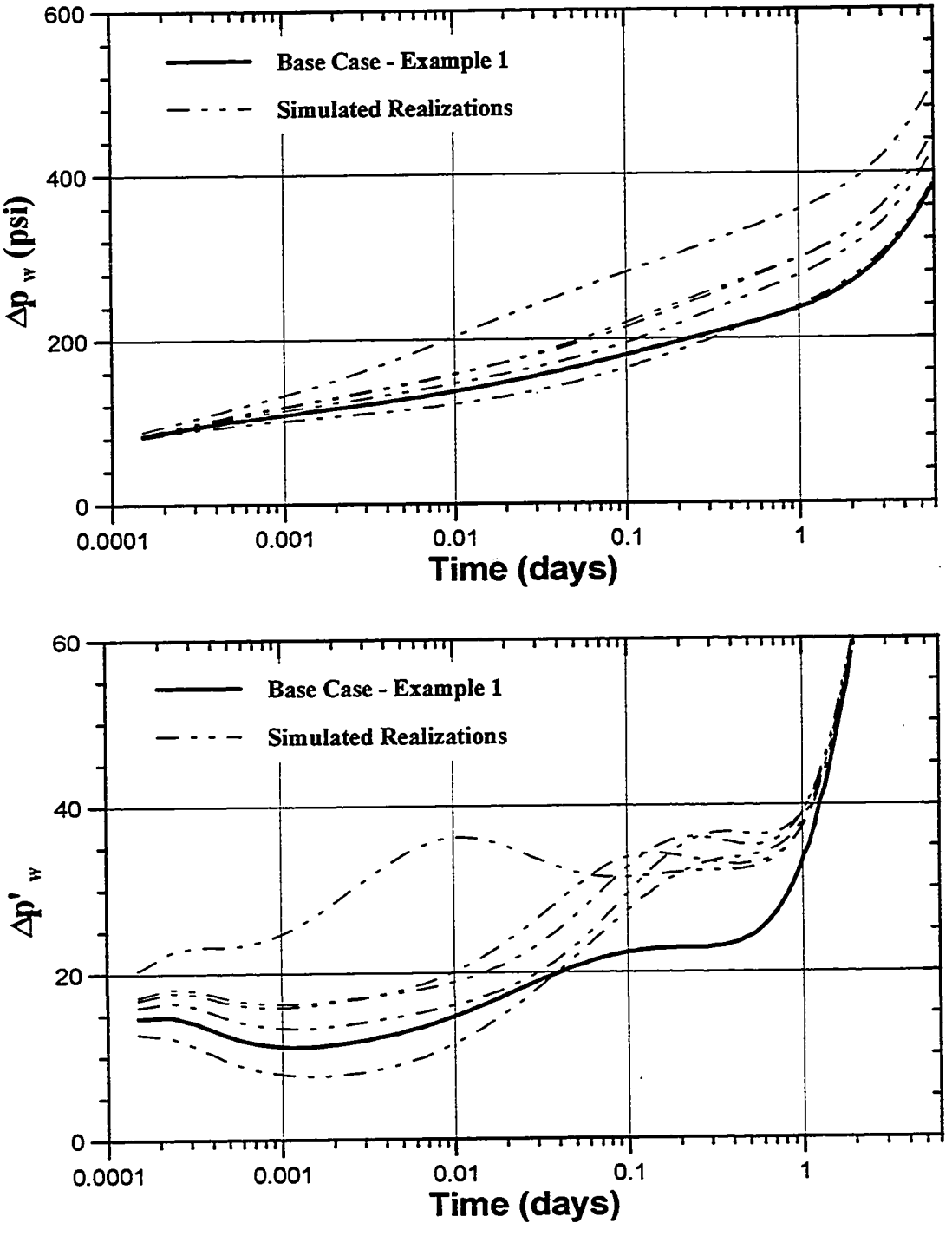

Figure 5.3 - Pressures and pressure derivatives of simulated permeability realizations honoring only the variogram constraint compared to the base case response for example 1.

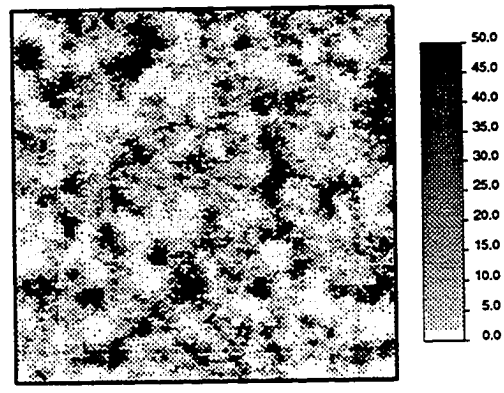

Figure 5.4a - Base case permeability distribution generated by Turning Bands (range = 310 ft $\sigma^2_{\ln k} = 1.61$).

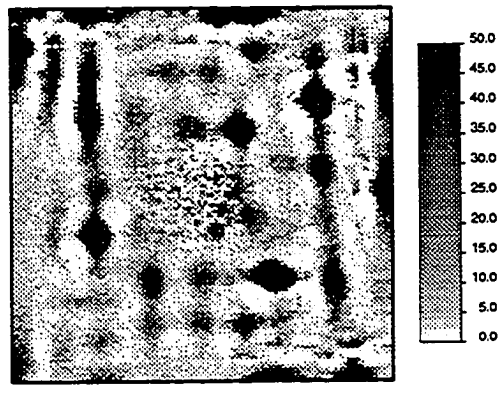

5.4b (seed = 1079601)

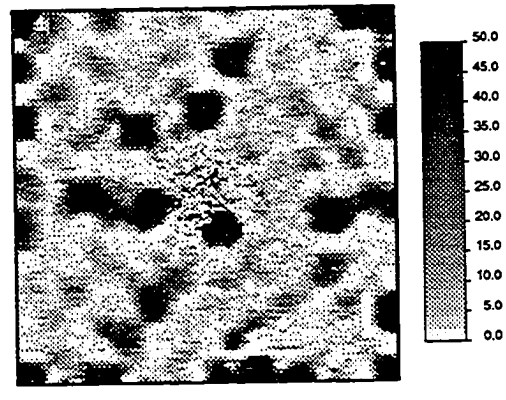

5.4c (Seed = 1079616)

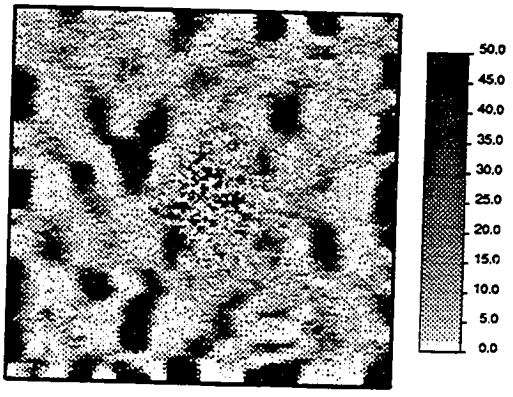

5.4d (Seed = 1079616)

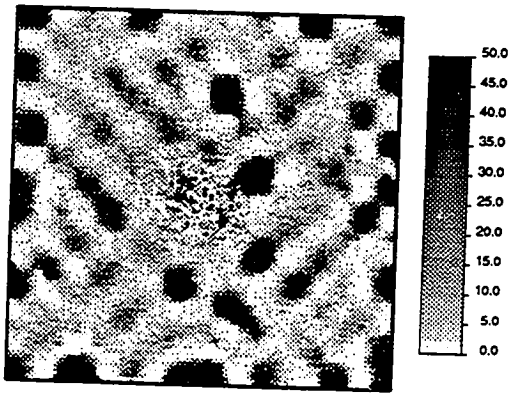

5.4e (Seed = 1079620)

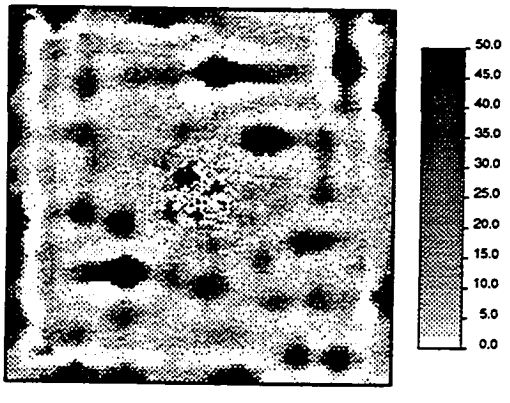

5.4f (Seed = 1079633)

Figure 5.4b - 5.4f - Simulated permeability distributions honoring variogram and Oliver well test constraints

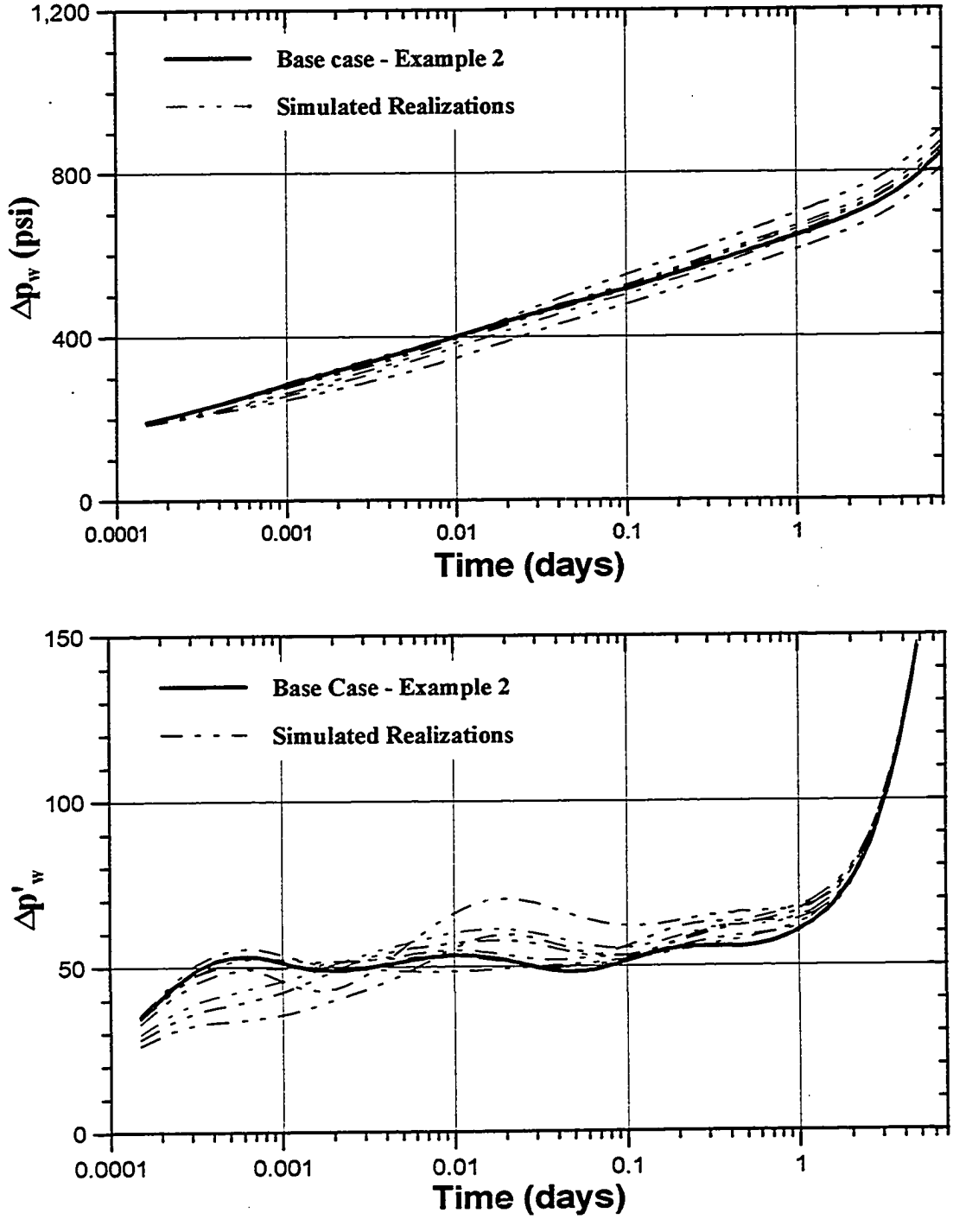

Figure 5.5 - Pressures and pressure derivatives of simulated permeability realizations honoring variogram and well test constraints compared to the base case response for example 2.

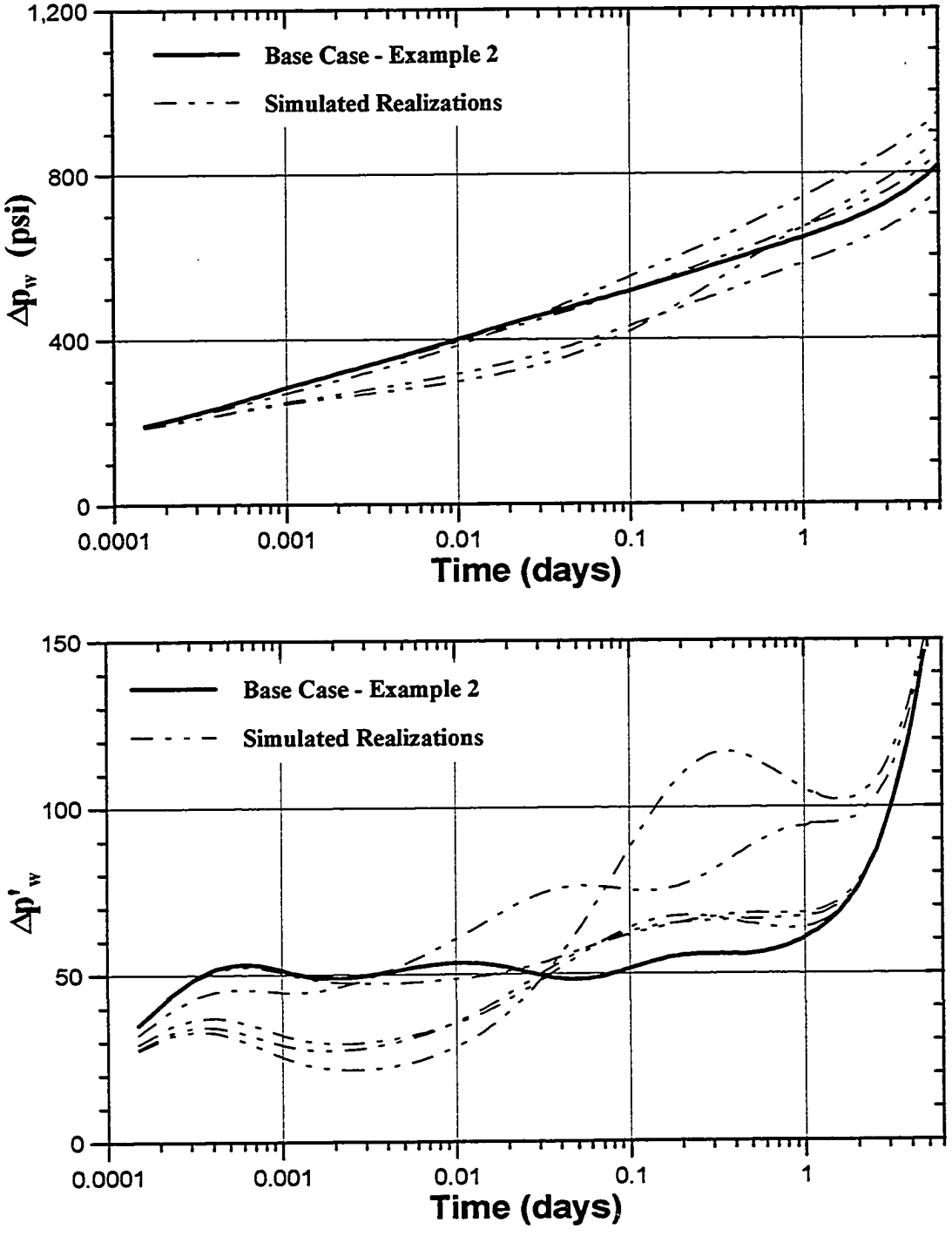

Figure 5.6 - Pressures and pressure derivatives of simulated permeability realizations honoring only the variogram constraint compared to the base case response for example 2.

Example 3

Figure 5.7a shows the base case permeability field for this example and Figures 5.7b-5.7f show simulated permeability fields honoring the spatial statistics and well test information constraints. Note that for this particular example the correlation range of the variogram is 2100 ft which is half the length of one side of the reservoir. From a qualitative perspective the permeability values near the center of the reservoir appear to be lower than those further away and the distribution of permeabilities have a radial characteristic. A comparison of pressures and pressure derivatives to the base case are shown in Figure 5.8. Figure 5.9 shows pressure responses for the same case for which the well test information is not honored and only the variogram is honored in regenerating the distribution. The pressure response for these cases is reproduced poorly.

The heterogeneity parameters for the three examples are given in Table 5.2.

Table 5.2- Summary of Heterogeneity Parameters for the Examples Investigated

	$\sigma^2_{\ln k}$	Range (ft)	HI	V
Example 1	0.92	600	0.124	0.6
Example 2	1.61	310	0.20	0.8
Example 3	0.92	2100	0.45	0.6

The heterogeneity index is defined in Reference 45 as:

$$H.I.=\frac{\sigma^2_{\ln k} range}{\Delta x N_x}, \qquad (5.1)$$

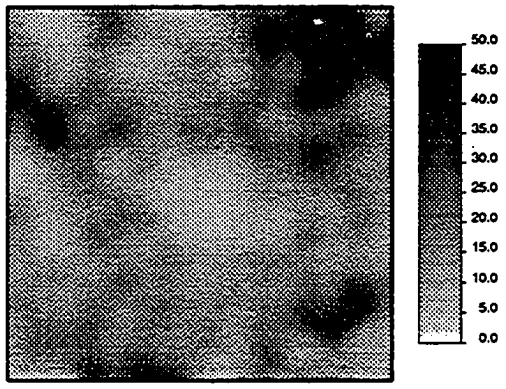

Figure 5.7a - Base case permeability distribution generated by Turning Bands (range = 2100ft $\sigma^2_{\ln k} = 0.92$).

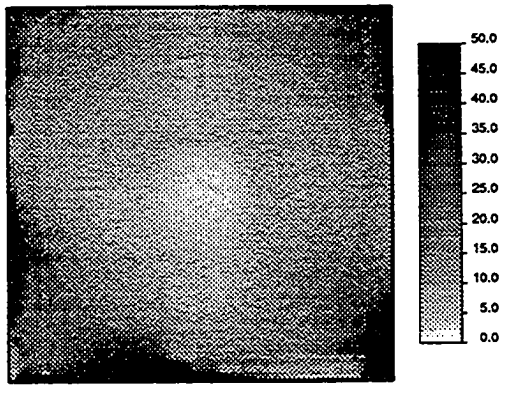

5.7b (seed = 1079613)

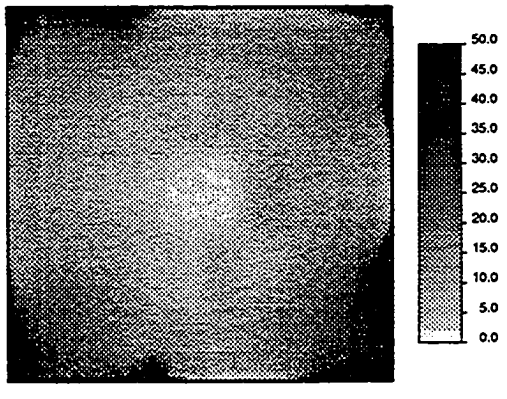

5.7c (Seed = 1079608)

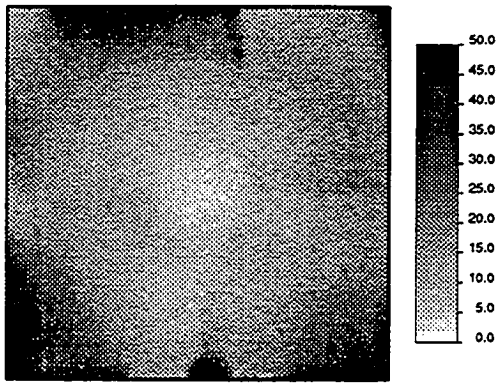

5.7d (seed = 1079622)

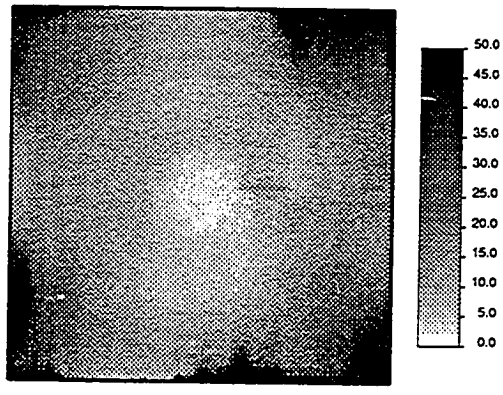

5.7e (seed = 1079635)

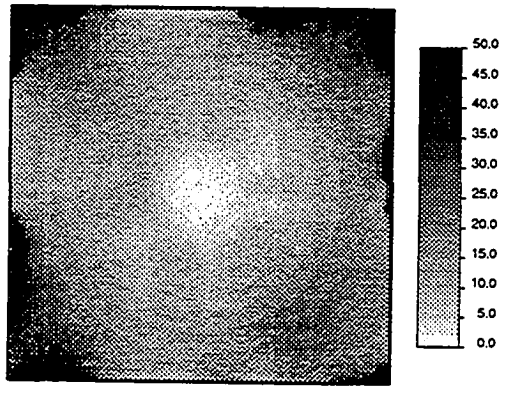

5.7f (Seed = 1079643)

Figure 5.7b - 5.7f - Simulated permeability distributions honoring variogram and Oliver well test constraints

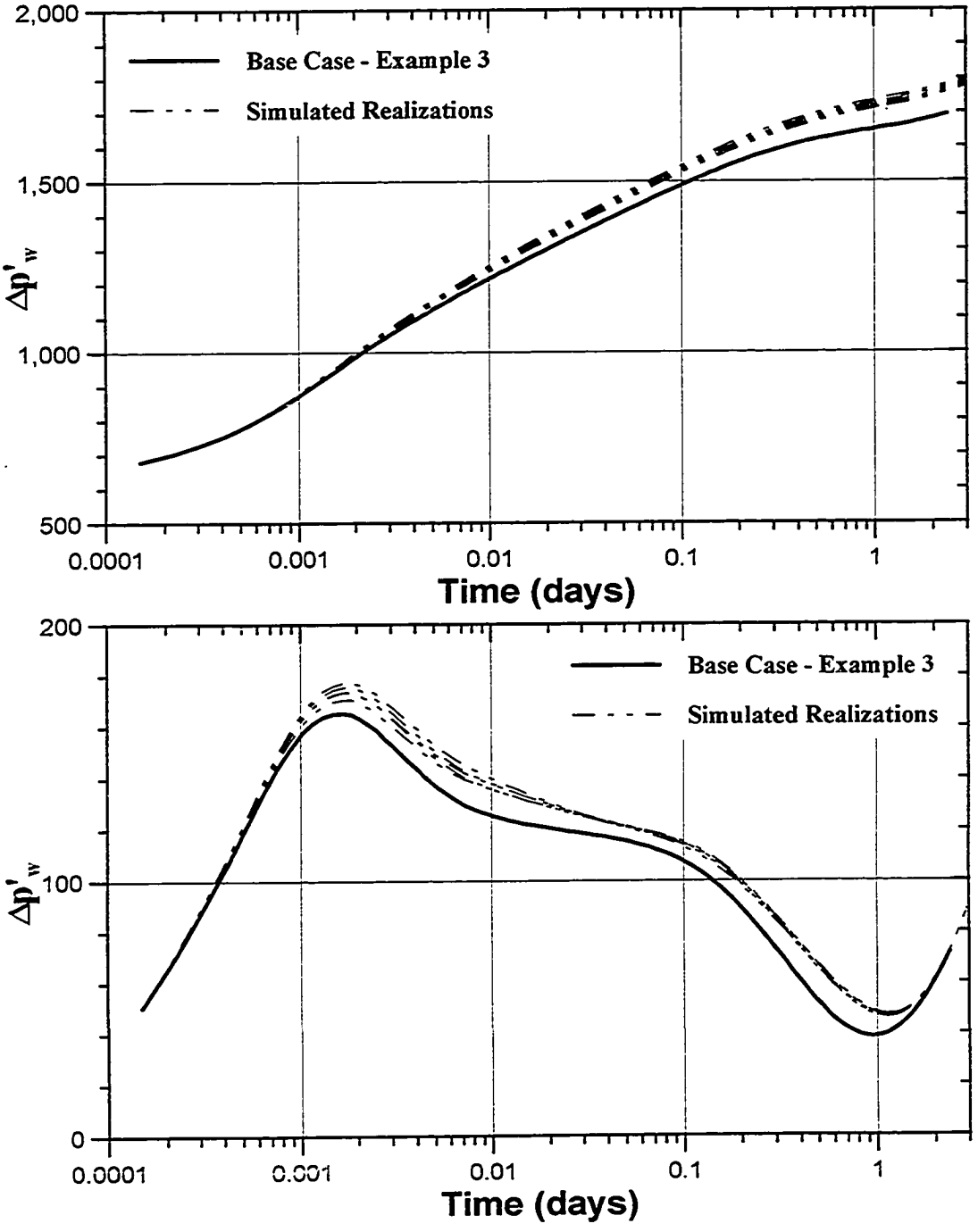

Figure 5.8- Pressures and pressure derivatives of simulated permeability realizations honoring variogram and well test constraints compared to the base case response for example 3.

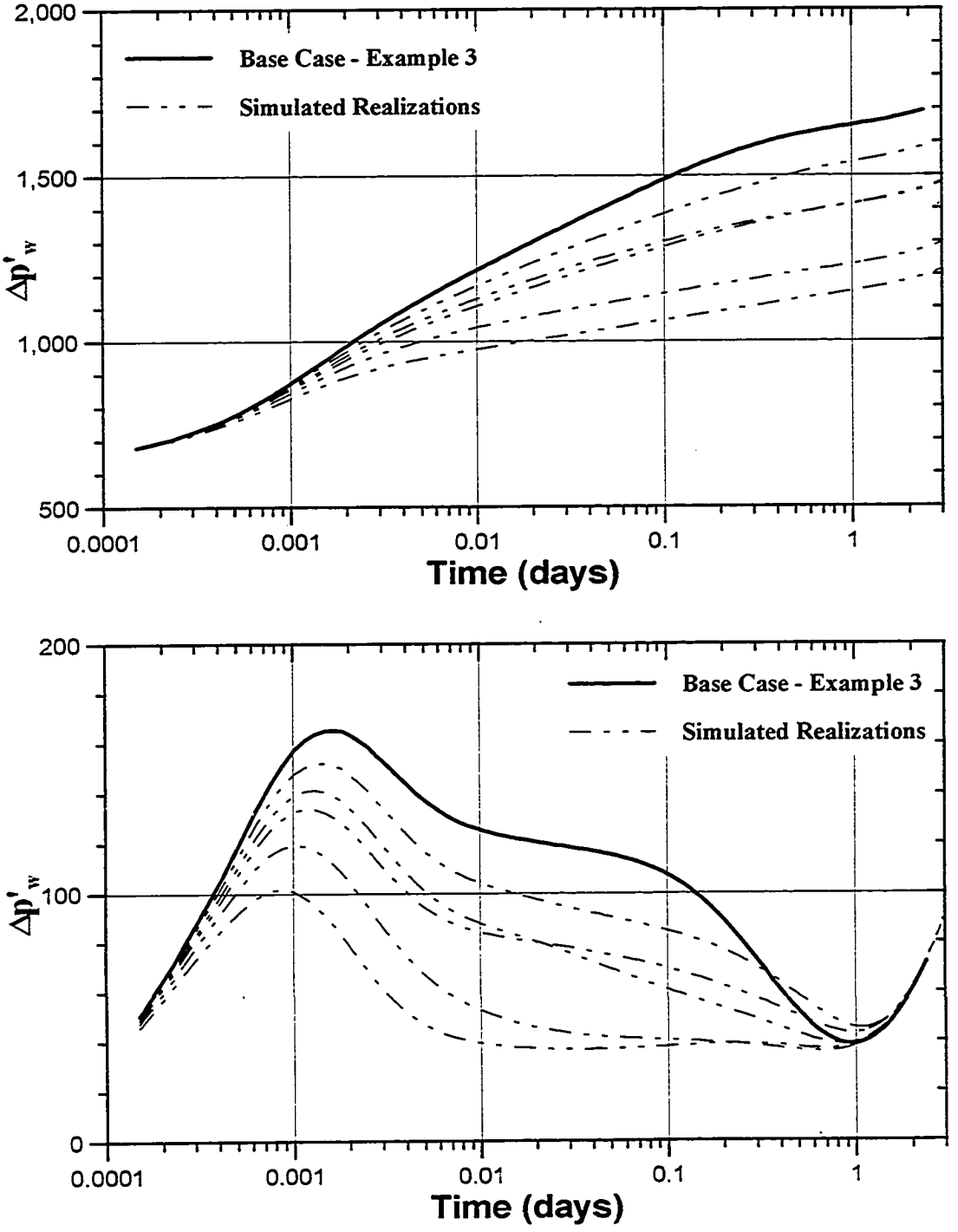

Figure 5.9 - Pressures and pressure derivatives of simulated permeability realizations honoring only the variogram constraint compared to the base case response for example 3.

Reference 46 defines the Dykstra Parson's coefficient, V, as:

$$V = 1 - \frac{1}{\exp(\sigma^2_{\ln k})}. \tag{5.2}$$

Note that for example 1 and 3 the multiple generated realizations consistently reproduce the pressures and pressure derivatives that match the base case pressure response. However, in example 2, the pressure responses of the simulated cases are not as consistent in reproducing the base case response. Note that, in example 2 the variance of the distribution is high and the range is low. For practical purposes, the pressure derivative shown in Figure 5.5, for this example may be considered as that of a homogeneous reservoir. The "homogeneous" pressure response is also observed for reservoirs in which the permeability distribution is completely random, i.e., the permeability distribution has no spatial correlation. This effect may apply to example 2-- the base case permeability distribution with the low correlation range shown in Figure 5.4a results in a relatively constant instantaneous well test permeability, $\hat{k}$, as shown in Figure 5.10. The equivalent permeability, $\bar{k}_e$, calculated by Oliver's method is also relatively constant as shown in Figure 5.10. The overall effect is that the pressure response is that of a homogeneous or completely random heterogeneous reservoir. This can be attributed to the low correlation range of the variogram used to develop the description and the reservoir image can interpreted to be that of a permeability distribution that is completely random (see Figure 5.4a).

5.1.2 ISA Results

In Section 3.2.2.2, it was observed that both the area based geometric average, $\bar{k}_g$, and the area based harmonic average, $\bar{k}_h$, give reasonable approximations to the ISA radial permeability distribution, k_{ISA}. We consider examples in which both averaging

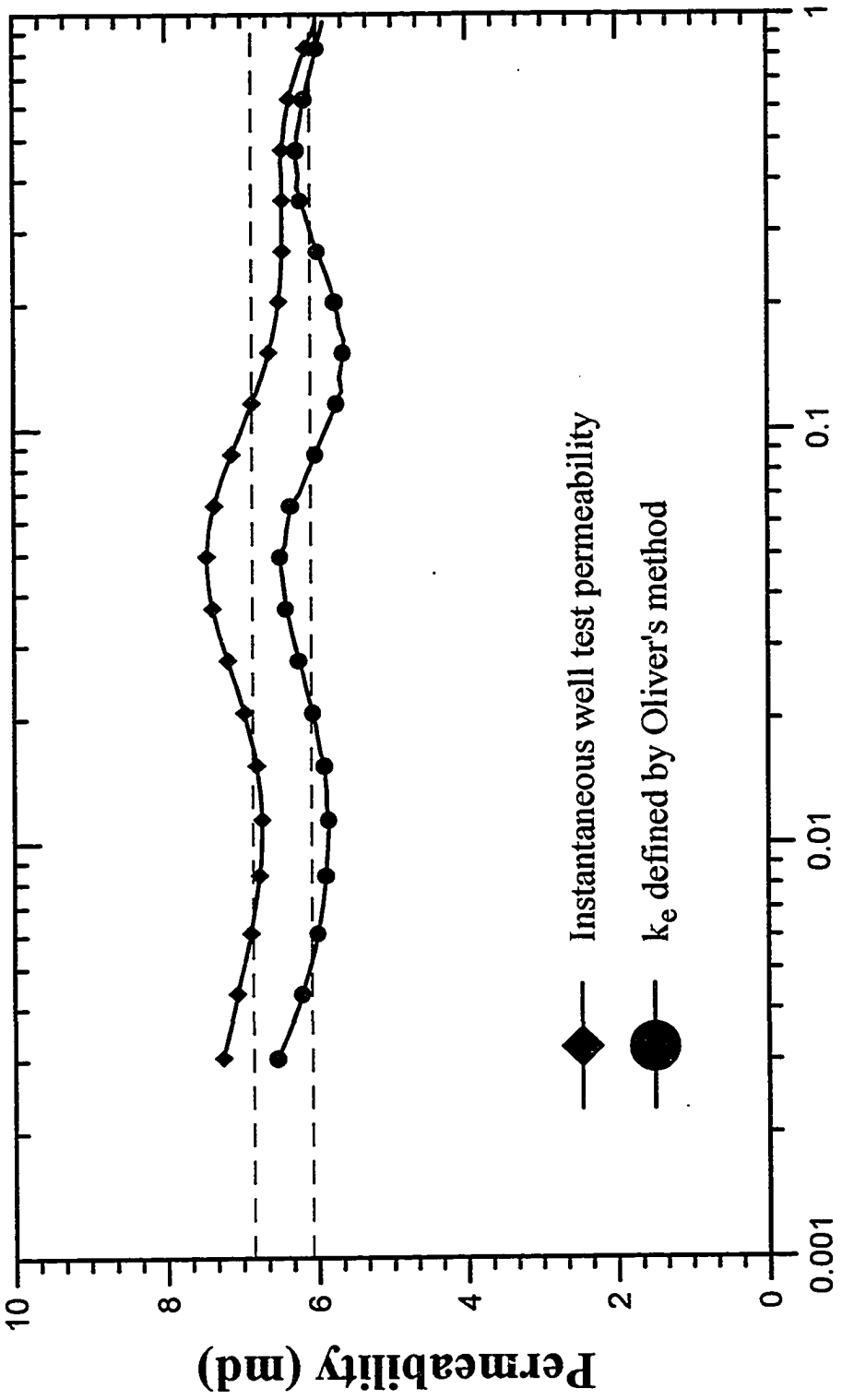

Figure 5.10 - Illustration of the instantaneous well test permeability and the Oliver derived permeability, k_e, for example 2.

techniques are used to generate the areal permeability distribution using the simulated annealing procedure given in Chapter IV. The equivalent radial permeability distribution derived by ISA, k_{ISA}, the conditioning data, and the univariate and spatial statistics are honored in the annealing algorithm.

The input parameters for the first example are given in Table 5.3. The truth case is the areal permeability distribution shown in Figure 3.1 with the pressure response shown in Figure 3.3.

Figures 5.11b-5.11c show the reproduced permeability fields honoring the input constraints. Figure 5.11a shows the base case for this example. The area based geometric average, $\bar{k}_g$, is used to approximate the ISA equivalent permeability, k_{ISA}. Figure 5.12 compares the pressure responses of the multiple realizations to the base case pressure response.

Figure 5.13a-5.13c shows the reproduced permeability distributions, where the area based harmonic average, $\bar{k}_h$, is used to approximate k_{ISA}. The base case permeability field is shown in Figure 5.11a. Figure 5.14 compares the pressure response of the multiple realizations to the base case pressure response.

For this example, we observe that when we perform harmonic averaging of grid block permeabilities within our radii of investigation to produce our distribution, the resulting pressure response matches the base case pressure response better than geometric averaging of grid block permeabilities.

Figure 5.15 shows the pressure and pressure derivative response compared to the base response for a second example. In this case geometric averaging of grid block permeabilities was used. Figure 5.16 shows the pressure response for the same example, where harmonic averaging of grid block permeabilities is used. When harmonic averaging is used the pressure derivative is better reproduced; however, the geometric averaging reproduces the pressure better.

Table 5.3 - Simulated Annealing Input Data - ISA

Number of grid blocks (x,y,z)	115x115x1
Block dimensions (Δx,Δy,Δz)	35*ft* x 35*ft* x 10*ft*
Variogram type	Spherical - isotropic
Sill	440.0
Range	590.0 *ft*

Well Test Information

n	r_{min}	r_{max}	k_{ISA}
1	64.53	91.40	33.18
2	91.40	115.8	34.28
3	115.8	138.24	23.04
4	138.24	159.92	20.33
5	159.92	181.71	19.72
6	181.71	203.98	19.13
7	203.98	227.00	18.00
8	227.00	250.92	16.51
9	250.92	275.96	15.02
10	275.96	302.98	13.75
11	302.98	330.19	12.74
12	330.19	360.05	12.04
13	360.05	392.24	11.60
14	392.24	427.29	11.40
15	427.29	465.88	11.43
16	465.88	508.73	11.69
17	508.73	556.52	12.05
18	556.52	610.10	12.42
19	610.10	670.46	12.74
20	670.46	738.57	12.99
21	738.57	815.63	13.17
22	815.63	902.83	13.33
23	902.83	1001.22	13.45
24	1001.22	1111.72	13.47
25	1111.72	1234.12	13.23
26	1234.12	1366.35	12.43
27	1366.35	1504.50	10.98

Conditioning Data	$x(ft)$	$y(ft)$	$z(ft)$	$k_{\bar{s}}(md)$
	2012.5	2012.5	17.5	34.3

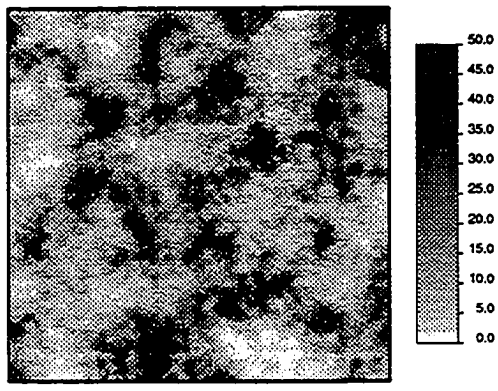

Figure 5.11a - Base case permeability distribution generated by Turning Bands (range = 600 ft $\sigma^2_{\ln k} = 0.92$).

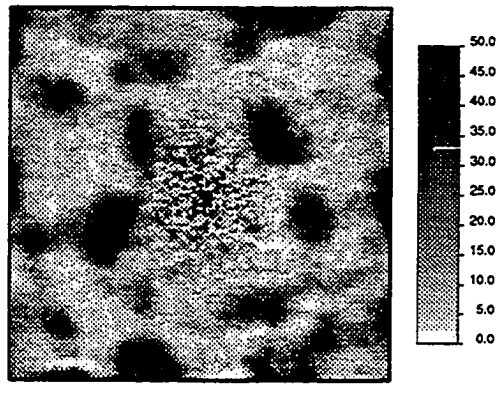

5.11b (Seed = 1079607)

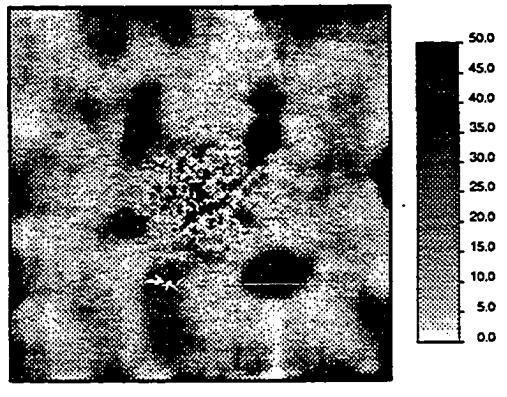

5.11 c (Seed = 1079622)

Figure 5.11b-5.11c - Simulated permeability distributions honoring variogram and ISA permeability distribution with a geometric area based permeability average

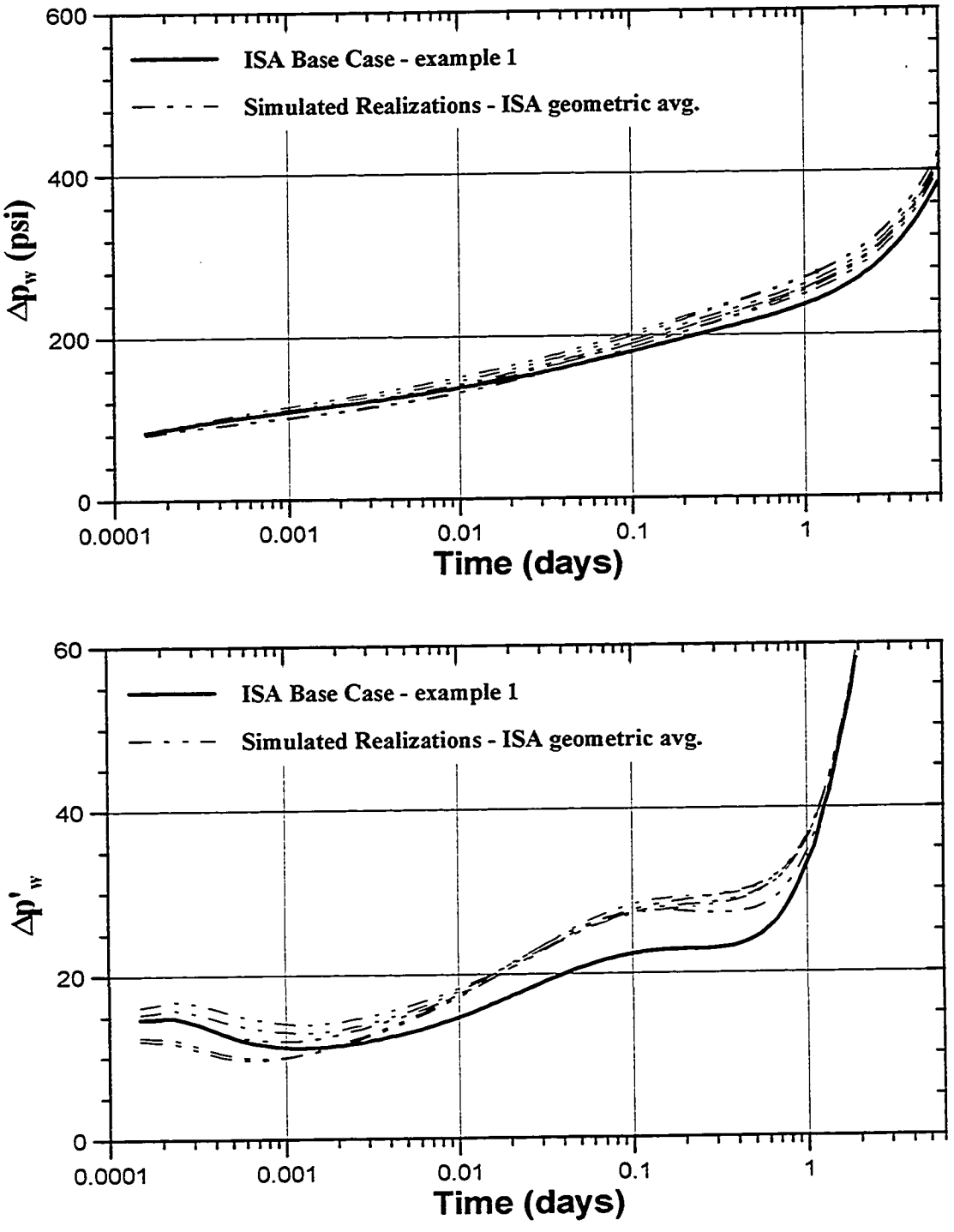

Figure 5.12 - Pressure and pressure derivative of simulated permeability fields honoring variogram and well test constraints compared to the base case response. k_{ISA} is approximated by $\overline{k_g}$.

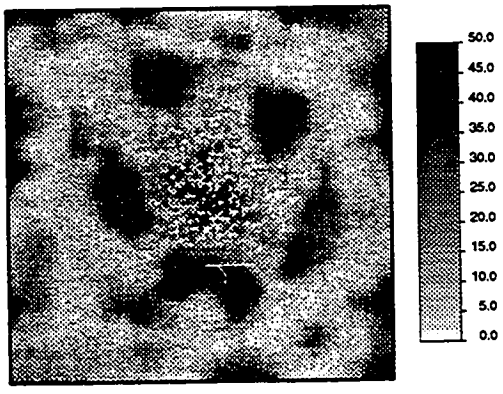

5.13a (Seed = 1079613)

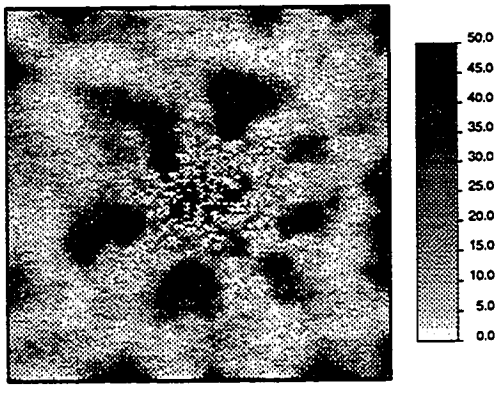

5.13b (Seed = 1079630)

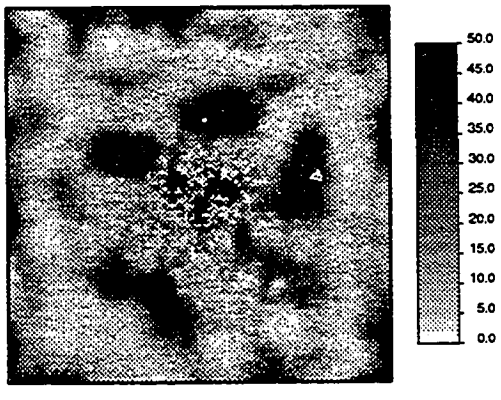

5.13c (Seed = 1079614)

Figure 5.13a-5.13c - Simulated permeability distributions honoring the variogram and the ISA radial permeability distribution with an area based harmonic permeability average.

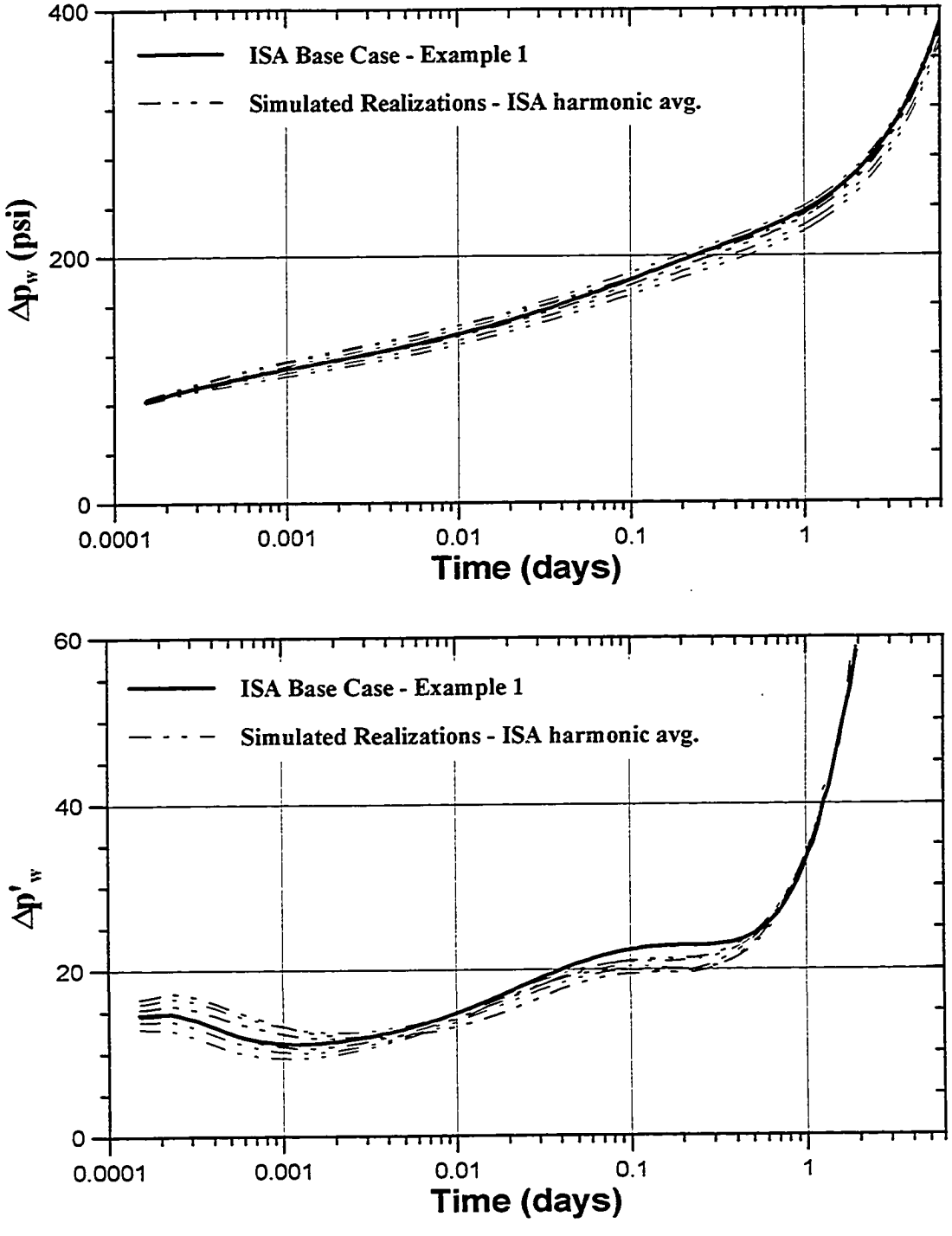

Figure 5.14 - Pressure and pressure derivative of simulated permeability fields honoring variogram and well test constraints compared to the base case response. k_{ISA} is approximated by $\bar{k}_h$.

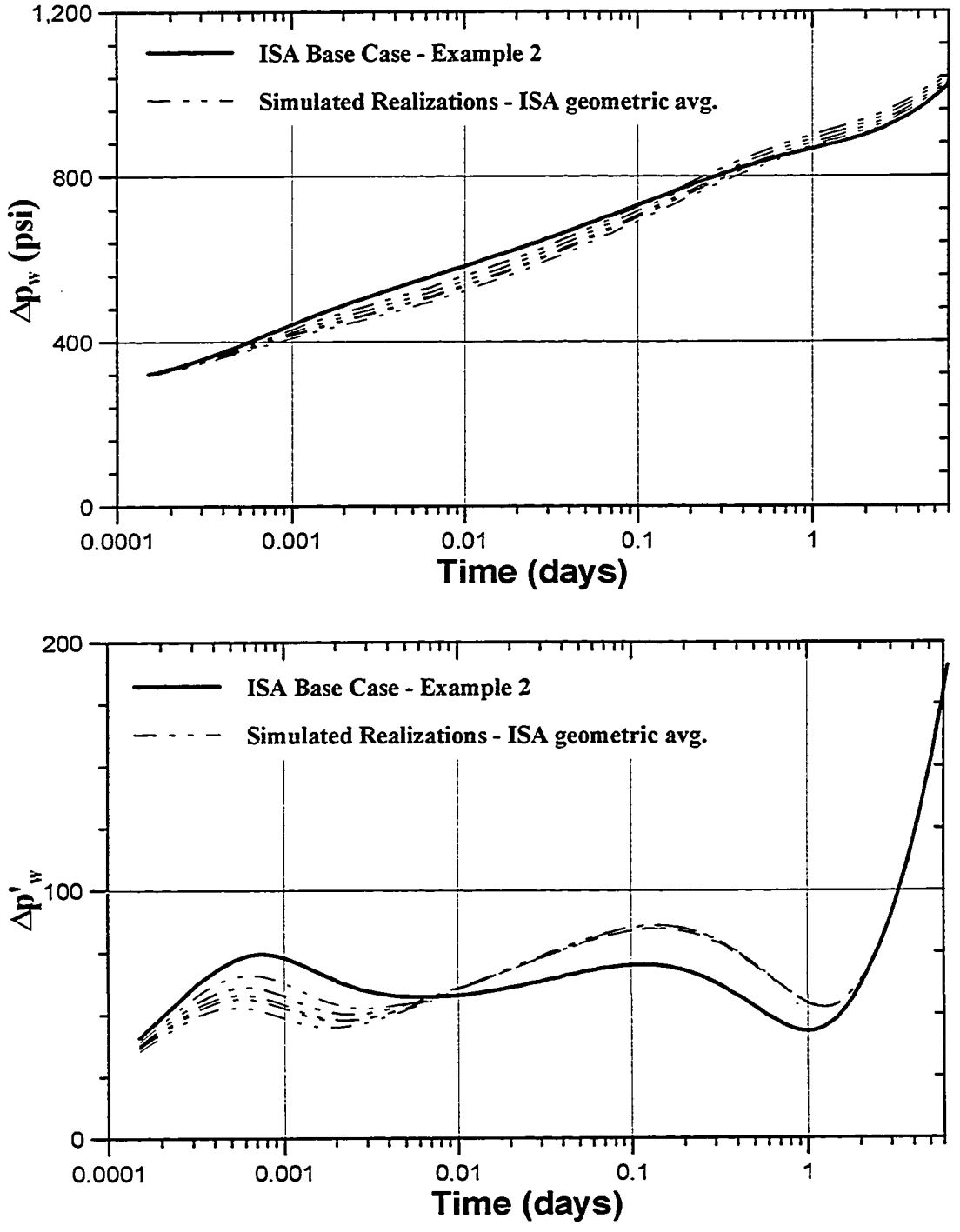

Figure 5.15 - Pressure and pressure derivative of simulated permeability fields honoring variogram and well test constraints compared to the base case response. k_{ISA} is approximated by $\bar{k}_g$.

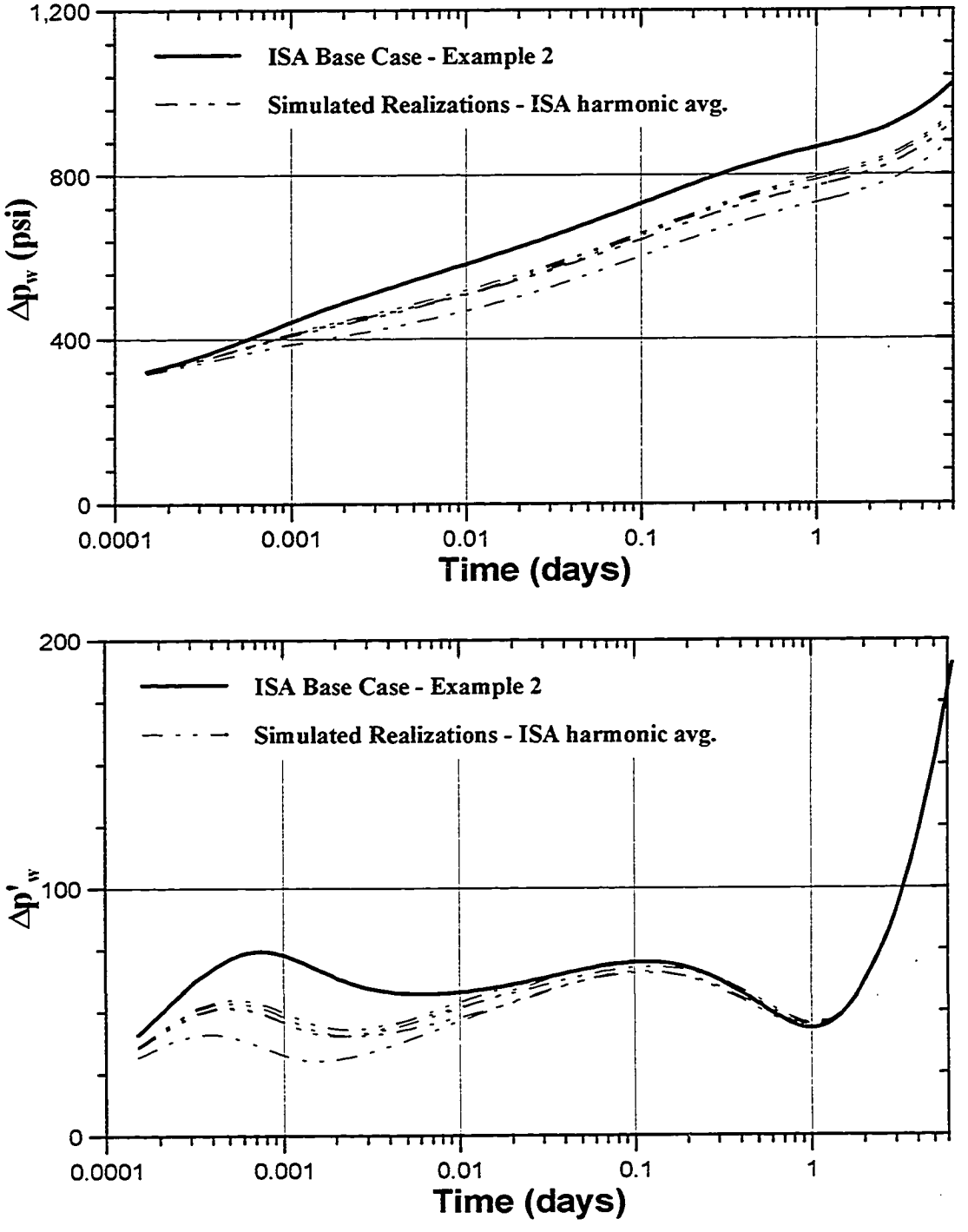

Figure 5.16 - Pressure and pressure derivative of simulated permeability fields honoring variogram and well test constraints compared to the base case response. k_{ISA} is approximated by $\overline{k_h}$.

In general, for all the realizations generated by the two methods to incorporate well test information (Oliver or ISA procedure), we observe that the reproduced images of the permeability distribution, do not agree with the base case images. We also observe that the reproduced permeability images are characteristically radial in appearance. This is expected, since the simulated annealing algorithm is constrained only to the variogram and a radial permeability distribution. In order to generate a more realistic image we would have to include more constraints, such as more conditioning data and production data. Incorporating production data constraints such as primary and secondary recovery information are described in Reference 27.

5.1.3 Computational Cost of Each Method

The advantage of using the ISA algorithm is that the simulated annealing procedure considering ISA is faster than that considering the Oliver procedure. This is clearly illustrated in Figure 5.17; for the same convergence tolerance, the Oliver procedure requires greater CPU time. We also observe that for the ISA procedure the update of the well test component of the energy function consumes less time than the update of the variogram component, where as in the Oliver method the well test update consumes the most time. This is because, ISA defines an equivalent permeability within an inner and outer radius of investigation and there is no overlap of the different radii of investigation.

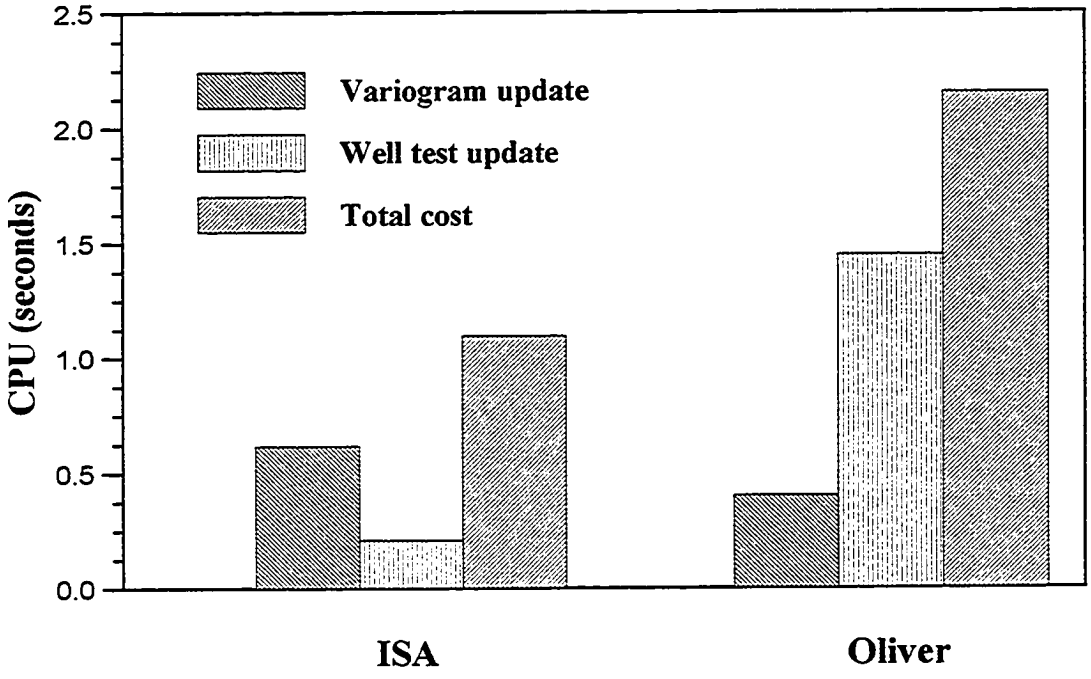

Figure 5.17 - Illustration of the CPU consumption of the simulated annealing algorithm for the ISA and Oliver method.

5.2 Effect of Porosity Variation

So far, we have presented cases in which we have studied heterogeneous reservoirs with variations in permeability only. In this section, we investigate the effect of porosity variations on the pressure response of a reservoir during a drawdown test. In our analysis we consider a procedure similar to that outlined by Feitosa.[2] He considered permeability and porosity heterogeneities for an r-θ distribution. We consider permeability heterogeneities for an x-y areal distribution.

We generate two base case heterogeneous systems. For the first case, we generate a heterogeneous reservoir with variable permeability and porosity. The base case permeability distribution is shown in Figure 5.18 and the histogram of the distribution in Figure 5.19. A permeability-porosity transform is performed using the following equation given in Reference 50:

$$\phi = \left[\frac{\sqrt{k}S_{wi}}{100}\right]^{1/.225}, \tag{5.3}$$

where S_{wi} is the irreducible water saturation, which in our case is assumed to be 0.3. The transform of permeability values to porosity values by this equation is shown in Figure 5.20.

In the second case, we consider the same permeability distribution shown in Figure 5.18 with a constant porosity of 0.144. This is the average porosity of the transformed porosity distribution determined by Equation 5.3.

For both cases a fluid simulation is performed in the heterogeneous medium using ECL 100. The resulting pressures and pressure derivatives are shown in Figure 5.21.

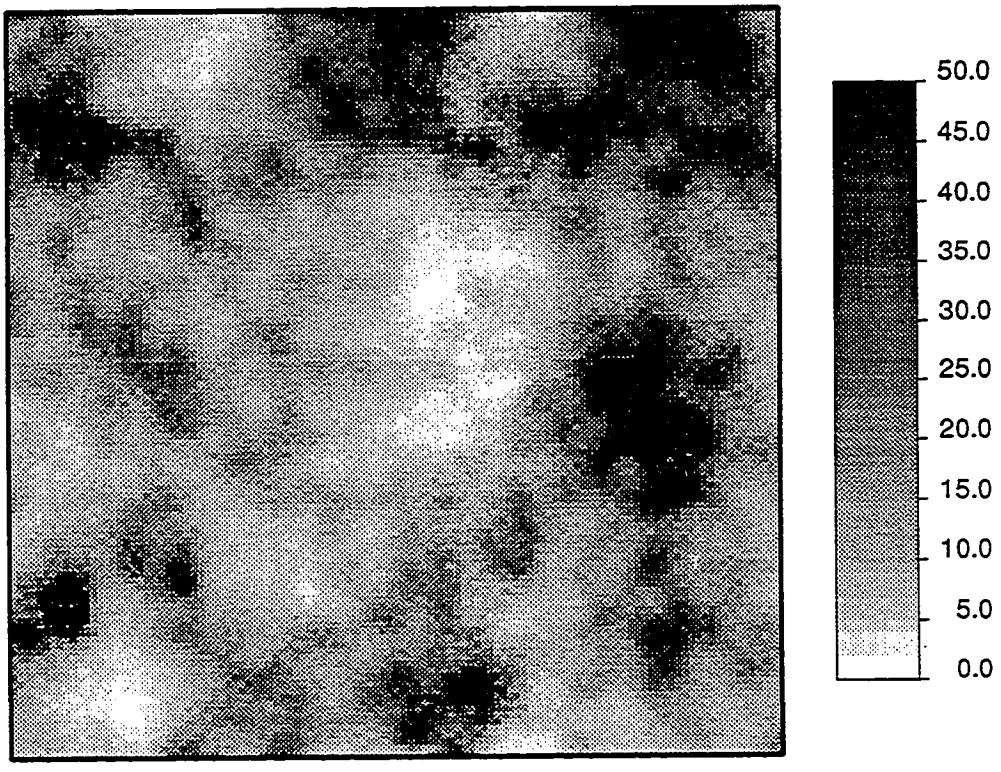

Figure 5.18 - Base case permeability distribution, for investigating the effect of porosity. Generated by Turning Bands (seed = -18, range = 960ft, $\sigma^2_{\ln k} = 0.92$, $\bar{k} = 20$md)

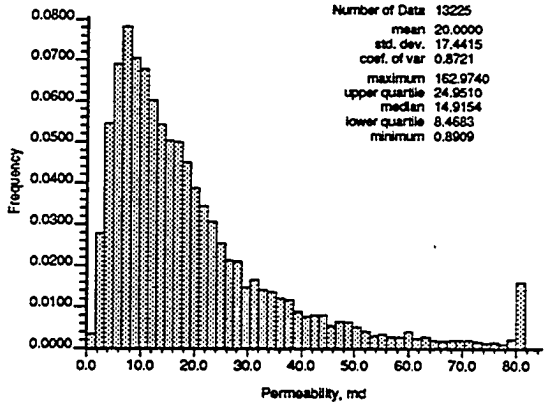

Figure 5.19 - Permeability histogram

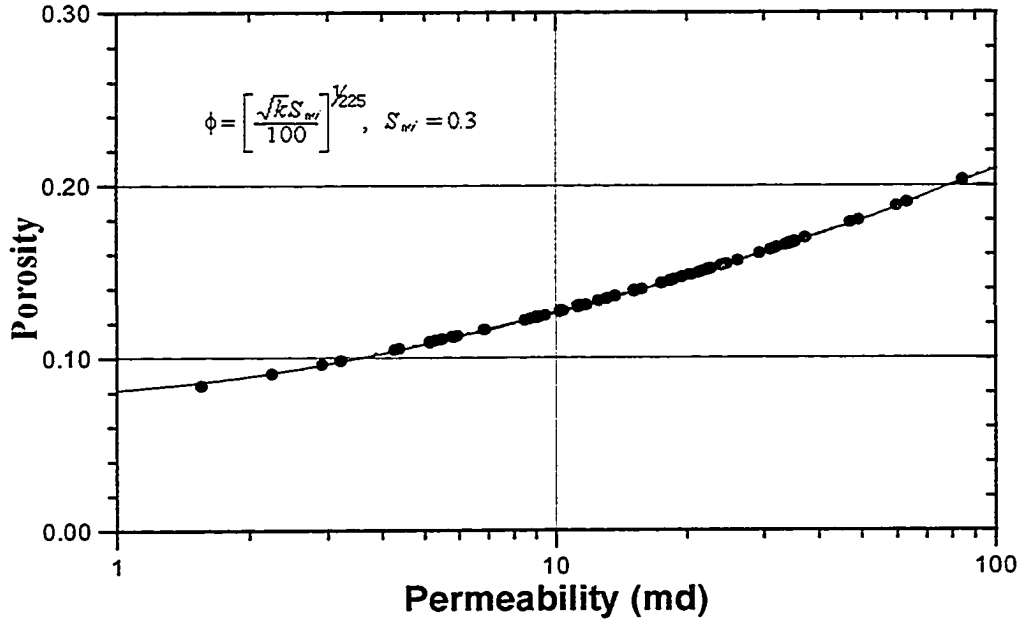

Figure 5.20 - Permeability-porosity transformation.[50]

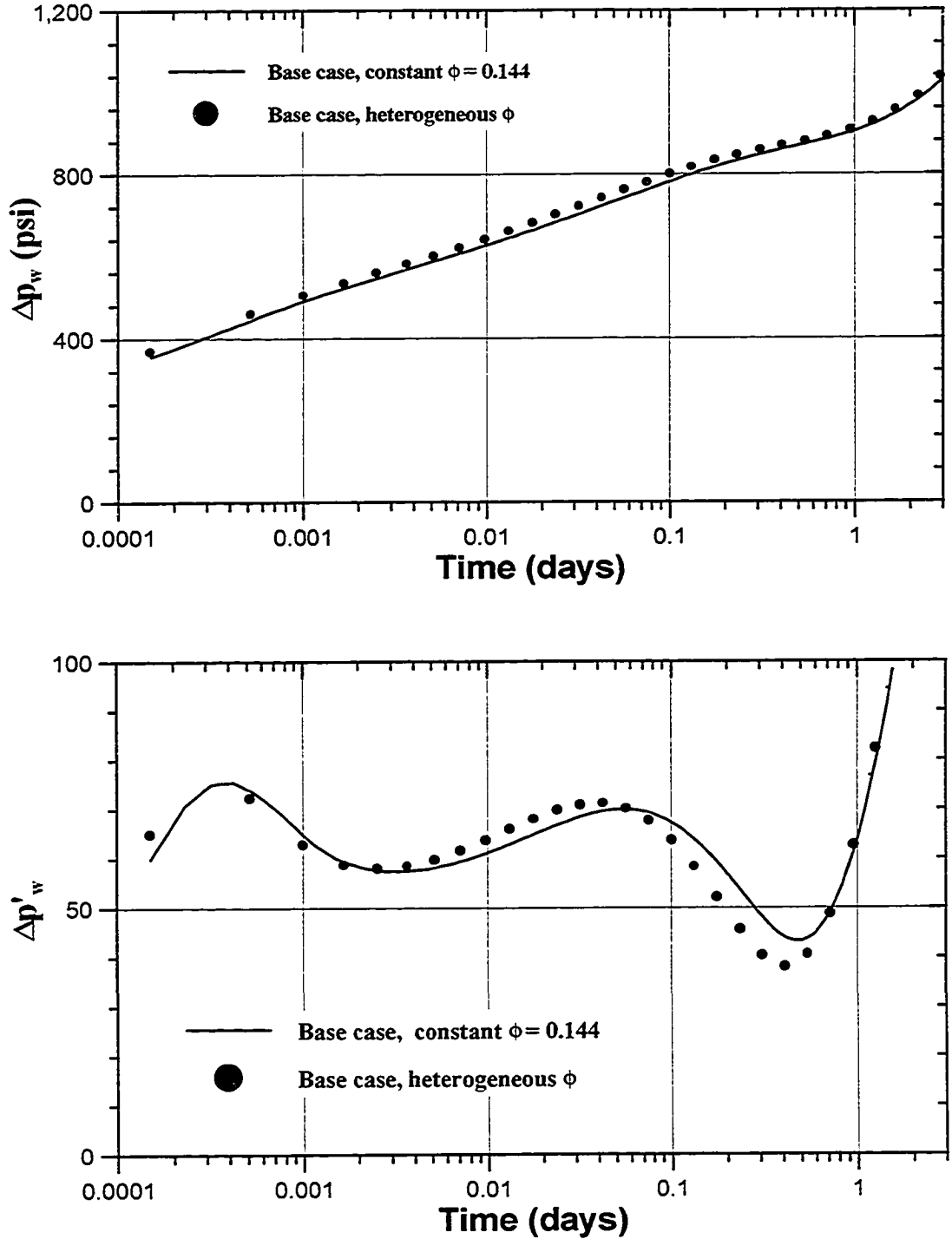

Figure 5.21 - Comparison of pressures and pressure derivatives between heterogeneous distributions with a variation in permeability and porosity, and only permeability.

Observe that the differences in the pressure and pressure derivative between the two simulations are relatively small.

We also consider, an example in which we consider heterogeneities in porosity and a constant permeability of 20 md. The fluid simulation of a drawdown in this heterogeneous medium are shown in Figure 5.22. Note that the pressure derivative is approximately constant.

We solve the inverse problem of describing the permeability distribution assuming that univariate and spatial statistics, and the pressure response during a drawdown of the reservoir are known. We use the pressure response of the reservoir in which both the permeability and porosity vary.

The method of simulated annealing using Oliver's solution (Chapter IV) is used to develop the permeability distribution. The input parameters to the simulated annealing algorithm are given in Table 5.4. The resulting permeability field is shown in Figure 5.23. Porosity values are assigned to corresponding grid blocks using the transform equation (Eq. 5.3). A fluid flow simulation is then performed in the heterogeneous porous medium. The results of the pressure responses for the case in which both permeability and porosity vary and also the case for which only permeability varies and porosity is constant at 0.144 are shown in Figure 5.24. These are compared to the base case pressure response.

From our analysis, we can conclude that, for practical purposes, porosity variations have a minimal effect on the pressure response of a reservoir. This is important, since reservoir descriptions must not only describe heterogeneities in permeability but also in porosity; therefore, the effect of porosity in the use of describing reservoir heterogeneity with well test information must be minimal.

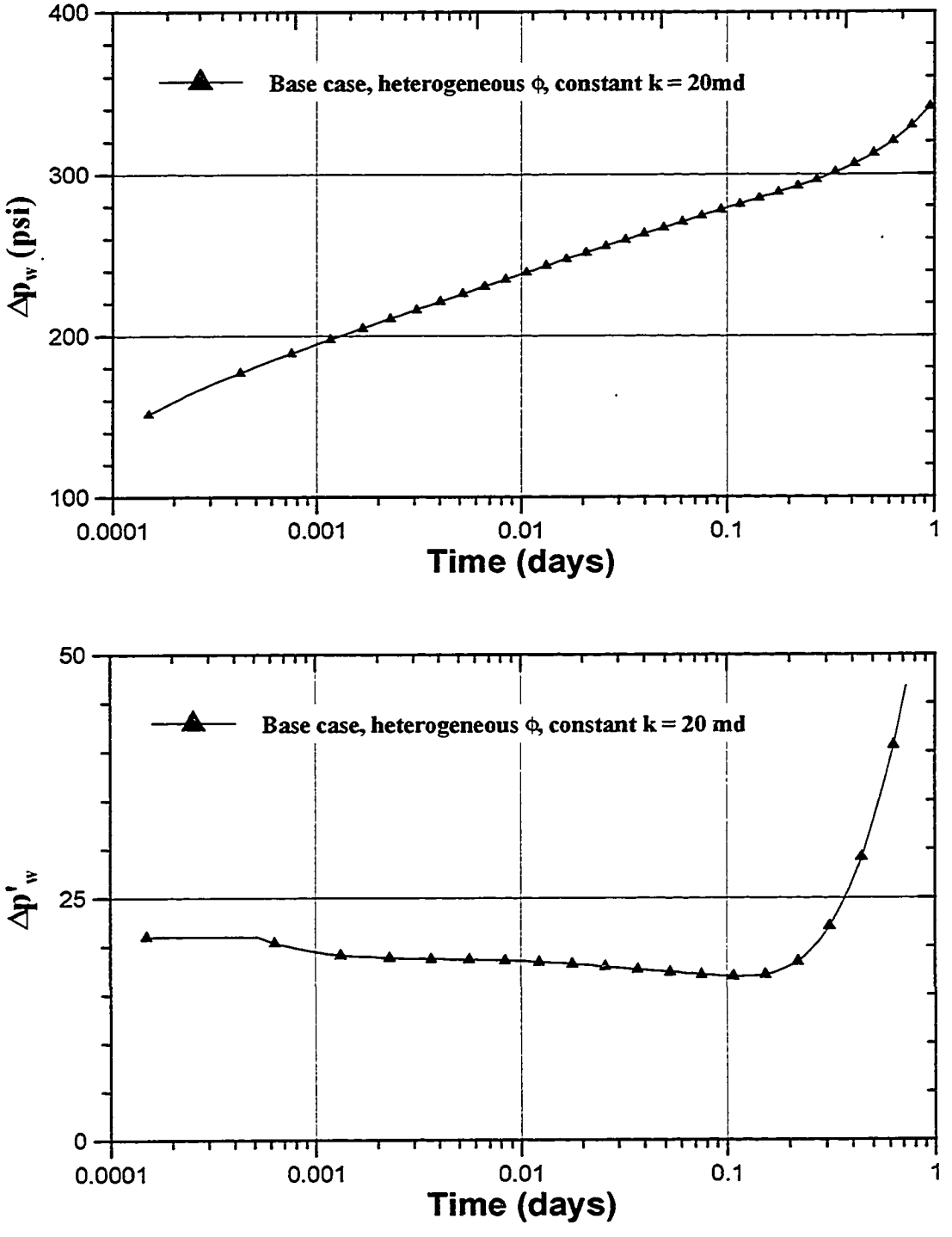

Figure 5.22 -Pressure and pressure derivative of a heterogeneous medium with variable porosity and a constant permeability of 20 md.

Table 5.4 - Simulated Annealing Input Data - Example Considering Heterogeneous Medium in Porosity and Permeability

Number of grid blocks (x,y,z)	115x115x1
Block dimensions ($\Delta x, \Delta y, \Delta z$)	35*ft* x 35*ft* x 10*ft*
Variogram type	Spherical - isotropic
Sill	263.0
Range (*ft*)	600.0

Well Test Information

n	t (days)	r_{min}	r_{max}	$\hat{k}$
1	1.67×10^{-3}	5.4	106.1	6.14
2	3.06×10^{-3}	7.4	143.7	6.21
3	5.62×10^{-3}	10.0	195.0	5.98
4	1.24×10^{-2}	14.8	288.8	5.52
5	2.56×10^{-2}	21.4	418.2	5.14
6	4.95×10^{-2}	29.7	578.2	5.09
7	9.38×10^{-2}	40.8	796.2	5.57
8	1.54×10^{-1}	52.3	1019.4	6.52
9	2.35×10^{-1}	64.6	1259.2	7.90
10	3.33×10^{-1}	77.0	1501.1	9.15
11	4.42×10^{-1}	88.6	1727.4	9.43
12	5.45×10^{-1}	98.4	1919.1	8.87

Conditioning Data	$x(ft)$	$y(ft)$	$z(ft)$	$k_s(md)$
	2012.5	2012.5	17.5	6.95

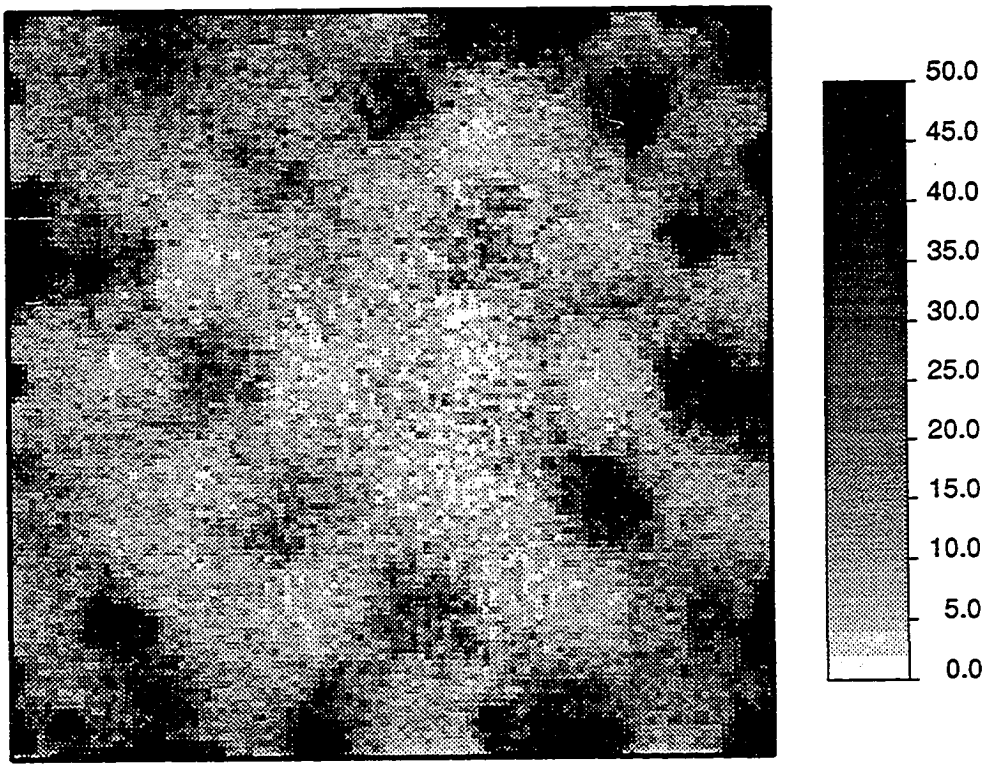

Figure 5.23 - Simulated permeability distribution honoring the constraints given in Table 5.4.

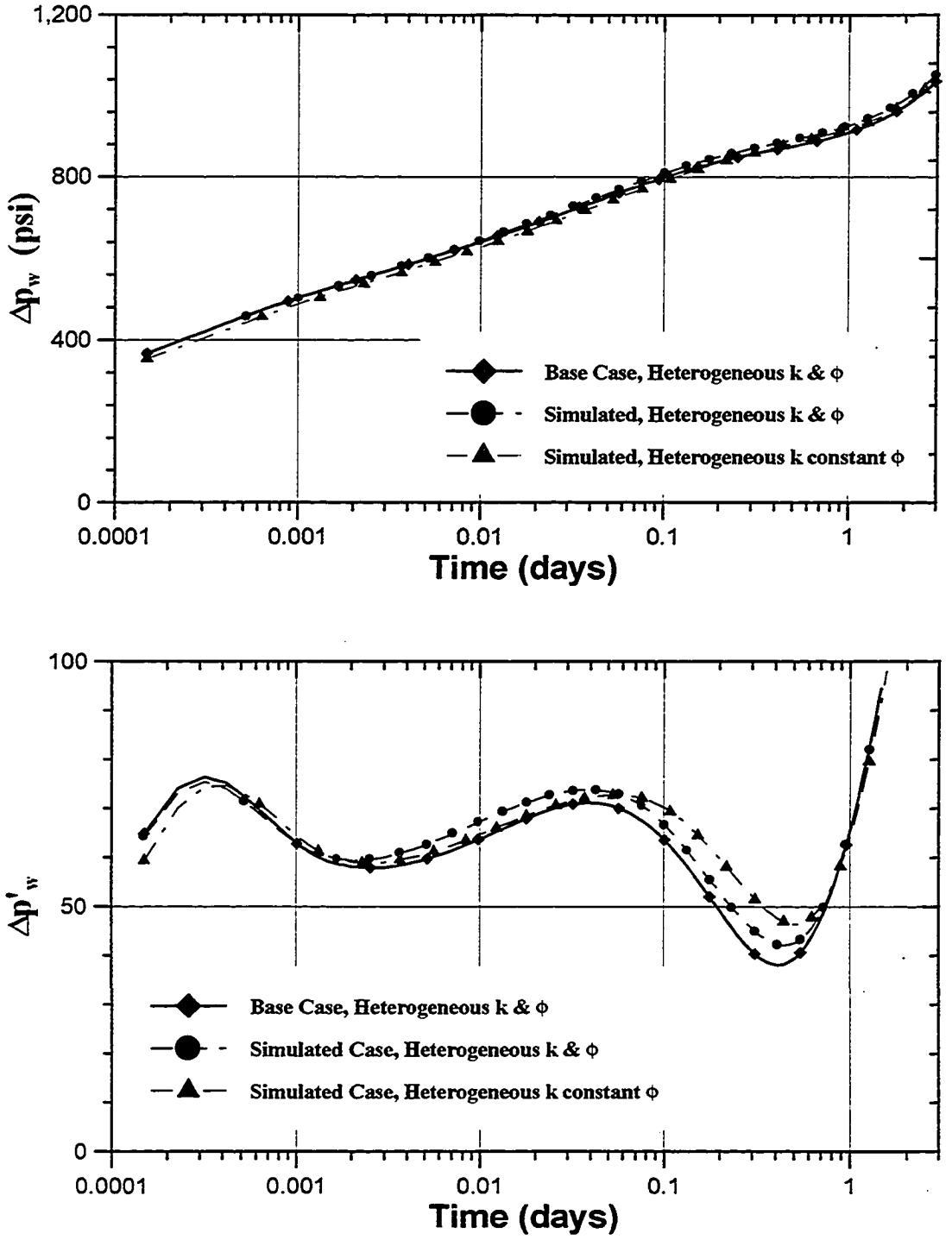

Figure 5.24- Comparison of the pressure response between the base case and simulated heterogeneous systems.

5.3 Effect and Incorporation of Anisotropy

The application of anisotropy to geostatistics is defined by the variogram model. Variogram models define zonal and/or geometric anisotropy (Figure 5.25).[11] A zonal anisotropy is one in which the sill value changes in direction and the range remains constant. In geometric anisotropy, the sill remains constant and the range varies -- see Figure 5.25. Variogram anisotropy may be observed in river channel deposits, where the spatial continuity of reservoir properties is greater in one direction than another. The effect of anisotropy on the fluid flow in a reservoir will affect the pressure response of a well test. In this study we consider an anisotropic reservoir drained by a single well producing at a constant rate at the center of the reservoir. In order to incorporate the effect of anisotropy on the pressure response, we develop a gridding scheme for the simulated annealing algorithm which allows for the incorporation of anisotropy in an isotropic domain.

5.3.1 Base Cases

Base case reservoir descriptions, considering geometric anisotropy, are developed using the simulated annealing algorithm. The reservoir dimensions and anisotropic variogram models for base case permeability distributions are given in Table 5.5.

We consider only geometric anisotropy in these examples. In order to be able to incorporate the permeability information from a well test into the simulated annealing

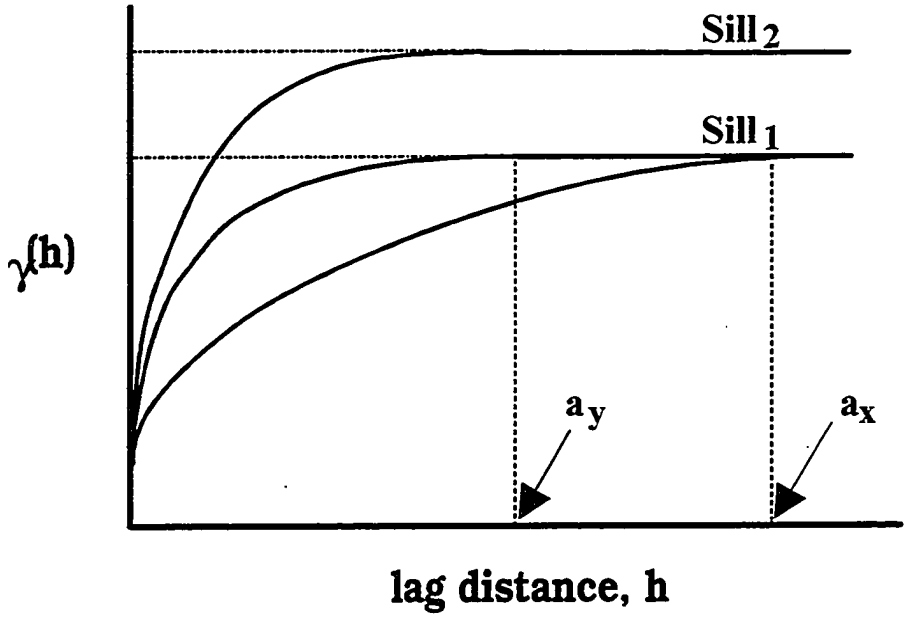

Figure 5.25 - Variogram models illustrating zonal and geometric anisotropy.

Table 5.5- Summary of Variogram Parameters used to Generate the Base Case Anisotropic Permeability Distributions.

	Range in x-direction (ft)	Range in y-direction (ft)	Sill x-direction	Sill y-direction
Example 1	1500	550	350	350
Example 2	3200	550	400	400
Example 3	3200	420	150	150

algorithm, we consider a variogram model in which the range in the x-direction is greater than that in the y-direction ($a_x > a_y$) (Figure 5.25). This simplifies the inverse problem described in Section 5.3.2. The base case permeability distributions for the three examples are shown in Figure 5.26. The corresponding pressure and pressure derivative response for these examples are shown in Figure 5.27. For these examples, the reservoir descriptions are created by forcing a permeability streak along the x-direction such that the producing well lies within the streak. This was achieved by using high permeability values along the location of the streak as conditioning values. The resulting permeability distribution resembles that of a channel sand reservoir. Figures 5.28 and 5.29 show equipotential contours of the flow simulation, for example 1, at 0.15 days and 0.29 days, respectively. Note that equi-potential pressure profile in the reservoir is approximately circular closer to the center of the reservoir and elliptical further away. The major axis of the ellipse is along the x-direction.

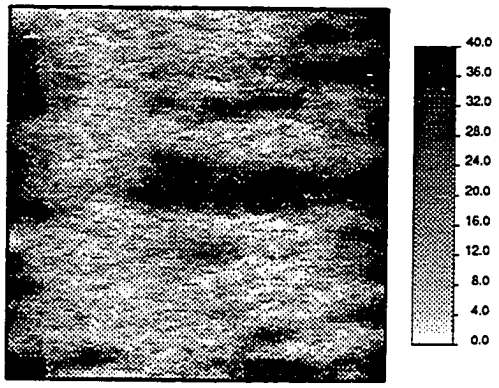

Example 1 - a_x = 1500 ft, a_y = 550 ft

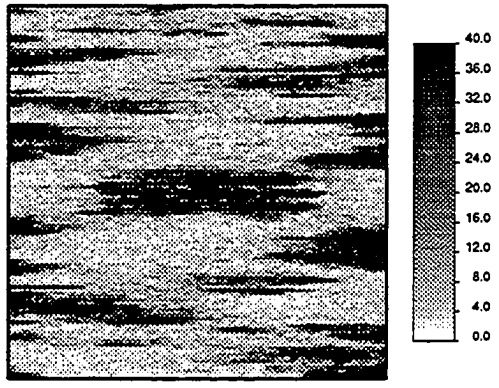

Example 2 - a_x = 3200 ft, a_y = 550 ft

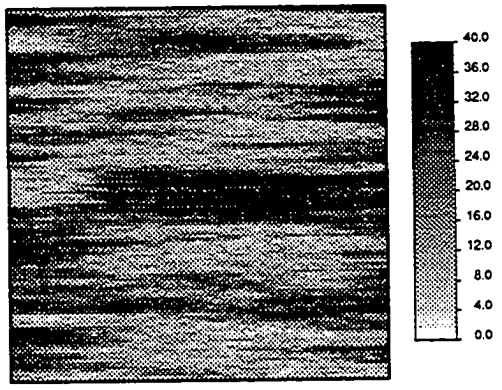

Example 3 - a_x = 3200 ft, a_y = 450 ft

Figure 5.26 - Base case anisotropic permeability distributions, properties are summarized in Table 5.5.

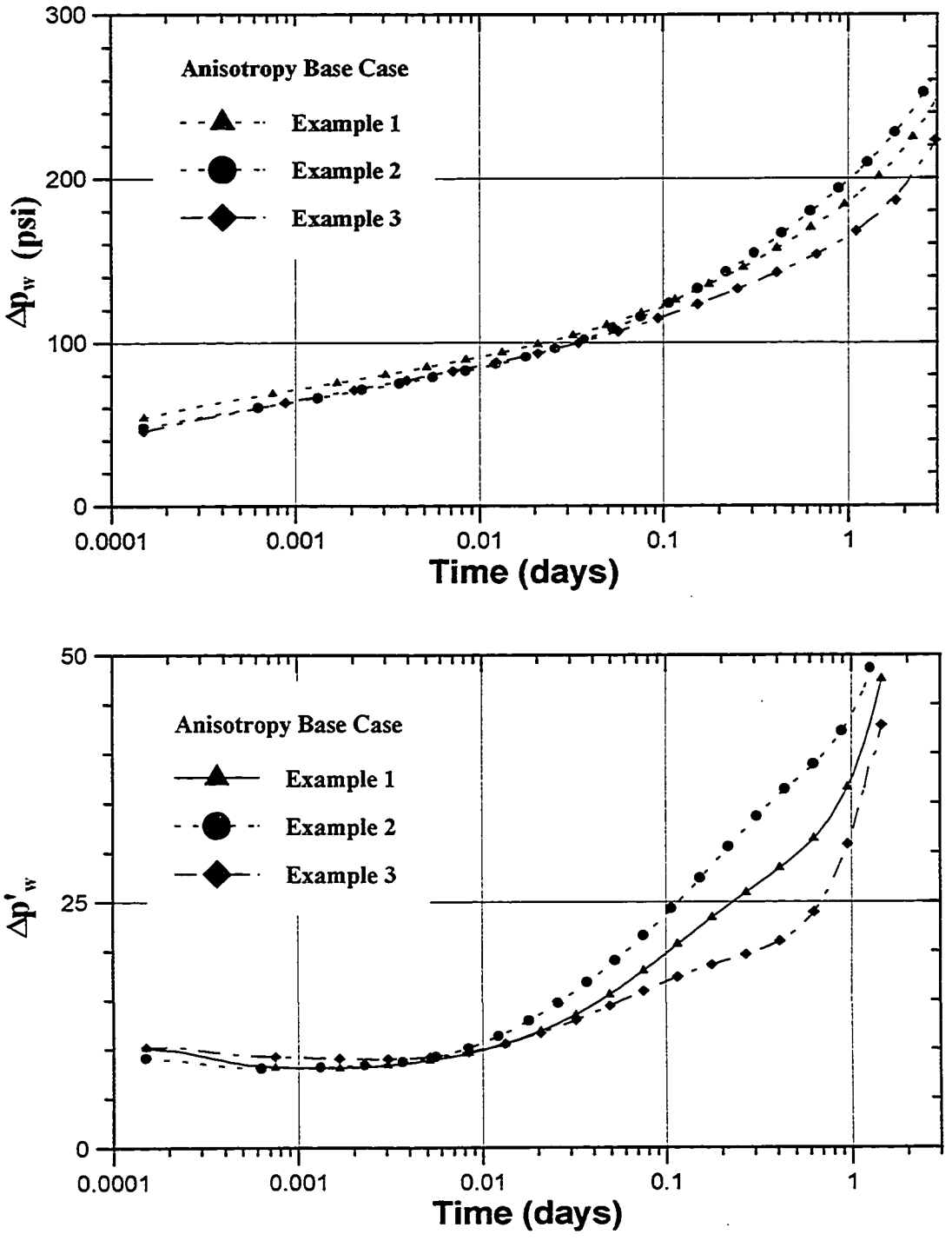

Figure 5.27 - Pressure and pressure derivative for the anisotropic permeability fields shown in Figure 5.26.

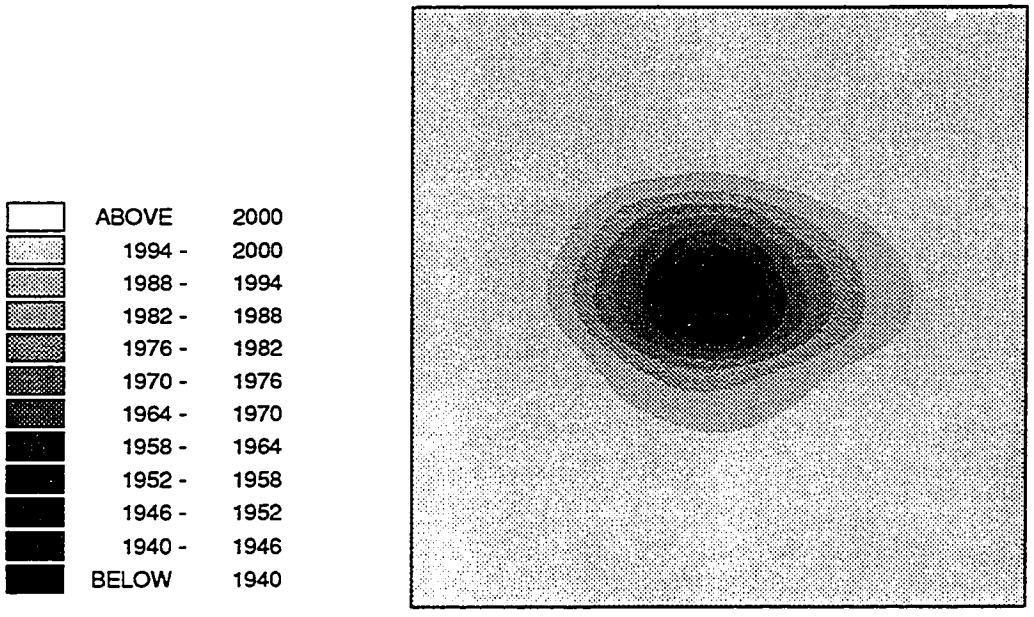

Figure 5.28 - Pressure contours for the permeability field shown in Example 1 of Figure 5.26 at a time step of 0.15 days during the flow simulation.

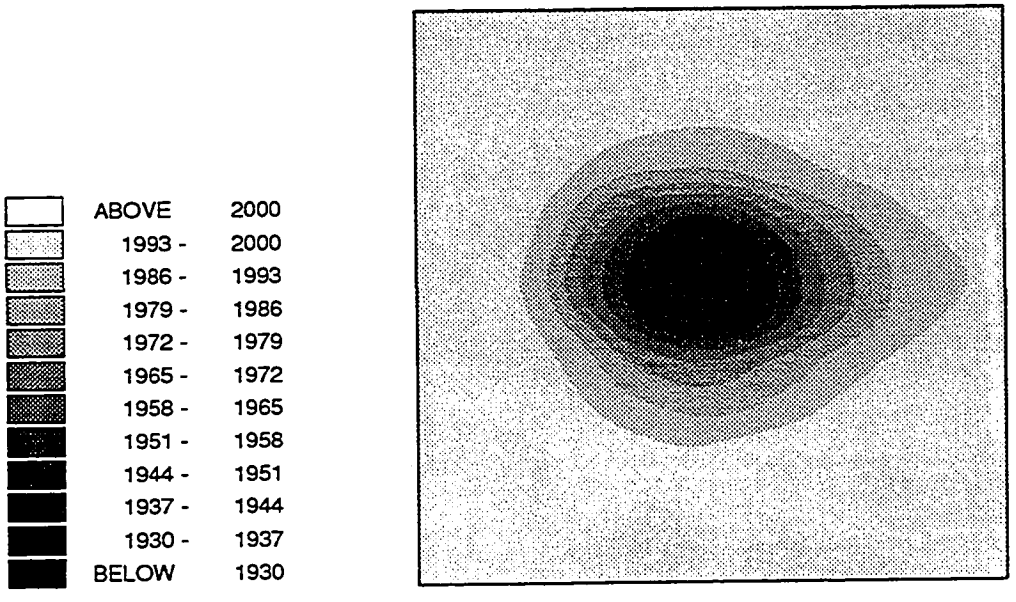

Figure 5.29 - Pressure contours for the permeability field in Example 1 of Figure 5.26 at a time step of 0.29 days during the flow simulation.

5.3.2 Reservoir Description Incorporating Anisotropy

The method of simulated annealing along with Oliver's solution is used to develop a reservoir descriptions that honor anisotropy. The method must honor the anisotropic variogram models and the permeability information obtained from the pressure response of an anisotropic reservoir.

In order to facilitate a solution to the problem, we only consider anisotropy defined in two principle directions: x and y. Figures 5.28 and 5.29 show that a reservoir drained by a single well, in which the range of the variogram in the x-direction is greater than that in the y-direction causes the equipotential profile to be elliptical. The major axis of the drainage ellipse is along the variogram direction of higher range.

For a steady state anisotropic problem, Muskat[51] considers an anisotropic medium in which $k_x \neq k_y$. Muskat claims that the effect of anisotropy in a porous media can be replaced by an equivalent *shrinking* or *expansion* of the coordinate system, for which the transformed coordinates from (x, y) to (x', y') are defined by:

$$x' = \frac{x}{\sqrt{k_x}} \quad \text{and} \quad y' = \frac{y}{\sqrt{k_y}} \tag{5.4}$$

By analogy we hypothesize that a similar transformation of coordinates should apply to an areally heterogeneous anisotropic medium. For our study we consider geometric anisotropy in which the range of the x-direction variogram (a_x) is different from the range of the y-direction variogram (a_y). Note that for our example in which $a_x > a_y$ results in the elliptical drainage profile shown in Figure 5.28 and 5.29. This effect will also be observed if $k_x > k_y$. Although on a local scale (individual grid blocks) we have an isotropic medium, on a larger scale, due to variogram anisotropy, we have an apparent

anisotropic permeability medium. We hypothesize that this variogram anisotropy ratio is representative of the apparent large scale permeability anisotropy. By analogy to Equation 5.4 we assume the following transformation of grid block dimensions:

$$\Delta x' = \frac{\Delta x}{\sqrt{a_x}} \text{ and } \Delta y' = \frac{\Delta y}{\sqrt{a_y}}, \tag{5.5}$$

For our study since $\Delta x = \Delta y$ the anisotropy factor can be defined as:

$$a_f = \frac{\Delta y'}{\Delta x'} = \sqrt{\frac{a_x}{a_y}}. \tag{5.6}$$

In order to incorporate the anisotropy effect, due to the pressure response, the grid dimensions are modified as illustrated in Figure 5.30 and are redefined by:

$$\Delta x' = \Delta x \text{ and } \Delta y' = a_f \Delta y. \tag{5.7}$$

The grid dimension modifications are only for permeability averaging within annular regions, and do *not* apply when the spatial statistics are honored. Figure 5.30 shows that if the major axis of the ellipse is along the x-direction and the minor axis of the ellipse is along the y-direction, then the reservoir, for the purpose of radial permeability averaging, is elongated in the y-direction. The overall effect is the incorporation of an elliptical drainage of the reservoir.

5.3.3 Results and Discussions on the Incorporation of Anisotropy

The grid dimensions modifications in permeability averaging are incorporated with Oliver's procedure (Chapter IV) in the simulated annealing algorithm to reproduce permeability distributions. We investigate three different examples with varying anisotropy ratios, summarized in Table 5.5.

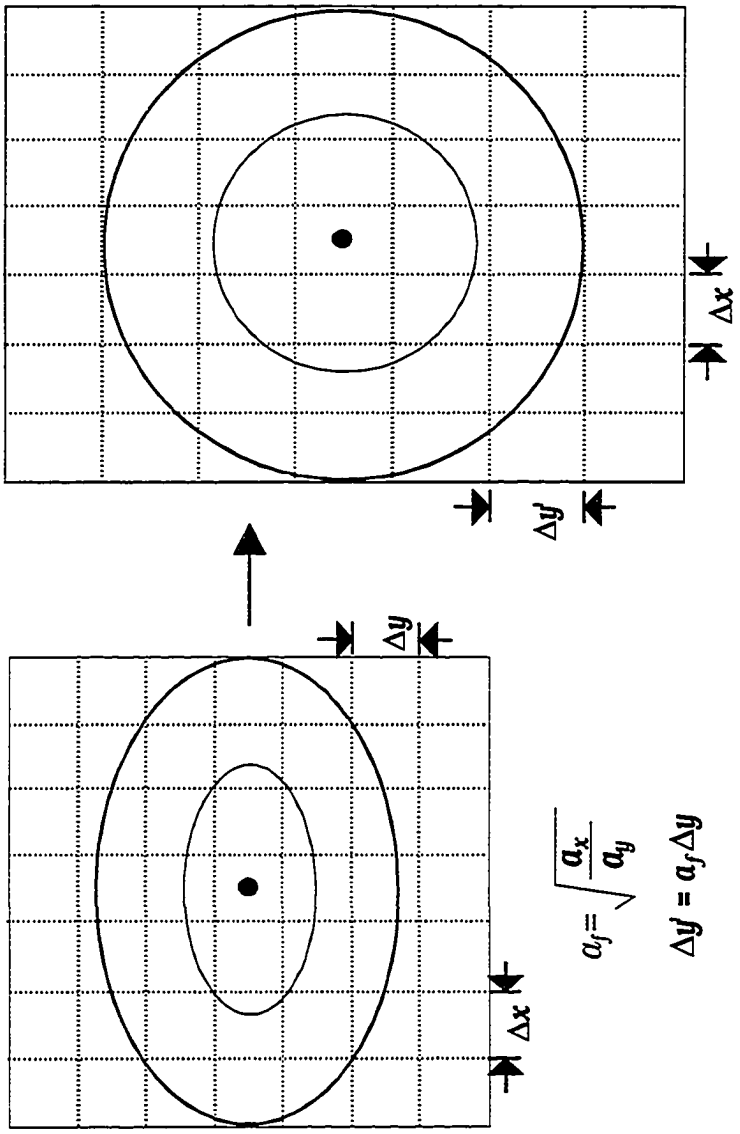

Figure 5.30 - Transformation of areal grid to incorporate anisotropy from well-test information.

Results for Example 1

Equation 5.6 is used to calculate the anisotropy factor, for example 1 (a_x = 1500 and a_y = 550) a_f = 1.65. In the simulated annealing procedure the grid dimensions for the purpose of radial permeability averaging are modified by Equation 5.7. Table 5.6 summarizes the input data for the simulated annealing algorithm. Figure 5.31 shows examples of permeability fields generated honoring the anisotropic variogram and pressure response of the anisotropic reservoir in example 1. In Figure 5.32 the pressures and pressure derivatives of the simulated cases are compared to the base case pressure. We also consider the pressure response of simulated permeability fields where anisotropy in permeability averaging is not considered, i.e., an anisotropy factor of 1.0 is used. The pressure responses of these simulations are shown in Figure 5.33.

Results for Example 2

We investigate a second example for which the base case permeability field is shown in Figure 5.34a. Once again conditioning values are used such that a streak with high permeability values is located along the center of the reservoir. For this example a_x = 3200 and a_y = 550, resulting in an anisotropy ratio, a_f = 2.41. A numerical drawdown simulation in the permeability field gives the pressure response. Table 5.7 summarizes the input data for the simulated annealing algorithm. The simulated annealing procedure outlined above is used to reproduce the permeability fields shown in Figures 5.34b and 5.34c. The pressure responses of multiple realizations honoring the variogram and anisotropic pressure transient response are shown in Figure 5.35. These pressure responses are compared to the base case. Figure 5.36 shows the pressure response of simulated permeability fields where the effect of the pressure response due to variogram anisotropy is not included in the permeability averaging process, i.e., a_f = 1.0.

Table 5.6 - Simulated Annealing Input Data - Anisotropy Example 1

Number of grid blocks (x,y,z)	115x115x1	
Block dimensions ($\Delta x, \Delta y, \Delta z$)	35*ft* x 35*ft* x 10*ft*	
Variogram type	Spherical	
	x	y
Sill	350.0	350.0
Range (*ft*)	1500.0	550.0

Well Test Information

n	t (days)	r_{min}	r_{max}	$\hat{k}$
1	7.5×10^{-4}	5.6	109.1	44.23
2	1.86×10^{-3}	8.1	158.7	44.13
3	5.18×10^{-3}	13.6	264.9	40.62
4	9.82×10^{-3}	18.7	364.8	36.44
5	1.79×10^{-2}	25.3	493.1	31.57
6	2.99×10^{-2}	32.7	636.9	27.10
7	4.95×10^{-2}	42.0	819.0	23.10
8	7.07×10^{-2}	50.2	978.6	20.48
9	1.08×10^{-1}	62.1	1210.4	17.81
10	1.65×10^{-1}	74.0	1443.9	16.01
11	2.04×10^{-1}	85.2	1662.3	14.85
12	2.52×10^{-1}	94.7	1847.3	14.11
13	3.11×10^{-1}	101.6	1981.8	13.67

Conditioning Data	$x(ft)$	$y(ft)$	$z(ft)$	$k_{\bar{s}}(md)$
	2012.5	2012.5	17.5	30.0

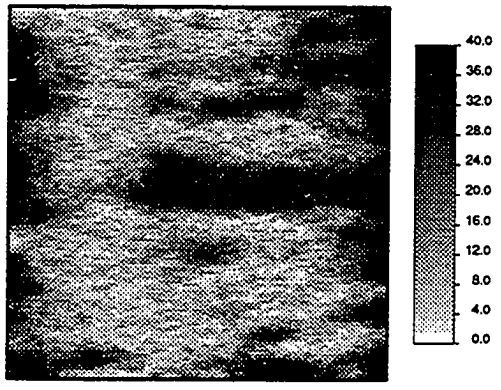

5.31a - Base case permeability distribution a_x = 1500 ft, a_y = 550 ft

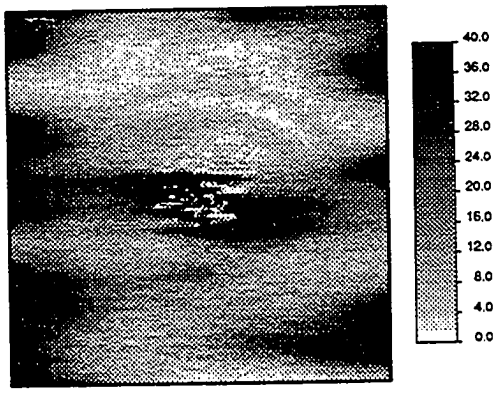

5.31b - Seed = 1079614

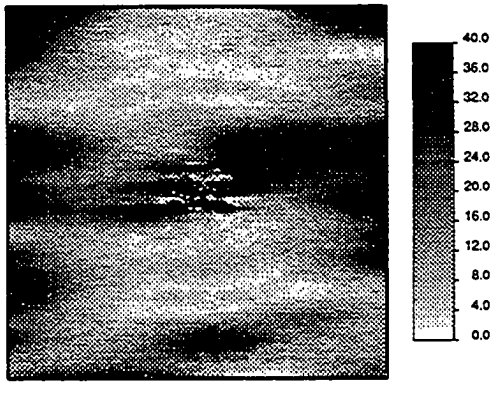

5.31c - Seed = 1079618

Figure 5.31 - Bass case and simulated permeability distributions incorporating well test and variogram anisotropy for example 1.

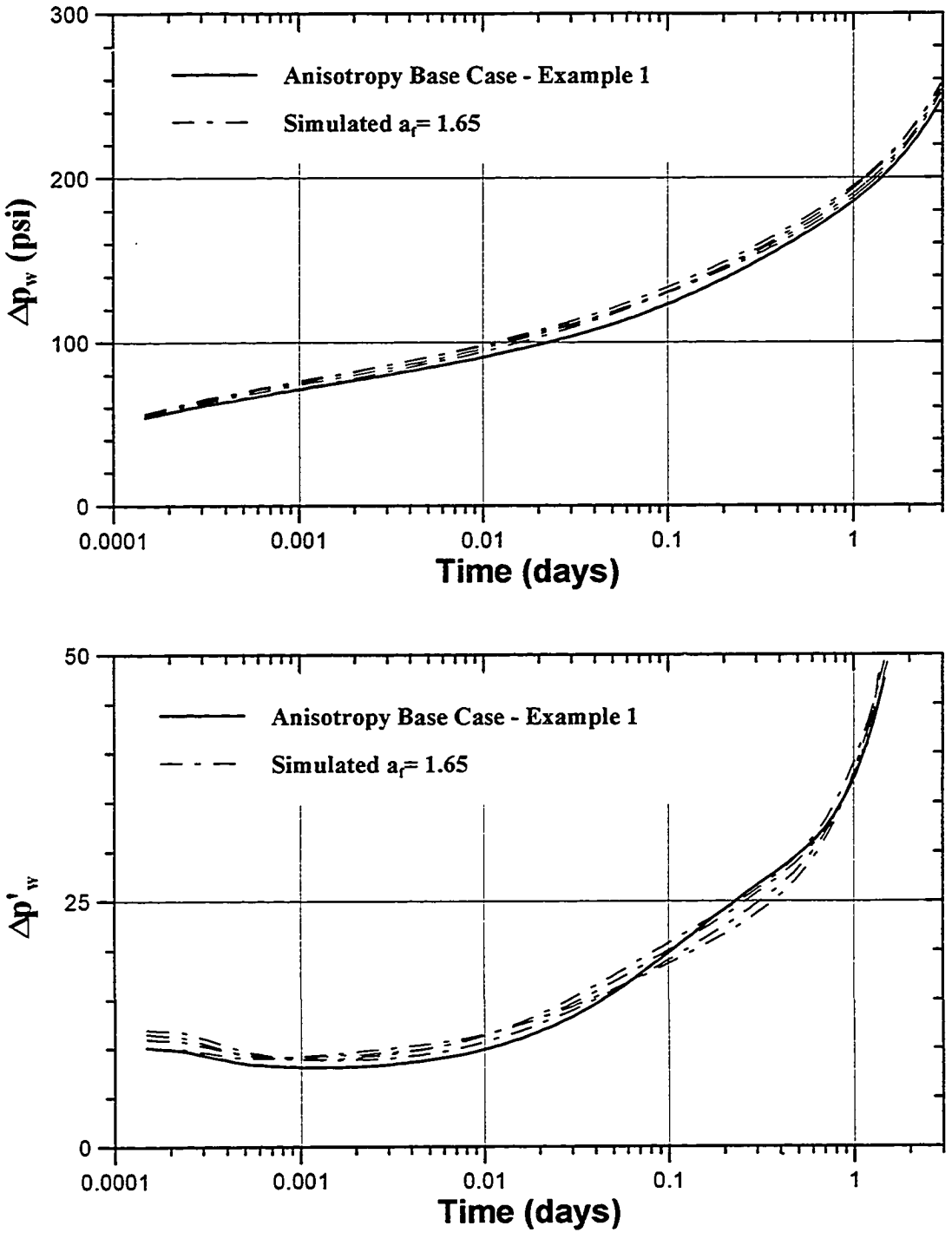

Figure 5.32 - Comparison of pressure and pressure derivatives between the base case and simulated distributions honoring anisotropic variogram and radial anisotropy well test information (a_f=1.65) for example 1.

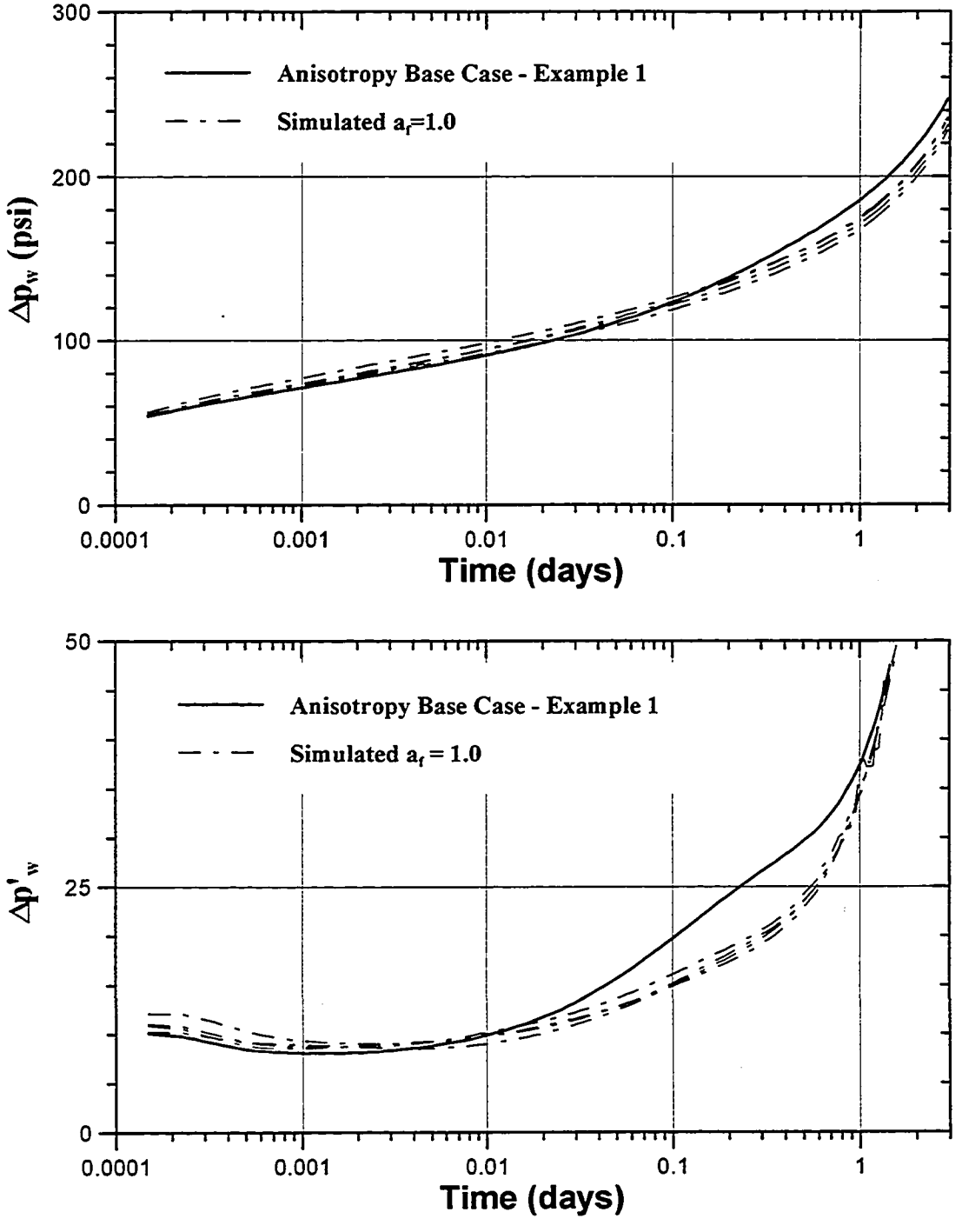

Figure 5.33 - Comparison of pressure and pressure derivatives between the base case and simulated distributions honoring anisotropic variogram and radial well test information (a_f=1.0) for example 1.

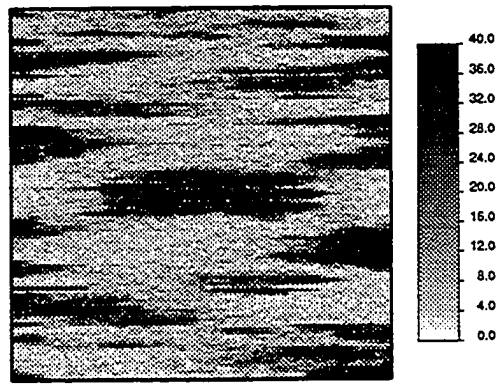

5.34a - Base case permeability distribution a_x = 3200 ft, a_y = 550 ft

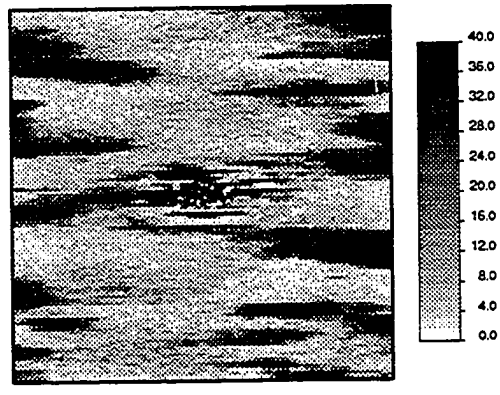

5.34 b - Seed = 1079633

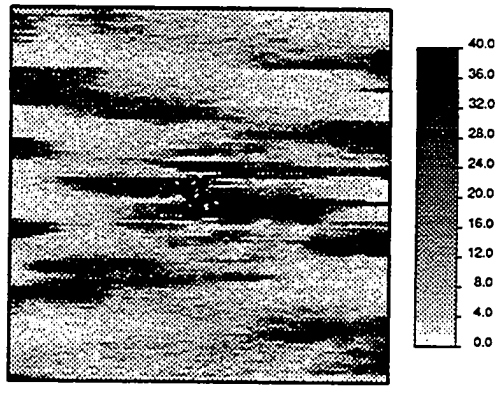

5.34c - Seed = 1079604

Figure 5.34 - Base case and simulated permeability distributions incorporating well test and variogram anisotropy for example 2.

Table 5.7 - Simulated Annealing Input Data - Anisotropy Example 2

Number of grid blocks (x,y,z)	115x115x1	
Block dimensions ($\Delta x, \Delta y, \Delta z$)	35*ft* x 35*ft* x 10*ft*	
Variogram type	Spherical	
	x	y
Sill	400.0	400.0
Range (*ft*)	3200.0	550.0

Well Test Information

n	t (days)	r_{min}	r_{max}	$\hat{k}$
1	7.5×10^{-4}	5.6	109.1	44.37
2	1.86×10^{-3}	8.1	158.7	43.26
3	5.18×10^{-3}	13.6	264.9	39.65
4	9.82×10^{-3}	18.7	364.8	34.05
5	1.79×10^{-2}	25.3	493.1	27.87
6	2.99×10^{-2}	32.7	636.9	23.80
7	4.95×10^{-2}	42.0	819.0	19.38
8	7.07×10^{-2}	50.2	978.6	17.12
9	1.08×10^{-1}	62.1	1210.4	14.80
10	1.65×10^{-1}	74.0	1443.9	13.15
11	2.04×10^{-1}	85.2	1662.3	12.03
12	2.52×10^{-1}	94.7	1847.3	11.31
13	3.11×10^{-1}	101.6	1981.8	10.90

Conditioning Data	$x(ft)$	$y(ft)$	$z(ft)$	$k_s(md)$
	2012.5	2012.5	17.5	70.0

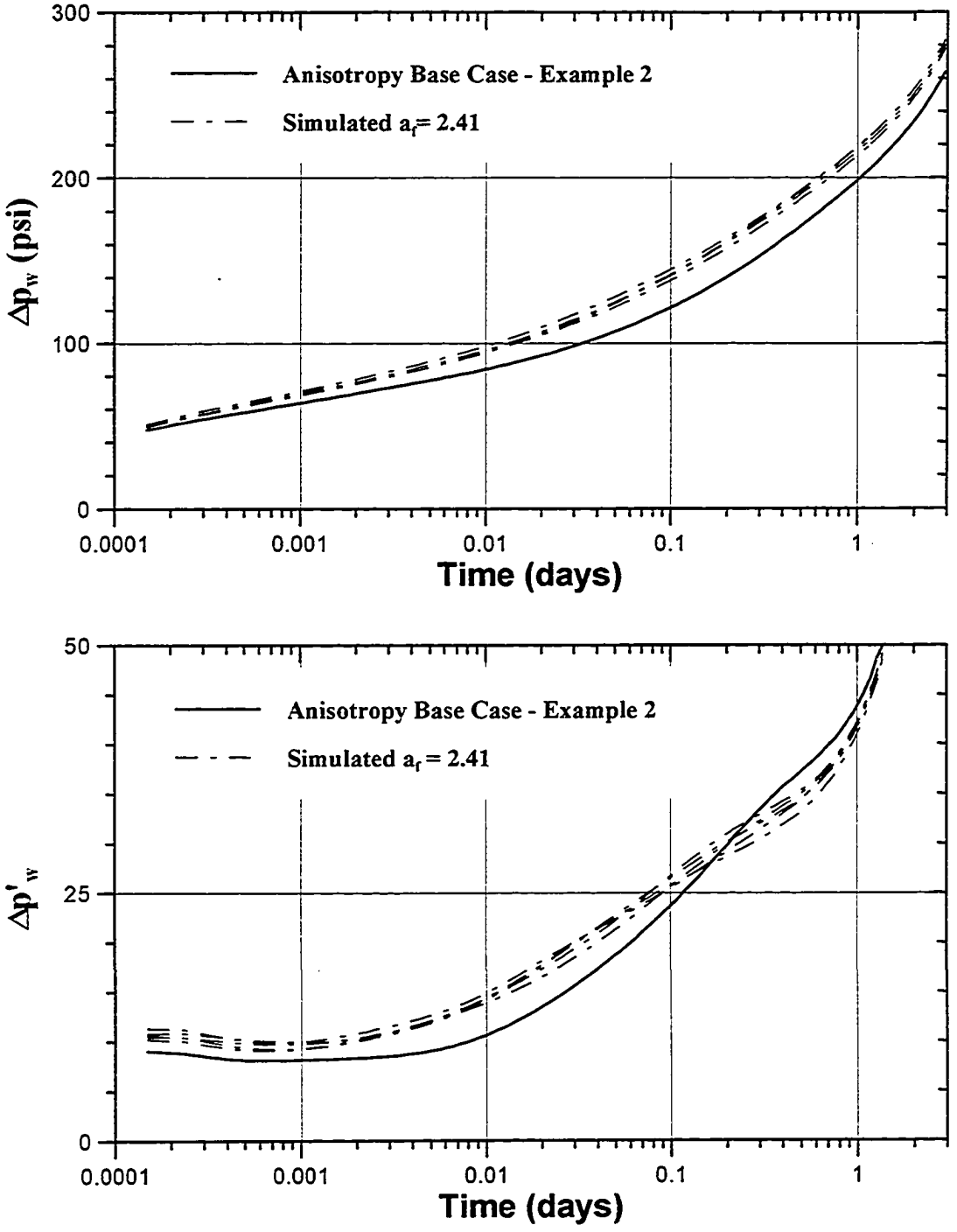

Figure 5.35 - Comparison of pressure and pressure derivatives between the base case and simulated distributions honoring anisotropic variogram and radial anisotropy well test information (a_f=2.41) for example 2.

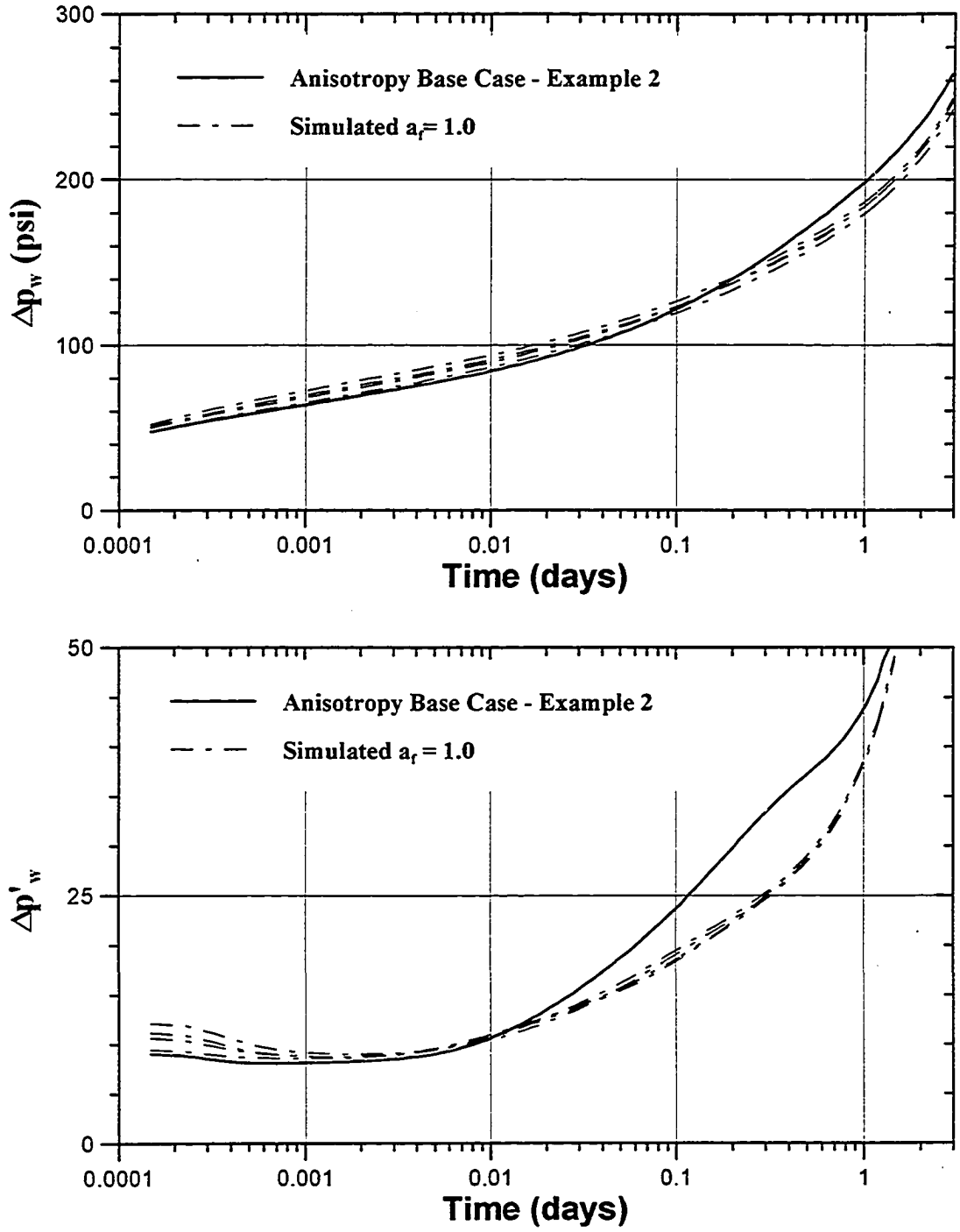

Figure 5.36 - Comparison of pressure and pressure derivatives between the base case and simulated distributions honoring anisotropic variogram and radial anisotropy well test information (a_f=1.0) for example 2.

Results for Example 3

For the third example we investigate a permeability field with an even higher anisotropy ratio, a_f = 2.74. Table 5.8 summarizes the input data for the simulated annealing algorithm. The base case permeability field and the simulated permeability fields are shown in Figure 5.37. The pressure and pressure derivative responses of the simulated examples are compared to the base case response shown in Figure 5.38. Figure 5.39 compares the pressure response for permeability fields with a_f= 1.0.

For the three examples studied, we observe that the pressure response is consistent from simulation to simulation. Note that for the first two examples, when the anisotropy effect due to the pressure response is considered in permeability averaging, the pressure response matches the base case pressure response better than when anisotropy is not considered. The improvement in the match is especially noticeable at later times, before pseudo steady-state flow occurs. This implies that, for these examples, we were better able to capture the elliptical flow phenomena due to anisotropy by considering the defined anisotropy ratio in the radial permeability averaging. For the third example, with the highest anisotropy ratio, when anisotropy is considered in permeability averaging there is no significant improvement in the reproduced pressure response when compared to the pressure response when anisotropy is not considered in permeability averaging. However, for this example it should be noted that the transition from transient to pseudo-steady state flow is captured better when anisotropy is considered in the permeability averaging process.

For the three examples studied, the inclusion of anisotropy in permeability averaging during the simulated annealing process improves the reproduction of the pressure response. Therefore, the effect of variogram anisotropy on the pressure response can be accounted for.

Table 5.8 - Simulated Annealing Input Data - Anisotropy Example 3

Number of grid blocks (x,y,z)	115x115x1	
Block dimensions ($\Delta x, \Delta y, \Delta z$)	35*ft* x 35*ft* x 10*ft*	
Variogram type	Spherical	
	x	y
Sill	150.0	150.0
Range (*ft*)	3200.0	420.0

Well Test Information

n	t (days)	r_{min}	r_{max}	$\hat{k}$
1	7.5×10^{-4}	6.2	120.9	38.88
2	1.32×10^{-3}	8.2	160.0	39.50
3	3.06×10^{-3}	12.5	243.9	39.94
4	6.62×10^{-3}	18.4	358.8	39.85
5	1.24×10^{-2}	25.1	490.0	34.58
6	2.08×10^{-2}	32.6	635.8	30.81
7	3.46×10^{-2}	42.1	820.0	27.23
8	4.95×10^{-2}	50.3	981.0	24.93
9	7.59×10^{-2}	62.3	1214.6	22.60
10	1.08×10^{-1}	74.3	1449.8	21.00
11	1.43×10^{-1}	85.6	1669.7	19.99
12	1.77×10^{-1}	95.2	1855.8	19.36
13	3.11×10^{-1}	101.6	1981.8	10.90

Conditioning Data	$x(ft)$	$y(ft)$	$z(ft)$	$k_{\bar{s}}(md)$
	2012.5	2012.5	17.5	80.0

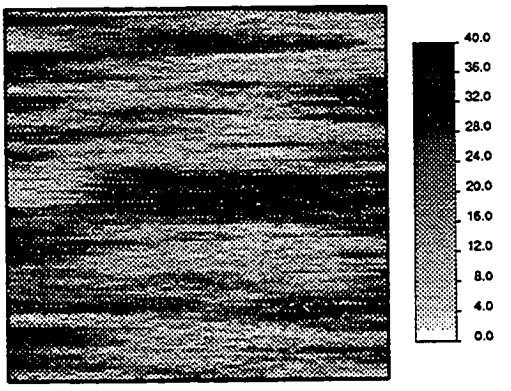

5.37a - Base case permeability distribution a_x = 1500 ft, a_y = 550 ft

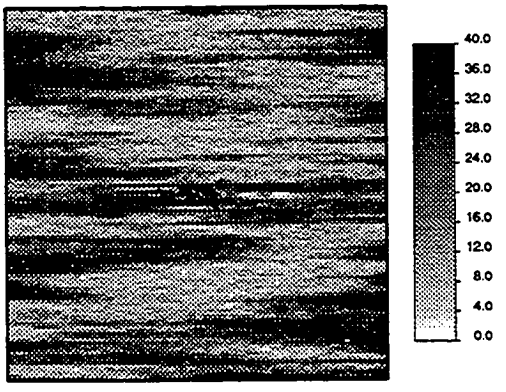

5.37b - Seed = 1079624

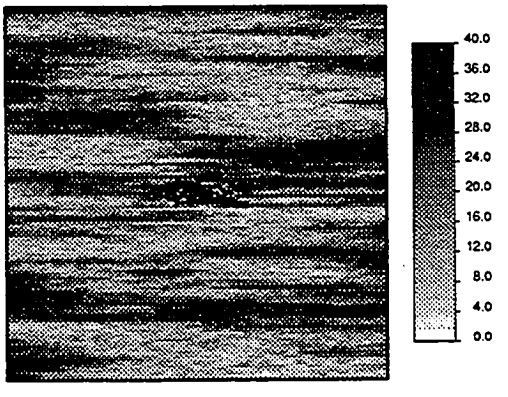

5.37c - Seed = 1079612

Figure 5.37 - Bass case and simulated permeability distributions incorporating well test and variogram anisotropy for example 3.

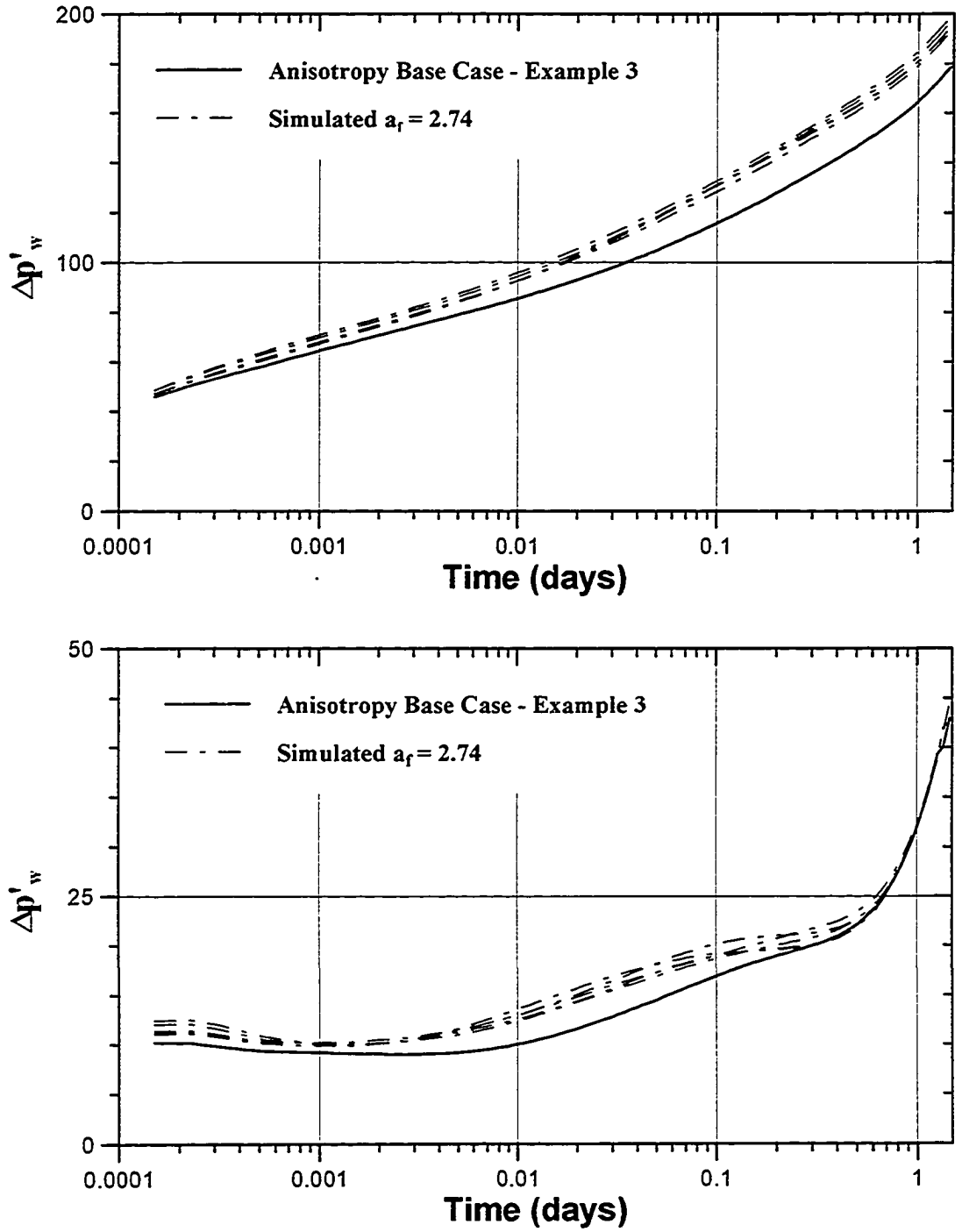

Figure 5.38 - Comparison of pressure and pressure derivatives between the base case and simulated distributions honoring anisotropic variogram and radial anisotropy well test information (a_f=2.74) for example 3.

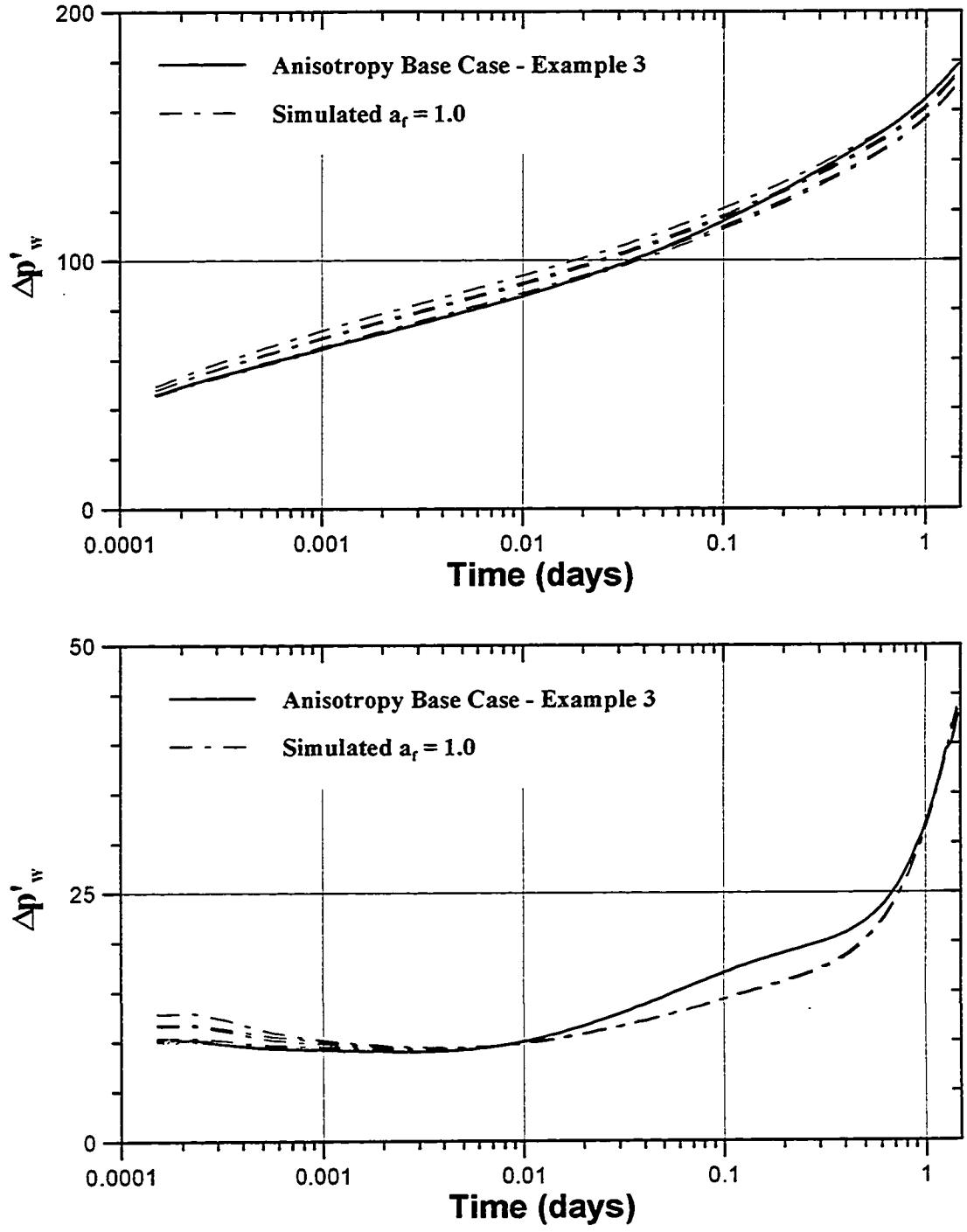

Figure 5.39 - Comparison of pressure and pressure derivatives between the base case and simulated distributions honoring anisotropic variogram and radial anisotropy well test information (a_f=1.0) for example 3.

CHAPTER VI

CONCLUSIONS

This chapter summarizes the observations and contributions of this dissertation. At the end, the important conclusions of this work are enumerated and recommendations for future work are made.

The objective of this work has been to incorporate well test data with the spatial and univariate statistics to develop alternate equiprobable reservoir descriptions.

In Chapter III we addressed the forward problem. Permeability fields with varying degrees of heterogeneity were generated using Turning Bands Method. Numerical fluid flow drawdown simulations for a producing well at the center of the permeability fields were performed. We considered flow of a single-phase slightly compressible fluid of constant viscosity. The permeability distributions and their respective pressure responses were assumed to be the *truth* or *base* cases.

Using the analytical solutions for well testing in heterogeneous reservoirs developed by Oliver[1] and Feitosa,[2] appropriate radii of investigation were defined and the type of permeability average that should be used between the radii determined.

By examining Oliver's solution, it was indicated that the instantaneous well test permeability derived from the pressure data represents a weighted harmonic average of some arbitrary radial permeability distribution. By performing numerical experiments on the base case permeability distributions and by using their respective pressure responses, we showed that the instantaneous well test permeability determined from the pressure data at time, t, could be approximated by a weighted harmonic average in the radial direction,

of an area-based geometric average in the theta-direction, of areally distributed grid block permeabilities within the defined radii of investigation. The harmonic average in the radial direction was weighted according to the weighting or kernel function defined by Oliver.

The Inverse Solution Algorithm (ISA) developed by Feitosa,[2] defines an equivalent radial permeability distribution. Numerical experiments on our base cases showed that the equivalent ISA permeability defined for an annular region of the reservoir could be approximated by an area-based harmonic or geometric average of grid block permeabilities in the theta direction.

Therefore, the instantaneous well test permeability or the equivalent radial permeability distribution defined by ISA could be explicitly related to the distribution of small scale permeabilities within annular regions of an areal (x-y) reservoir.

In Chapter IV, a detailed description of the simulated annealing algorithm was presented. The algorithm generates alternate equiprobable reservoir descriptions that honor the following constraints:

- the univariate statistics (cdf),
- the spatial statistics (variogram),
- the conditioning data,
- the well test pressure transient information.

The observations made in Chapter III, concerning the application of Oliver's method and Feitosa's Inverse Solution Algorithm (ISA) to an areally (x-y) heterogeneous reservoir, were used to honor the well test constraint. These observations were:

(i) For Oliver's method the instantaneous well test permeability, $\hat{k}$, could be approximated by an equivalent permeability, $\overline{k}_e$, which is an area-based geometric average of grid block permeabilities in the θ-direction, followed by averaging in the radial direction using Oliver's kernel function to determine appropriate weights.

(ii) The equivalent radial permeability distribution determined by ISA could be approximated by an area-based harmonic or geometric average of grid block permeabilities in the θ-direction.

The simulated annealing objective function was modified to include the spatial statistics and well test information. In Oliver's method, in order to honor the well test component of the energy function, perturbations or swaps of grid block permeabilities were made until the equivalent permeability within the defined inner and outer radii of investigation matched the instantaneous permeability. For ISA, a similar objective function based on approximating the equivalent ISA radial permeability distribution by an area-based harmonic or geometric average of the grid block permeabilities within an annular region were defined.

Weights to each component (variogram and well test) of the objective function were appropriately assigned by performing numerical experiments with the annealing simulation and the minimum number of iterations required to achieve stable estimates of the weights for each component of the objective function were determined.

By demonstrating the ability of the simulated annealing algorithm to honor well test information as well the spatial statistics, we showed the robustness and flexibility of the simulated annealing algorithm to enable the incorporation of additional constraints.

In Chapter V, we used the simulated annealing algorithm described in Chapter IV to generate alternate equiprobable reservoir descriptions that honor the spatial statistics and the well test information.

Numerical fluid flow drawdown simulations were performed in the simulated permeability fields. The pressure responses of the simulated fields were compared to their respective *base* or *truth* cases.

When using the Oliver method a good match between the pressure responses of the simulated case and base case was observed. In addition, the pressure transient drawdown results were consistent from simulation to simulation.

For the ISA method, we observed that an area-based harmonic average of the grid block permeabilities reproduced the base case pressure response better than an area based geometric average. In these cases, also, the pressure responses were consistent from simulation to simulation.

Furthermore, we observed that when the well test constraint is not used to reproduce the permeability distribution, i.e., the reservoir description is constrained only to the spatial statistics, the pressure responses of the base and the simulated permeability distribution are in poor agreement.

A comparison of the CPU requirements for each method revealed that the cost of updating the well test component for the ISA method is less than that for the Oliver method.

In the remaining part of Chapter V we looked at applications and extensions of the inverse modeling technique to related problems when well test data is incorporated into developing a reservoir description.

The effect of porosity heterogeneities on the pressure response during a drawdown test was studied. We investigated drawdown simulations in a porous medium heterogeneous in porosity and permeability. We observed that the effect of porosity heterogeneities is small and thus can be ignored when honoring well test data to develop the reservoir description.

We considered the effect of anisotropy on the pressure response, during a pressure transient test, and its incorporation into the reservoir description. The effect of an elliptical equipotential profile due to the drainage of an anisotropic reservoir was incorporated into the permeability averaging process. We observed that by defining an anisotropy ratio based on the ranges of the x- and y-direction variograms, we were able to capture the effect of anisotropy on the pressure response. We studied three examples, with varying anisotropy ratios, and observed that in general when anisotropy is incorporated into the permeability averaging process the match between the pressure response of the simulated

permeability fields and the base case response improved. The improvement was especially noticeable for the transition from infinite-acting to pseudo-steady sate flow.

The important conclusions and observation of this dissertation are listed below:

1. The analytical solutions of Oliver[1] and Feitosa[2] were used to describe an appropriate averaging of areal permeability distributions, within an inner and outer radii of investigation.
2. The simulated annealing algorithm was used to develop reservoir descriptions that honor the univariate and spatial statistics and the pressure response of a reservoir for a single well. The pressure response of the reservoir was honored by using the averaging techniques for the Oliver method or ISA. We have therefore demonstrated the robustness and flexibility of the simulated annealing algorithm to incorporate additional constraints imposed by other sources of information.
3. The overall computational cost of the simulated annealing algorithm is less for the ISA procedure than for Oliver's method.
4. We were able to consistently match the simulated permeability fields pressures and pressure derivatives, with those of the base case.
5. In contrast when the well test constraint is not considered in reproducing the permeability fields, the pressure and pressure derivatives compared unfavorably with those of the base case.
6. We observed that heterogeneities in porosity have a minimal effect on the pressure response during a well test, thus porosity heterogeneities can be ignored when honoring well test data in the reservoir description.
7. By modifying the gridding scheme for the permeability averaging process in the simulated annealing algorithm, we were able to incorporate the effect of anisotropy on the pressure response during a drawdown test.

Recommendations

The recommended future work in this area includes the following:

1. The methodology of incorporating the pressure response during a well test should be applied to existing field data , and the method's practicality demonstrated.
2. The method must be extended to handle build-up data.
3. Well test information from multiple wells within a reservoir will provide more information that the reservoir description can be constrained to. By honoring the information from multiple well tests the extremities of permeability distributions in a reservoir may be captured. In addition, by extending Oliver's solution and ISA to results from interference tests, information about the interwell permeability connectivity may be captured.
4. Furthermore, the value of information obtained from the multi-well study needs to be quantified. This can be done by performing waterflood fluid-flow simulations in the simulated permeability fields and comparing them to base case results and observations.
5. The method of simulated annealing must be extended to incorporate multiple sources of information, such as primary and secondary performance parameters and geophysical data, to develop the best possible reservoir description.
6. The simulated annealing algorithm is computationally demanding and by imposing more constraints on the algorithm, the computational cost becomes even higher. Therefore the efficiency of the algorithm must be improved. The incorporation of multiple constraints makes the algorithm ideal for solution by parallel processing, in which each update component of the energy function can be solved by a separate node.

7. Parameters in the incorporation of well test data must be optimized to reduce the computational cost. In particular a sensitivity analysis of the following parameters must be performed:
   - For Oliver's method an optimum number of instantaneous permeability values, $\hat{k}$, from the pressure derivative data must be determined such that the pressure response of the reservoir is reproduced. For our investigation we used *enough* permeability values such that trends in the pressure derivative were captured.
   - An optimum minimum number of Coat's grid radial divisions must be determined. In our study we used 50 radial Coat's grid divisions.
   - In our simulation studies we used *enough* grid blocks such that we are able to honor the area-based permeability averages. A sensitivity study for selecting sufficient grid blocks within the simulation domain must be performed such that the pressure transient information is still effectively captured.
   - The convergence tolerance of the simulated annealing algorithm must be redefined. The present convergence tolerance is arbitrary and results in an *over-kill* of the simulation process. A definition based on relative change of the energy function from one iteration step to the next may be more appropriate.

The long term recommendations for future work include:

1. Methods for incorporating well tests data for three dimensional systems need to be studied.
2. Incorporation of well test data for multi-phase flow reservoirs.

NOMENCLATURE

Symbol

a_f	anisotropy ratio
A	radius of investigation coefficient
$A_{\bar{s}}$	area of grid block in the annular ring at location vector $\bar{s}$, ft^2
A_r	area of annular region, ft^2
B	formation volume factor, *bbl/STB*
C	class interval for the sample cdf
c_t	total compressibility psi^{-1}
E	objective or energy function
E'	objective function after an update
E_0	normalizing constant for objective function
h	thickness, *ft*
$\bar{h}$	lag distance vector for variograms
HI	heterogeneity index
$\bar{k}$	average permeability, *md*
$\bar{k}_a$	arithmetic permeability average within an annular region, *md*
k_D	dimensionless permeability
$\bar{k}_e$	equivalent permeability, *md*
$\bar{k}_g$	geometric permeability average within an annular region, *md*
$\bar{k}_h$	harmonic permeability average within an annular region, *md*
k_{ISA}	ISA derived equivalent radial permeability, *md*
$k(r,\theta)$	permeability at location (r,θ) for a radial heterogeneous reservoir
k_{ref}	arbitrary reference permeability, *md*

$k_{\bar{s}}$	grid block permeability, *md*
$\overline{k}_{wt}$	well test permeability from the semilog straight line, *md*
$\hat{k}$	instantaneous well test permeability, *md*
$K(r_D, t_D)$	weighting or kernel function
l'	index defining the transformed grid block at, $\bar{s}$ ', for the muti-well study
m	semilog straight line slope
M	number of iterations
N_c	number of conditioning data
N_d	number of variogram directions
N_f	number of classes for distribution function
N_h	number of variogram lag distances
N_o	number of constraints for a conditional simulation
N_p	number of pairs in a variogram
N_s	number of grid blocks in the simulation domain
N_r	number of radial divisions in the simulation grid
N_t	total number of time points valid for Oliver's solution
N_w	total number of well test constraints
N_x	number of grid blocks in x
N_y	number of grid blocks in y
O_x	coordinate of x-origin of the reservoir, *ft*
O_y	coordinate of y-origin of the reservoir, *ft*
p_D	dimensionless pressure
p_i	initial reservoir pressure, *psia*
p_0	central grid block pressure, *psia*
p_{wf}	well flowing pressure, *psia*
p_{wd}	dimensionless well flowing pressure

p'_{wd}	dimensionless pressure derivative
q	rate, *STB/D*
r	radius, *ft*
r_{cmax}	radius from the well to furthest corner of the gridblock, *ft*
r_{cmin}	radius from the well to closest corner of the grid block, *ft*
r_D	dimensionless radius
r_{Dmax}	maximum dimensionless radius defined by the weighting function
r_{Dmin}	minimum dimensionless radius defined by the weighting function
r_e	reservoir radius to nearest no flow boundary, *ft*
r_w	wellbore radius, *ft*
R	random number
s	skin
$\bar{s}$	grid block location vector
$\bar{s}'$	transformed grid block location vector for the multi-well study
S_{wi}	initial water saturation
t	time, *days*
t_D	dimensionless time
$\hat{t}_D$	instantaneous dimensionless time
T^r	temperature control parameter
T^o	initial temperature control parameter
V	simulation variable
V	Dykstra-Parson's coefficient
w_i	weight of annular region
$W_{1/2,1/2}$	Whitaker function
x	x-direction grid block coordinate, *ft*
y	y-direction grid block coordinate, *ft*
α	convergence rate factor

ε_a	convergence tolerance based on acceptance ratio
ε_v	convergence tolerance based on objective function
γ	variogram
γ_o	specified variogram model for a conditional simulation
γ_s	sample variogram of simulation variable
λ	variogram correction term
ω	power for permeability averaging
ϕ	porosity
ψ	weight of objective function component
$\sigma^2_{\ln k}$	variance of the logarithm of the permeability distribution
μ	viscosity, *cp*
μ_k	mean permeability, *md*
ΔE^k	change in objective function at iteration k
$\Delta p'_w$	instantaneous logarithmic pressure derivative, *psi*
Δx	grid block dimension in x, *ft*
Δy	grid block dimension in y, *ft*

REFERENCES

1. Oliver, D.S.: "The Averaging Process in Permeability Estimation from Well-Test Data," *SPEFE* (Sept. 1990) 319-324.
2. Feitosa, G.: "Well Test Analysis for Heterogeneous Reservoirs," Ph.D. dissertation, University of Tulsa, Tulsa, OK (1993).
3. Pérez, G.: "Stochastic Conditional Simulation for Description of Reservoir Properties," Ph.D. dissertation, University of Tulsa, Tulsa, OK (1991).
4. Aasum, Yngve: "Effective Properties of Reservoir Simulator Grid Blocks," Ph.D. Dissertation, University of Tulsa, Tulsa, OK (1992).
5. Warren, J.E. and Price, H.S.: "Flow in Heterogeneous Porous Media," *SPE Journal* (Sept. 1961), 153-169.
6. Jones, A., King, P., McGill, C., and Williams. J: "Renormalization: A Multilevel Methodology for Upscaling," poster presented at the 1991 3rd International Reservoir Characterization Technical Conference, Tulsa, OK, Nov. 3-5.
7. Journel, A.G. and Huijbregts,C.J.: *Mining Geostatistics*, Academic Press, New York (1978).
8. Haldorsen, H. H. and Damsleth, E.: "Stochastic Modeling," Journal of Petroleum Technology (April 1990) 404-12.
9. Damsleth, E., Tjolse, C.B., Omre, K.H. and Haldorsen, H.H.: " A Two-Stage Stochastic Model Applied to a North Sea Reservoir," paper SPE 20605 presented at the 1990 SPE Annual Technical and Exhibition, New Orleans, LA Sept. 23-26.
10. Galli, A., Guerillot, D., Ravenne, C., and HERESIM Group: "Combining Geology, Geostatistics and Multiphase Fluid Flow for 3D Reservoir Studies," paper presented

at the Second European Conference on the Mathematics of Oil Recovery, Paris, France, 1990.

11. Isaaks, E.H. and Srivastava, R.M.: *Applied Geostatistics*, Oxford University Press, New York (1989).
12. Journal, A.G. and Alabert, F.G.: "A New Method for Reservoir Mapping," *JPT* (Feb. 1990) 212-218.
13. Deutsch, C.V. and Journel A.G.: GSLIB Oxford University Press
14. Hewett, T.A. and Behems, R.A.: "Conditional Simulation of Reservoir Heterogeneity with Fractals," *SPEFE* (Sept. 1990) 217-225.
15. Shibli, S. " An Approach to Generating Reservoir Property Descriptions Using a Stochastic Conditional Simulation Method", MS Thesis, University of Tulsa, Tulsa, OK (1992).
16. Mantoglou, A. and Wilson, J.L.: "The Turning Bands Method for Simulation of Random Fields Using Line Generation by a Spectral Method," Water Resources Research (Oct. 1982) 1379-94.
17. Huang, X.: "Application of the Genetic Algorithm to Reservoir Description," MS Thesis, University of Tulsa, Tulsa, OK (1993).
18. Sen, M., Datta Gupta, A., Stoffa, P.L., Lake, L.W., Pope, G.A.: "Stochastic Reservoir Modeling Using Simulated Annealing and Genetic Algorithms," paper SPE 24754 presented at the 1992 Annual Technical Conference and Exhibition, Washington, D.C., Oct. 3-7.
19. Farmer, C.L.: "Numerical Rocks, The Mathematical Generation of Reservoir Geology," paper presented at the 1989 Joint IMA/SPE European Conference Cambridge University, July 25-27.
20. Ouenes, A.: "Application of Simulated Annealing to Reservoir Characterization and Petrophysics Inverse Problems," Ph.D. Dissertation, The New Mexico Institute of Mining and Technology, Socorro, NM (1992).

21. Deutsch, C.V. and Journel, A.G.: "Annealing Techniques Applied to the Integration of Geological and Engineering Data," Report for the Stanford Center for Reservoir Forecasting (1992). Stanford University.

22. Doyen, P.M. and Guidish, T.M.: "Seismic Discrimination of Lithology: A Bayesian Approach," Western Atlas International, Middlesex, England.

23. Al-Kaabi, A.U. and Lee, W.J.: "Using Artificial Neural Networks to Identify the Well Test Interpretation Model," paper SPE 20332 presented at the Fifth SPE Petroleum Conference held in Denver, CO, June 25-28, 1990.

24. Kirkpatrick, S., Gelatt, C.D. Jr., and Vecchi, M.P.: "Optimization by Simulated Annealing," Science (May 13 1983) 671-680.

25. Fasanino, G. and Molinard, J.E.: "Inverse Modeling of Gas Reservoirs," paper SPE 15592 presented at the 1986 Annual Technical Conference and Exhibition, New Orleans, LA, Oct. 5-8.

26. Long, J.C.S., Doughty, C., Hestir, K., and Martel, S.: "Modeling Heterogeneous and Fractured Reservoirs with Inverse Methods Based on Iterated Function Systems," paper presented at the Third International Reservoir Characterization Technical Conference, Tulsa, OK, Nov. 3-5, 1991.

27. Hird, K.: "A Conditional Simulation Method for Reservoir Description Using Geological and Well Performance Constraints." Ph.D. dissertation, University of Tulsa, Tulsa, OK (1993)

28. Earlougher, R.C. Jr.: *Advances in Well Test Analysis*, Monograph Series, SPE, Richardson, TX (1977).

29. Van Poolen, H.K.: "Radius of Drainage and Stabilization-Time Equations," *Oil and Gas J.* (Sept. 14, 1964) 138-146.

30. Lee, John: *Well Testing*, SPE, Dallas (1982).

31. Matthews, C.S. and Russell, D.G.: *Pressure Buildup and Flow Tests in Wells*, Monograph Series, SPE, Richardson, TX (1967)

32. De Costa e Silva, A.J.: "A New Approach to the Characterization of Reservoir Heterogeneity Based on the Geomathematical Model and Kriging Technique" paper SPE 14275 presented at the 1985 Annual Technical Conference and Exhibition, Las Vegas, Sept. 22-25.

33. Ben-Rached, L.:" An Application of Geostatistical Techniques for Reservoir Performance Prediction" MS thesis, University of Tulsa, Tulsa, OK (1991).

34. Jensen, J.L., Lake, L.W., and Hinkley, D.V.: "A Statistical Study of Reservoir Permeability: Distributions Correlations and Averages," paper SPE 14270 presented at the 1985 Annual Technical Conference and Exhibition, Las Vegas, NV, Sept. 22-25.

35. Gómez-Hernández, J.J. and Gorelick, S.M.: "Effective Groundwater Model Parameter Values: Influence of Spatial Variability of Hydraulic Conductivity, Leakance and Recharge," *Water Resources Research*, 25(3), 405-419, 1989.

36. Alabert, F.G.: "Constraining Description of Randomly Heterogeneous Reservoirs to Pressure Test Data: A Monte Carlo Study," paper SPE 19600 presented at the 1989 Annual Technical Conference and Exhibition, San Antonio, TX, Oct. 8-11.

37. Rosa, A.J. and Horne, R.N.: "Reservoir Description by Well Test Analysis Using Cyclic Flow Rate Variation," paper SPE 22698 presented at the 1991 Annual Technical Conference and Exhibition, Dallas, TX, Oct. 6-9.

38. Oliver, D.S.: "Estimation of Radial Permeability Distribution from Well Test Data," paper SPE 20555 presented at the 1990 Annual Technical Conference and Exhibition, New Orleans, LA, Sept. 23-26.

39. Yang, A.: "Program TBM-Turning Bands Method to Generate 2-D Random Fields with Autocorrelation," FORTRAN Source Code, University of Texas, Austin, TX (1987).

40. *ECLIPSE 100 - Black Oil Simulator*, ECL-Bergeson Petroleum Technologies, Inc., Oxfordshire, England (1990).

41. Peaceman, D.W. : "Interpretation of Well-Block Pressures in Numerical Reservoir Simulation," *SPE of AIME* (1978).

42. Whittaker, E.T. and Watson, G.N.: *A Course in Modern Analysis*, Cambridge University Press, Cambridge (1952).

43. Lifu Chu, personal communication, Sept. 1993.

44. MacDonald, R.C., and Coats, K.H.: "Methods for the Numerical Simulation of Water and Gas Coning." paper SPE 2796 presented at the Second Symposium on Numerical simulation of Reservoir Performance, Dallas, TX, Feb. 5-6, 1970.

45. Mishra, S., Brigham, W.E., and Orr, F.M. Jr.: "Tracer and Pressure Test Analysis for Characterization of Areally Heterogeneous Reservoirs," paper SPE/DOE 17365 presented at the 1988 SPE/DOE Enhanced Oil Recovery Symposium, Tulsa, OK, April 17-20.

46. Craig, F.F., Jr.: *Reservoir Engineering Aspects of Waterflooding*, Monograph Volume 3, SPE of AIME, Dallas, TX (1971).

47. Burden, R.L. and Faires, J.D: *Numerical Analysis*, Prindle, Weber, and Schmidt, Boston, MA (1985).

48. Metropolis, N., Rosenbluth, A.W., Rosenbluth, M.N., Teller, A.G., and Teller, E. "Equation of State Calculations by Fast Computing Machines," The Journal of Chemical Physics (June 1953) 1087-92.

49. Aarts, E. and Korst, J.: *Simulated Annealing and Boltzman Machines: A stochastic Approach to combinatorial Optimization and Neural Computing*, John Wiley & Sons Ltd., Chichester (1989).

50. *Log Interpretation Charts*, Schlumberger Educational Services, USA (1991).

51. Muskat, Morris : *Physical Principles of Oil Producation*, International Human Resources Development Corporation, Boston, MA (1981), pp 262-263.

APPENDIX A

In this appendix we present the calculation procedure to determine the area of the grid blocks that fall within an annular ring of defined minimum and maximum radii. Recall that the two-dimensional simulation grid has i=1,2,.....N_s grid blocks and j=1,2,.....N_r radial divisions.

To begin with, the simulation domain is divided into 4 quadrants (I, II, III and IV) as shown in Figure A.1. We consider the annulus defined between r_{j-1} and r_j for j=1,2,....N_r. Figure A.1 also shows that for each annular region under consideration a grid-block within the simulation domain will have an area within the annulus defined by 5 possible arrangements which are defined by the following criteria:

$$
\begin{aligned}
&r_{c\max} > r_{j-1} > r_{c\min} && \text{.....Block A}\\
&r_{c\max} > r_j > r_{c\min} && \text{..... Block B}\\
&(r_{c\max} > r_{j-1} > r_{c\min}) \text{ and} (r_{c\max} > r_j > r_{c\min}) && \text{..... Block C}\\
&(r_{c\max} < r_{j-1}) \text{ and} (r_{c\min} > r_{j-1}) && \text{..... Block D}\\
&(r_{c\min} > r_j) \text{ or } (r_{c\max} < r_{j-1}) && \text{..... Block E,}
\end{aligned}
\qquad \text{(A.1)}
$$

where r_{cmin} and r_{cmax} are the radii defining the distance from the well to closest and furthest corners of the grid block, respectively. If the grid block is type D, i.e., the whole grid block is within the annulus under consideration, then $A_{\bar{s}} = \Delta x \times \Delta y$. If the grid block is type E, then $A_{\bar{s}} = 0$. We outline the procedure to calculate the area of the other types of gridblocks, but first we describe some important nomenclature relevant to the problem.

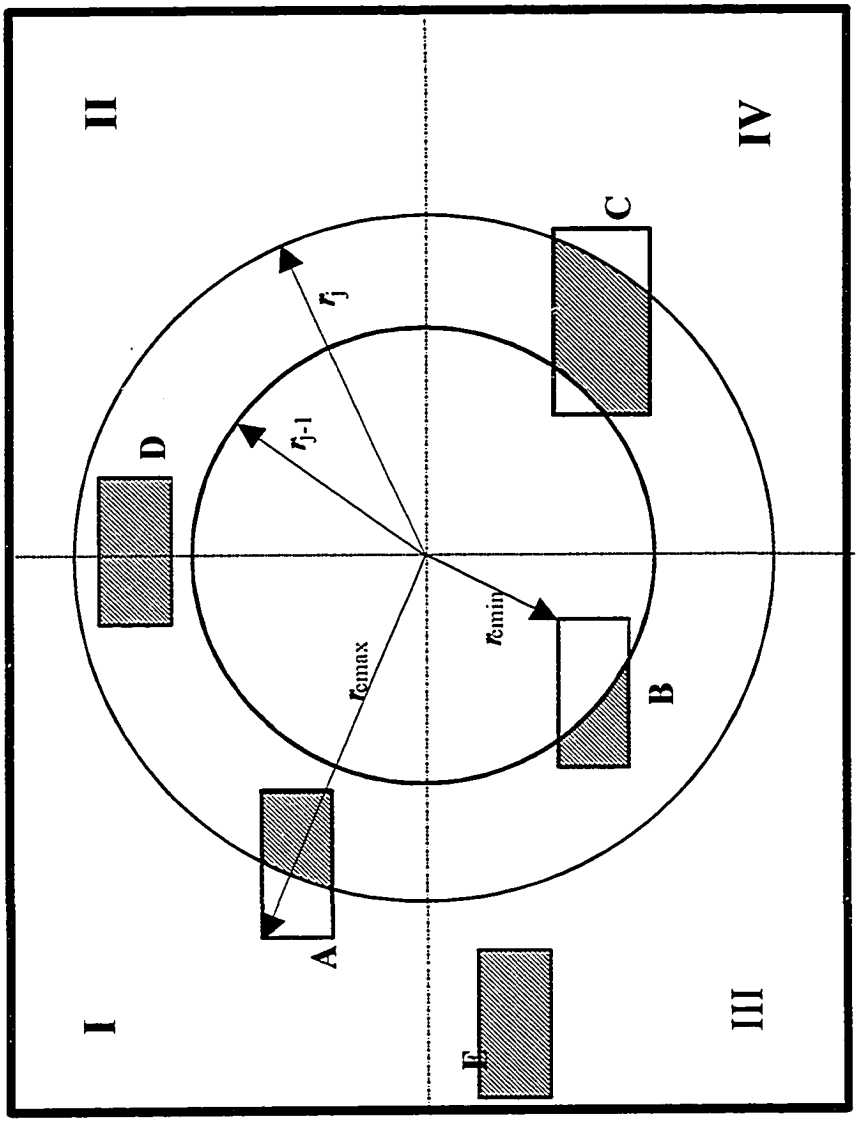

Figure A.1 - Simulation domain illustrating possible combinations of areas of grid blocks within the annulus

Grid Block Coordinates

The grid block coordinates are defined in Figure A.2. We also define the coordinates of the intersecting arc for the outer radius, r_j, at (x1,y1),(x2,y2).

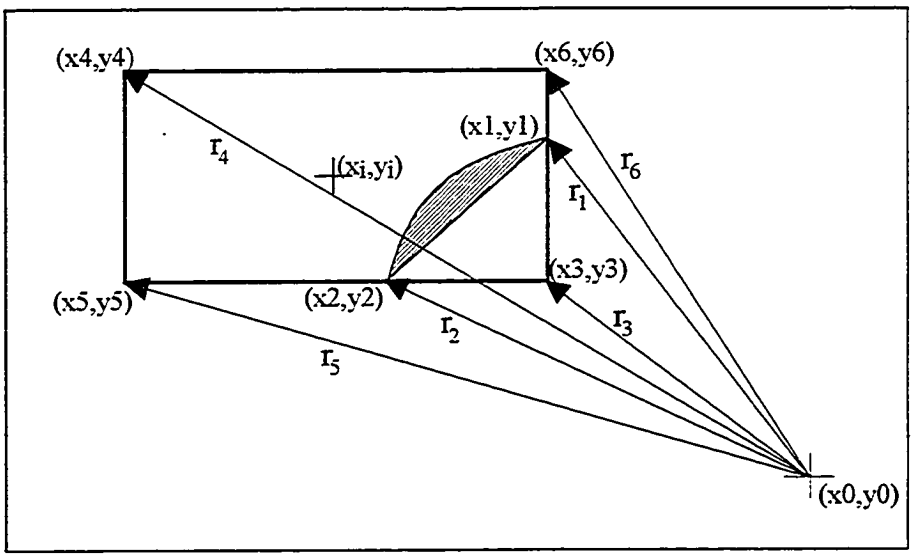

Figure A.2- Coordinates of the grid block and the intersecting arc.

Area of the Sector

The area of the shaded sector is defined by:

$$A_{sec} = \frac{1}{2} r_j^2 (\beta - \sin\beta), \tag{A.2}$$

where, β is the angle of sector, measured in radians, from the center $(x0,y0)$ of the reservoir defined by:

$$\beta = \tan^{-1}\frac{y1-y0}{x1-x0} + \tan^{-1}\frac{y2-y0}{x2-x0}. \tag{A.3}$$

Transformation of Coordinates

The coordinates of grid blocks in quadrants II, III, and IV are transformed to equivalent grid block coordinates of Quadrant I. The original coordinates of the grid block are given by $(x1, y1), (x2, y2), (x3, y3)$ and $(x4, y4)$. For each transformation we define corresponding integer flags, I_x and I_y, which are later used to calculate the locations of the intersection coordinates along the grid block.

For quadrant I we define the coordinates as:

$$\begin{aligned} &(x3', y3') = (x3, y3), \\ &(x4', y4') = (x4, y4), \\ &(x5', y5') = (x5, y5), \text{ and} \\ &(x6', y6') = (x6, y6) \\ &I_x = -1 \text{ and } I_y = 1. \end{aligned} \tag{A.4}$$

The transformation of a grid block in quadrant II to an equivalent grid block in quadrant I is given by the following transformation of coordinates.

$$\begin{aligned} &(x3', y3') = (x5, y5), \\ &(x4', y4') = (x6, y6), \\ &(x5', y5') = (x3, y3), \text{ and} \\ &(x6', y6') = (x4, y4) \\ &I_x = 1 \text{ and } I_y = 1. \end{aligned} \tag{A.5}$$

The transformation of a grid block in quadrant III to an equivalent grid block in quadrant I is given by the following transformation of coordinates:

$$
\begin{aligned}
&(x3', y3') = (x6, y6),\\
&(x4', y4') = (x5, y5),\\
&(x5', y5') = (x4, y4), \text{ and}\\
&(x6', y6') = (x3, y3)\\
&I_x = -1 \text{ and } I_y = -1.
\end{aligned}
\tag{A.6}
$$

The transformation of a grid block in quadrant IV to an equivalent grid block in quadrant I is given by the following transformation of coordinates:

$$
\begin{aligned}
&(x3', y3') = (x4, y4),\\
&(x4', y4') = (x3, y3),\\
&(x5', y5') = (x6, y6), \text{ and}\\
&(x6', y6') = (x5, y5)\\
&I_x = 1 \text{ and } I_y = -1.
\end{aligned}
\tag{A.7}
$$

The above coordinate transforms simplify the procedure for calculating the partial area of a grid block that falls within the annulus of consideration.

Intersection Coordinates of the Arc

We now list the equations used to calculate the unknown coordinates of the arc of the radius of interest intersecting the grid block.

If y1 is known then x1 is calculated by:

$$x1 = x0 + I_x\sqrt{r_j^2 - (y1 - y0)^2} \tag{A.8}$$

If x1 is known then y1 is calculated by:

$$y1 = y0 + I_y\sqrt{r_j^2 - (x1 - x0)^2} \tag{A.9}$$

If y2 is known then x2 is calculated by:

$$x2 = x0 + I_x\sqrt{r_j^2 - (y2 - y0)^2} \tag{A.10}$$

If x2 is known then y2 is calculated by:

$$y2 = y0 + I_y\sqrt{r_j^2 - (x2 - x0)^2} \tag{A.11}$$

In the section describing the calculation of area of the grid block intersected by the arc, we state the known coordinates for which the unknown coordinate locations are calculated by the above equations.

Area of Grid Block Type A

The circle defined by the outer radius, r_j, may intersect the grid block in a variety of ways and we describe each possible combination. For the sake of clarity, we define the title of the calculation procedure by its corresponding figure number, illustrating the type of grid block area within the annulus. The type of grid block area calculation is defined by a criteria based on the intersection points of the arc defining the radius and the grid block--this criteria is described. We then define the known coordinates of the arc of the outer radius intersecting the grid block. The unknown coordinate locations are calculated by Equations A.8-A.11. Finally, we describe the calculations for the area of the grid block within the annulus or the shaded region of the grid block, A_s^g.

Figure A.3

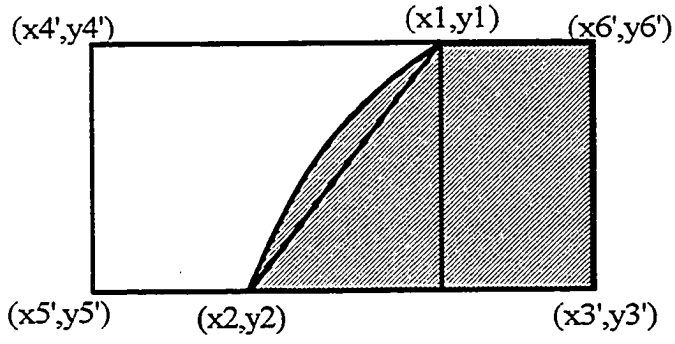

Figure A.3

Defining criteria:

$$r_6 < r_j < r_4 \text{ and } r_3 < r_j \le r_5 \tag{A.12}$$

Unknown coordinates of the intersecting arc:

$$y1 = y6', \quad y2 = y3', \tag{A.13}$$

Grid block area within the annulus, A_s^a:

$$A_s^a = \Delta y|x6' - x1| + \frac{1}{2}\Delta y|x2 - x1| + A_{sec} \tag{A.14}$$

Figure A.4

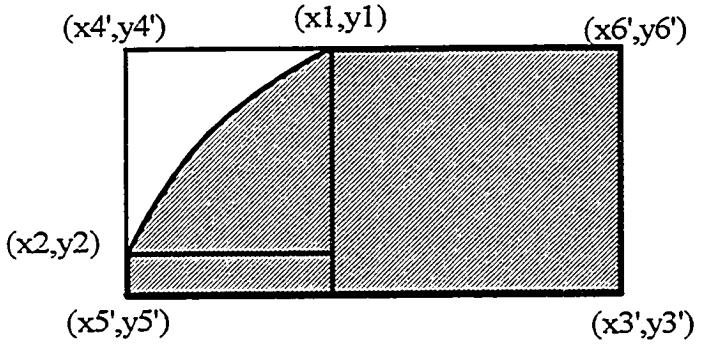

Figure A.4

Defining criteria:

$$r_6 < r_j < r_4 \text{ and } r_5 < r_j < r_4 \tag{A.15}$$

Unknown coordinates of the intersecting arc:

$$y1 = y4' \text{ and } x2 = x4'. \tag{A.16}$$

Grid block area within the annulus, A_s^a:

$$A_s^a = \Delta x \Delta y - \left(\frac{1}{2}|x2 - x1||y2 - y1| - A_{sec}\right) \tag{A.17}$$

Figure A.5

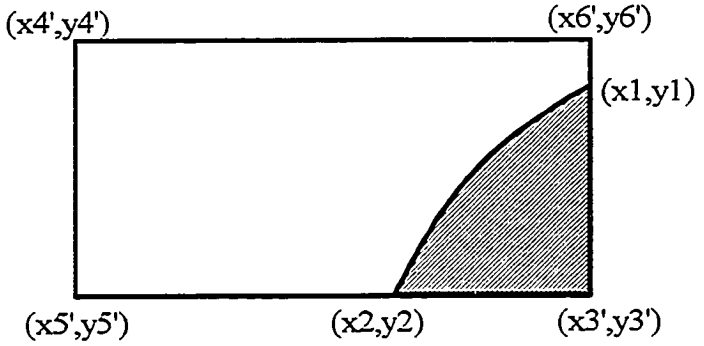

Figure A.5

Defining criteria:

$$r_3 < r_j \le r_6 \text{ and } r_3 < r_j < r_5 \tag{A.18}$$

Unknown coordinates of the intersecting arc:

$$x1 = x3' \text{ and } y2 = y3'. \tag{A.19}$$

Grid block area within the annulus, A_s^a:

$$A_s^a = \frac{1}{2}|x2 - x1||y2 - y1| + A_{sec} \tag{A.20}$$

Figure A.6

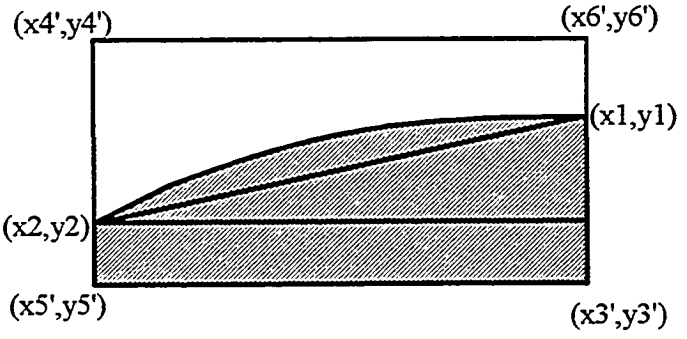

Figure A.6

Defining criteria:

$$r_5 < r_j < r_4 \text{ and } r_5 < r_j < r_6 \tag{A.21}$$

Unknown coordinates of the intersecting arc:

$$x2 = x4' \text{ and } x1 = x3'. \tag{A.22}$$

Grid block area within the annulus, A_s^a:

$$A_s^a = \frac{1}{2}|x2 - x1||y2 - y1| + |x2 - x1||y2 - y5'| + A_{sec} \tag{A.23}$$

We now outline the calculations for the area of a grid blocks within the annulus that fall on the x-dividing line along the center of the reservoir, i.e., $y_i = y_0$.

Figure A.7

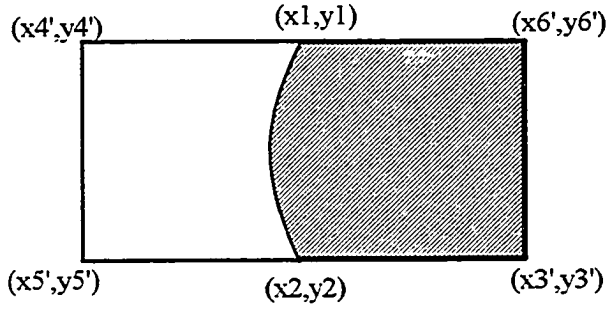

Figure A.7

Defining criteria:

$$y_i = y_0 \text{ and } r_6 < r_j \le |x4' - x0| \tag{A.24}$$

Unknown coordinates of the intersecting arc:

$$y1 = y6' \text{ and } y2 = y3'. \tag{A.25}$$

Grid block area within the annulus, A_s^a:

$$A_s^a = \Delta y|x1 - x6'| + A_{sec} \tag{A.26}$$

Figure A.8

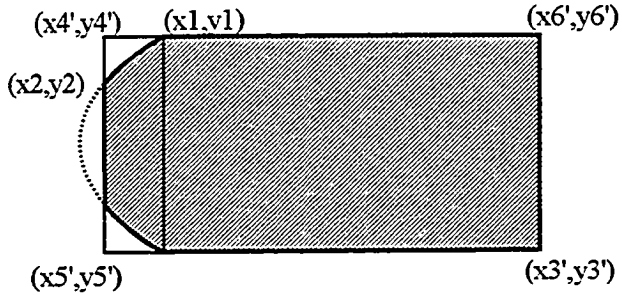

Figure A.8

Defining criteria:

$$y_i = y_0 \text{ and } |x4'\text{-}x0| > r_j > r_6 \tag{A.27}$$

Unknown coordinates of the intersecting arc:

$$x2 = x4' \text{ and } y1 = y4'. \tag{A.28}$$

Grid block area within the annulus, A_s^a:

$$A_s^a = \Delta x \Delta y - 2\left(\frac{1}{2}|x2 - x1||y2 - y1| - A_{sec}\right) \tag{A.29}$$

Figure A.9

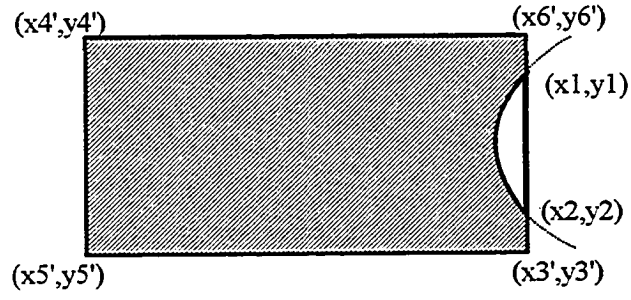

Figure A.9

Defining Criteria:

$$y_i = y_0 \text{ and } r_3 > r_j > |x3'\text{-}x0| \tag{A.30}$$

Unknown coordinates of the intersecting arc:

$$x1 = x3' \text{ and } x2 = x3'. \tag{A.31}$$

Grid block area within the annulus, A_s^g:

$$A_s^g = \Delta x \Delta y - A_{sec} \tag{A.32}$$

We now outline the calculations for the area of a grid blocks within the annulus that fall on the y-dividing line along the center of the reservoir, i.e., $x_i = x_0$.

Figure A.10

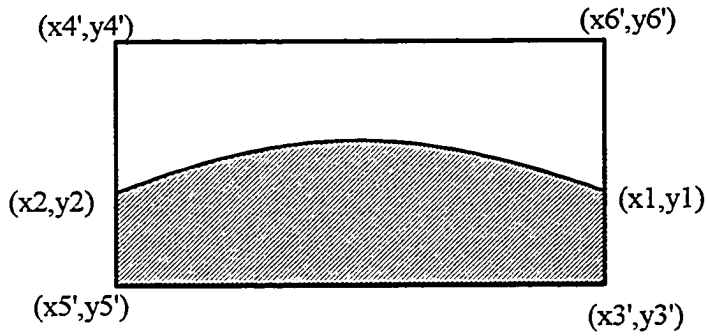

Figure A.10

Defining criteria:

$$x_i = x_0 \text{ and } |x3'\text{-}x0| < r_j < r_6 \tag{A.33}$$

Unknown coordinates of the intersecting arc:

$$x1 = x3' \text{ and } x2 = x4'. \tag{A.34}$$

Grid block area within the annulus, A_s^g:

$$A_s^g = |x2 - x1||y2 - y1| + A_{sec} \tag{A.35}$$

Figure A.11

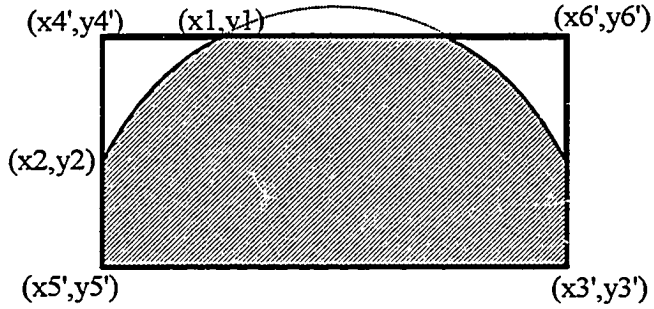

Figure A.11

Defining criteria:

$$x_i = x_0 \text{ and } r_6 > r_j > |y6' - y0| \tag{A.36}$$

Unknown coordinates of the intersecting arc:

$$x1 = x6' \text{ and } y2 = x6'. \tag{A.37}$$

Grid block area within the annulus, A_s^g:

$$A_s^g = \Delta x \Delta y - 2\left(\frac{1}{2}|x2 - x1||y2 - y1| - A_{sec}\right) \tag{A.38}$$

Figure A.12

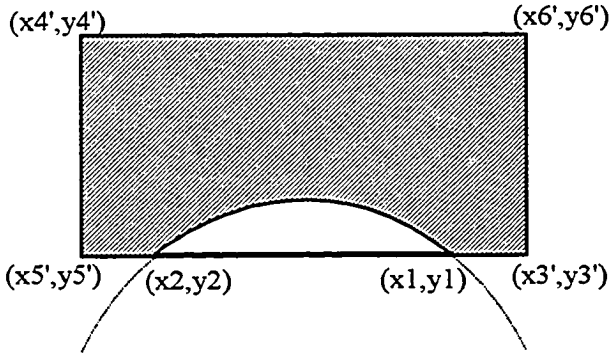

Figure A.12

Defining criteria:

$$x_i = x_0 \text{ and } r_5 > r_j > |y5' - y0| \tag{A.39}$$

Unknown coordinates of the intersecting arc:

$$y1 = y3' \text{ and } y2 = y3'. \tag{A.40}$$

Grid block area within the annulus, A_s^a:

$$A_s^a = \Delta x \Delta y - A_{sec} \tag{A.41}$$

A.2 Area of Grid Block Type B

In this case the arc of the circle defined by the inner radius, r_{j-1} intersects the grid block (Figure A.1). The grid block area is calculated with the same procedure as described for the calculation of the area of grid block type A. This area is then subtracted from the total area of the rectangular block:

$$A_s^B = \Delta x \Delta y - A_s \tag{A.42}$$

A.3 Area of Grid Block Type C

The grid block type C is intersected by both arcs defined by the inner and outer radii. In this case the area of the grid block within the annulus is defined by:

$$A_s^c = A_s^a - (\Delta x \Delta y - A_s^b) \tag{A.43}$$